On the use of C_2* emission spectroscopy for thermometry of flames in propulsion systems

Master Thesis

KSJ Chandra Sekharan

Delft University of Technology

TU Delft Delft University of Technology

Challenge the Future

MASTER THESIS

On the use of C_2* emission spectroscopy for thermometry of flames in propulsion systems

by

KSJ Chandra Sekharan

in partial fulfilment of the requirements for the degree of

Master of Science
in Aerospace Engineering

at the Delft University of Technology,
to be defended publicly on Thursday September 27, 2018 at 1:30 pm.

Supervisor :	Dr. ir. Alexis Bohlin
Thesis committee :	Dr. Arvind Gangoli Rao (Chairman, FPP, LR Faculty, TU Delft) Dr. Paul Roling (ATO, LR Faculty, TU Delft)

This thesis is confidential and cannot be made public until September 27, 2019.

TU Delft Delft University of Technology

Preface

I wish to thank my Supervisor Dr.Alexis Bohlin for his technical guidance and for his motivational mentorship throughout the whole duration of the thesis. He has been a very supportive guide. My parents have always been patient with me in various regards, they have supported my education and cared for my well-being by sacrificing their everyday pleasures all their lives. I express my heartfelt gratitude to my father Dr.Chandrasekharan and my mother Mrs.Padmavathi. Finally, I wish to acknowledge my love, Ms.Ramya, for having renewed zeal and passion for life in me, after grave setbacks, which motivated me for the successful completion of my thesis work.

Kalyan Surya Jagan, Chandra Sekharan.
Delft, September 2018.

Abstract

The developments in combustion technology has to be catered to in parallel by the development in the instrumentation employed in collection of combustion data, to get a better picture of the complex processes involved. In this regard, the flame temperature and equivalence ratio are the most important parameters that has to be studied to infer the combustion efficiency and emissions from combustion. Combustion reactions in flames give rise to the formation of various intermediate radicals, some of which are chemiluminescent by nature. The relative intensity of optical emissions from chemiluminescent radicals such as OH*(the asterisk is used as a notation for electronically excited states), CH* and C_2* can be used for flame thermometry and spatial analysis of flame structure in hydrocarbon flames. The C_2* radical and CH* radical is emphasized upon in this study for the analysis of laminar premixed hydrocarbon flames. Spatial distribution of these radicals is mapped from their chemiluminescence signals and recorded across various zones of the flame using a fiber optic bundle to capture incoming photons, a Czerny-Turner spectrometer encompassing a diffraction grating for optical dispersion and a CCD detector to record the spectrum. Local flame spectra recorded in the reaction zone of methane/air flames are known to exhibit strong emission signals from OH*, CH* and C_2* radicals. The peak intensity ratios of these radicals in the reaction zone are functions of local equivalence ratio. To sum up, spectral intensity measurements of such chemiluminescent radicals serve as tools for analyzing the local flame stoichiometry and for the measurement of local flame temperature.

In this thesis work, an experimental set-up is proposed to capture the spectral signals of a premixed, laminar, methane-air Bunsen flame at various spatial locations across the geometry of the flame. Using the emission spectra of this flame, the flame characteristics like relative intermediate radical species concentration, the spatial distribution of radicals, the flame equivalence ratio, the rotational and vibrational flame temperature and their degree of agreement with the adiabatic flame temperature are studied. It has been found that a definite relationship exists between the spectral signals emitted by these chemiluminescent radicals and the flame parameters such as equivalence ratio and adiabatic flame temperature.

Keywords:
combustion, chemiluminescence, spectroscopy, optical thermometry, rotational temperature, vibrational temperature, C_2 radical, flame equivalence ratio*

Contents

List of Figures

List of Tables

List of Symbols and Acronyms

TIT - Turbine Inlet Temperature

HEATTOP - High-temperature Engine Aero-Thermal measurements for gas Turbine life Optimization, Performance and condition monitoring

E - Energy of a photon

h - Planck's constant

ν - Frequency of a photon

c- Velocity of light

λ - Wavelength

σ - Wavenumber

T- Spectral term

m - The order pertaining to each radiation in the Spectral series

$\mathbf{R_H}$- Rydberg's constant

m - Mass

v - Velocity

a - Radius

n - Principal quantum number.

l - Orbital quantum number

j - Spin quantum number

m - Magnetic quantum number .

$\mathbf{Z_e}$- nuclear charge

$\mathbf{l_i}$- length of orbital angular momentum vector

$\mathbf{s_i}$- length of spin angular momentum vector

L - vector sum of all orbital angular momenta

S - sum of all the spin momenta

J - the total angular momentum

Λ - projection of vector L on the internuclear axis

Σ - projection of vector S on the internuclear axis

Ω - total electronic angular momentum about the internuclear axis of diatomic molecule

ΔE - the energy difference

$\mathbf{E_0}$ - the electronic energy of the molecule exclusive of the consideration of spins of the electrons

E_e- the energy of the valence electrons of the molecule

E_r- the energy of rotation of the molecule about a fixed axis

E_v- the energy of vibration of the molecule due to a periodic deformation.

E_t - the translational energy of the molecule

X- the fundamental multiplet of least energy level

R- the angular momentum of the molecule taken parallel to the axis of rotation

I- the moment of inertia of the diatomic system.

B- the rotational constant

D - another rotational constant when the effect of centrifugal stretching is taken into account

r - internuclear distance

r_e- the equilibrium internuclear distance

ν_{osc}- oscillation frequency of the Vibrational movement

G(v) - vibrational spectral terms of the harmonic oscillator

ω_e- the wave number related to the classic vibrational frequency

D_e - dissociation energy of the molecule

D_0 - zero-point energy

V - potential energy of the anharmonic oscillator can be represented by the Morse function

B_v - average rotational constant in a 'vibrating rotator'

B_e- rotational constant of a non-rotating molecule and

α_e, γ_e - rotational constants

$F_v(J)$ - the rotational term of the 'vibrating rotator'

Ψ_V - vibrational wavefunction

I - intensity of an electromagnetic radiation

T - absolute temperature at thermal equilibrium

n_i - average number of particles of a given chemical species

E_i - energy level of a given chemical species

g_i- the statistical weight of the energy level Ei

N_i - population of energy level Ei

N - the total number of particles of the species considered belonging to all energy levels

k- the Boltzmann Constant

$dN_{i\rightarrow j}$- the number of molecules undergoing transition from Ei to a lower energy state Ej in unit time

A_{ij} - Einstein transition probability of spontaneous emission

I_{em} - the energy emitted per unit time

ρ(ν) - spectral volume density

B_{ji}- Einstein transition probability of absorption

B_{ij}- Einstein transition probability of stimulated emission

S_{ij}- strength of line

f - oscillator strength

K - integrated absorption coefficient

α- constant dependent on the measuring instrument.

$a_{v' \rightarrow v''}$ - vibrational transition probability

$a_{m \rightarrow n}$- electronic transition probability

Chapter 1. Introduction

1.1 Background

Combustion is an inherent phenomenon in Aerospace Propulsion Systems. Temperature measurements in such systems can be broadly categorized into probe thermometry and optical thermometry. Optical thermometry, which encompasses several different methodologies, exploits the photon emission or absorption occurring in a combustion process. Chemiluminescence is the process of emission of light as a result of a chemical reaction. Spectroscopic studies using chemiluminescence of flames can help in determining the intensity distribution of products formed in the combustion process. In such combustion processes the number density of different intermediate species formed during combustion depends on the adiabatic flame temperature. The relative spectral line intensities observed from flame emission spectrum is a representative of the relative number density of different species formed in the combustion process. Hence using this correlation, the equivalence ratio and the flame temperature can be inferred by making use of the Boltzmann law which connects the thermodynamic temperature and the relative number density of different chemical species formed in the reaction. This thesis work will be concerned with elucidating the equivalence ratio and the thermodynamic temperature of such combustion flames by making spectroscopic quantitative measurements on the line intensities of spectra emitted by the Carbon molecule and CH molecule.

The particles of matter have translational, vibrational and rotational motions. The thermodynamic temperature is defined as the measure of the average energy of these motions. Hence in quantum mechanics there exists different temperatures for an excited particle, namely vibrational, rotational, electronic and translational temperatures. Generally, the translational temperature is referred to as the gas kinetic temperature and it is the commonly measured entity; by thermometric instruments like thermometers and thermocouples. In this thesis work the emission spectra of the Swan band of the C_2 radical and the CH radical will be analysed, using which the vibrational and rotational temperatures will be extracted. Finally, the degree of agreement of these temperatures with the gas kinetic temperature will be scrutinized. This thesis aims to investigate the feasibility of using emission spectroscopy as a means of non-intrusive temperature measurement for flames in combustion.

The usage of conventional intrusive thermometric probes such as thermocouples and gas analysers for combustion diagnostics have associated structural problems and aerodynamic instabilities, affecting the system under diagnosis [1]. Hence, better diagnostic tools are essential for monitoring such systems. Among the alternative choices, optical emission spectroscopy from spontaneous emissions of radicals formed in combustion reactions exhibits remarkable advantages as they are simple, low-cost and compact [2]. The payload weight is a very important limiting variable in the aerospace arena, and employing compact spectrometers for active, real-time, in situ, non-intrusive combustion diagnostics is an interesting choice [3]. Hence emission spectroscopy can be regarded as a powerful tool to

aid in active combustion diagnostics, in systems where a real time and in situ monitoring is necessary [4].

1.1.1 Drawbacks of conventional thermometric systems in gas turbine engines.

Commonly, intrusive electronic devices such as thermocouples, resistance thermometers and quartz resonance thermometers are used to measure gas temperatures at various locations in the jet engine [5]. To measure temperatures in high temperature regions such as the combustion zone in a gas turbine combustor, the existing state-of -the art methods such as thermocouples have certain drawbacks associated with them which are enlisted below:

- Being intrusive instruments, thermocouples disturb the flow field around the vicinity and can result in a change of flow dynamics, paving to way to an erroneous flame temperature measurement, called velocity error or impact error.
- There is always a time lag between the events occurring in a combustion flame and the events that are sensed by the thermocouple.
- The basic assumption while employing a thermocouple to measure the environmental temperature, is the prevalence of a constant potential difference when the temperature remains constant. But in real world applications, there is change in voltage over time even when the temperature remains a constant. This erroneous phenomenon is called drift and is an important source of error to be considered in thermocouple measurement
- With rapid growth in material sciences and cooling technologies, the turbine inlet temperature (TIT) has reached up to 2000K in modern gas turbines, where temperature measurement plays the pivotal role in efficiency determination. The thermocouples currently used in gas turbines have an operating temperature limitation of about 1300 K and, as a result the TIT is measured further downstream away from the combustor section. As a result of such a procedure an inherent uncertainty exists and in order to run the engine safely a wider margin of safety on the operating temperature is required. Accurate gas temperature measurements in the high temperature gas turbine environments are also required for component residual life prediction methods, cooling system design, combustor performance assessment and optimum engine control technologies [6].
- To measure temperatures in the high temperature regions such as the combustion zone in a combustor, the existing state-of -the art methods such as thermocouples need more improvisation for highly accurate measurements since they are intrusive devices which also require cooling systems to be located in such high temperature regions.

1.1.2 The need for development of optical thermometric systems in gas turbine engines.

The difficulties encountered with conventional thermometric systems are expected to be overcome by employing non-intrusive thermometric techniques, wherein optical emission thermometry is one such technique. Optical thermometry is a temperature measurement procedure that is based on the inferences from spectroscopic analysis. In contrast to intrusive temperature measurement techniques, such optical temperature measurement techniques do not interfere with the system under measurement.

In their 2013 research article in the Journal of Engineering Gas Turbines and Power, Michele et al from the material science department of the University of Cambridge have concluded that research activities are ongoing to improve the service life of the thermocouples at temperatures higher than 1300K [7], emphasizing the need for the development of better temperature measurement systems at very high temperature ranges. In larger engines TIT can be over 1750K [8] making the usage of conventional Nickel based thermocouples unusable. The HEATTOP(acronym for " High-temperature Engine Aero-Thermal measurements for gas Turbine life Optimization, Performance and condition monitoring") is a project funded by the European Community as part of the Sixth Framework Programme which targets the development and improvement of instrumentation to measure pressure, temperature (gas temperature, surface temperature, blade temperature), flow and tip clearance in gas turbines. A part of the project also emphasizes about the necessity for a thermometric system with a higher temperature measurement capability as put forward by several gas turbine manufacturers [9]. To give a picture of the magnitude of the temperatures involved, Fig.1 shows the gas-path temperatures for a typical subsonic engine, and for a typical after-burning supersonic engine.

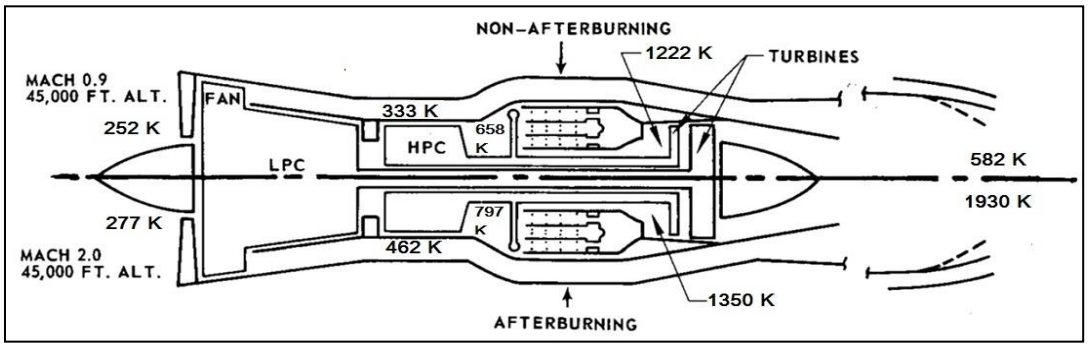

Figure 1: Gas-path temperatures in a typical gas turbine engine [10].

The positive assertions of cost, accuracy, transient capabilities and measurement range about emission spectroscopy are bolstered by the list compiled in Fig.2 taken from the Review of temperature measurement [10], 2000.

Method	Minimum temperature (°C)	Maximum temperature (°C)	Response	Transient capability	Sensitivity	Accuracy	High signal	Stability/ repeatability	Low thermal disturbance	Commercially available	Relative Cost
Gas thermometer	about −269	700	Slow	No	···	A standard	Yes	Yes	No	No	Very high
Liquid-in-glass thermometer	−200	600	Slow	Yes	1 °C	±0.02–±10 °C (ind) ±0.01 °C (lab)	Yes	Yes	No	Yes	Very low
Bimetallic strip	−73	540	Medium	Yes	···	±1 °C	Yes	Yes	Yes	Yes	Low
Thermocouple	−270	2300	Very fast	Yes	±10 μV/°C	±0.5–±2 °C	No	Yes	Yes	Yes	Very low
Suction pyrometer	−200	1900	Very fast	Yes	···	±5 °C of reading	Yes	Yes	No	Yes	Mid to high
Electrical resistance device	−260	1064	Fast	Yes	0.1 Ω/°C	The standard above 13 K	Yes	Yes	Yes	Yes	Mid to low
Thermistors	−100	700	Fast	Yes	10 mV/K	±0.01–±0.05 °C	Yes	Yes	Yes	Yes	Mid to low
Semiconductor devices	−272	300	Very fast	Yes	±1%	±0.1 °C	Yes	Yes	No	Yes	Low
Fiber optic probes	−200	2000	Fast	Yes	10 mV/°C	0.5 °C	Yes	Yes	Yes	Yes	Mid to high
Capacitance	−272	−170	Fast	Yes	Good	Poor	Yes	No	Yes	Yes	Mid
Noise	−273	1500	Fast	Yes	Good	Good	No	Yes	Yes	No	High
Chemical sampling	5	2100	Slow	No	···	±25 K	No	Yes	No	Yes	Mid
Thermochromic liquid crystals	−40	283	Medium	Yes	±0.1 °C	±1 °C	···	Yes	Yes	Yes	Low to Mid
Thermographic phosphors	−250	2000	Very fast	Yes	~0.05 °C	0.1%–5%	Yes	Yes	Yes	Yes	High
Heat sensitive paints	300	1300	Slow	No	···	±5 °C	Yes	Yes	Yes	Yes	Mid
Infrared thermometer	−40	2000	Very fast	Yes	~0.1 °C	±2 °C	Yes	Yes	Yes	Yes	Very high
Two color	150	2500	Very fast	Yes	1 °C/mV	±1%(±10 °C)	Yes	Yes	Yes	No	Very high
Line scanner	100	1300	Very fast	Yes	···	±2 °C	Yes	Yes	Yes	Yes	Very high
Schlieren	0	2000	Fast	Yes	N/A	N/A	Visual	Yes	Yes	Yes	Mid
Shadowgraph	0	2000	Fast	Yes	N/A	N/A	Visual	Yes	Yes	Yes	Mid
Interferometry	0	2000	Fast	Yes	N/A	N/A	Yes	Yes	Yes	Yes	High
Line reversal	727	2527	Very fast	No	Line of sight avg.	±10–15 K	Yes				Low
Absorption spectroscopy	20	2500	Very fast	No	Line of sight avg	15%	Yes	Yes	Yes	Yes	Low
Emission spectroscopy	20	2700	Very fast	Yes	Line of sight avg.	15%	Yes	Yes	Yes	Yes	Low
Rayleigh scattering	20	2500	Very fast	No	0.1 mm^3 in 100 °C	1%	Yes	Yes	Yes	No	Very high
Raman scattering	20	2227	Very fast	No	0.1 mm^3 in 100 °C	7%	Yes	Yes	Yes	No	Very high
CARS	20	2000	fast		1 mm^3 in 50 °C	5%	Yes	at atm	Yes	Yes	Very high
Degenerative four wave mixing	270	2600	Very fast	Yes	1 mm^3 in 50 °C	10%	Yes	at atm	Yes	No	Very very high
Luminescence	20	200	fast	Yes	1.5 nm in 200 °C	±5 °C	Yes	Yes	Yes	No	High
LIF	0	2700	Very fast	No	···	10%	Yes	Yes	Yes	No	Very high

Figure 2: Review of temperature measurement techniques [11].

1.2 Objective and research questions

The objective of this study is to acquire Optical Emission Spectra(OES) across a laminar premixed conical Bunsen flame, in order to use the spectral intensity measurements of such chemiluminescent radicals for analysing local flame stoichiometry and measurement of local flame temperature. The intensity profile of the C_2 and CH radicals across the flame zones are recorded experimentally and then analysed. Based on the research objective the following research questions are proposed:

1. Can the spatial distribution of the C_2^* radical across the flame front for a given equivalence ratio be mapped using the acquired OES?

2. In a hydrocarbon flame, will the peak emission intensity ratios of chemiluminescent radicals give a picture of the local flame stoichiometry? Can these peak emission intensity ratios in the flame reaction zone be used to determine the local equivalence ratio?

3. Is it possible to determine the C_2* Vibrational Temperature(T_v) and Rotational Temperature(T_r) in the flame reaction zone for a range of equivalence ratios by fitting the recorded experimental spectrum to a simulated theoretical spectrum?

4. What is the degree of agreement of the C_2* Rotational Temperature(T_r) with the theoretical adiabatic flame temperature(gas kinetic/translational temperature) at the respective spatial locations across the flame front? Is this a reliable source of thermometry for flames in combustion?

1.3 Report Outline

This master thesis report is divided into 8 chapters each of which addresses a specific purpose. Following the introduction, Chapter 2 to 4 will give an insight into the literature and background knowledge necessary to understand the research work with better perspective. The reader will get a basic understanding about premixed laminar hydrocarbon flames in Chapter 2. Chapter 3 gives a brief outlook of the Swan Band spectra, a familiar emission spectrum frequently encountered with Carbon Radicals in Hydrocarbon Flames. Chapter 3 also discusses the spectroscopic analysis of molecular spectra such as the Swan spectra. Chapter 4 deals with the core physical and quantum mechanical concepts behind spectroscopic thermometry which are required for a thorough understanding of this work. Having laid a basic platform to understand the physical concepts behind the thesis work, Chapter 5 gives a detailed description of the experimental setup and the procedure to capture the emission spectrum from a premixed laminar Bunsen flame. Chapter 6 deals with the theory behind theoretical spectroscopic modelling and the procedure for fitting the experimental spectrum to theoretical spectra to infer useful data from a recorded spectrum. A major portion of this chapter deals with the procedure for usage of BESP and NMT; these are open source software for spectroscopic thermometry, created by a team of researchers at The Center for Laser Applications, University of Tennessee Space Institute (UTSI), Tennessee, United States. The results obtained with regard to the research goals and the inferences from these results are presented in Chapter 7. Finally, Chapter 8 concludes the thesis work by giving a brief overall outlook of the research work performed, highlighting its main contributions and also gives recommendations for potential future research that can prove useful in this area.

Chapter 2. Premixed Laminar Hydrocarbon Bunsen Flame

In this chapter, the structure of a premixed laminar hydrocarbon flame, the various zones such as the cold-gas region, preheat zone, reaction zone and products zone in such a flame are discussed. Further the asymptotic representation of these zones and the divisions within the reaction zone are discussed upon.

2.1 Structure of the Flame

A premixed flame is self-sustaining propagation of a localized combustion zone at subsonic velocities [12], wherein the reactants; the fuel and oxidizer are mixed homogeneously before they reach the reaction front. In gas dynamics, such subsonic travel of a premixed flame is termed deflagration. The flame front propagates with a definite velocity termed flame speed depending on the convection-diffusion balance within the flame structure. When the velocity distribution of the unburnt pre-mixture is laminar, then such a combustion flame is termed premixed laminar flame. In the current study the fuel is methane and the oxidizer is air.

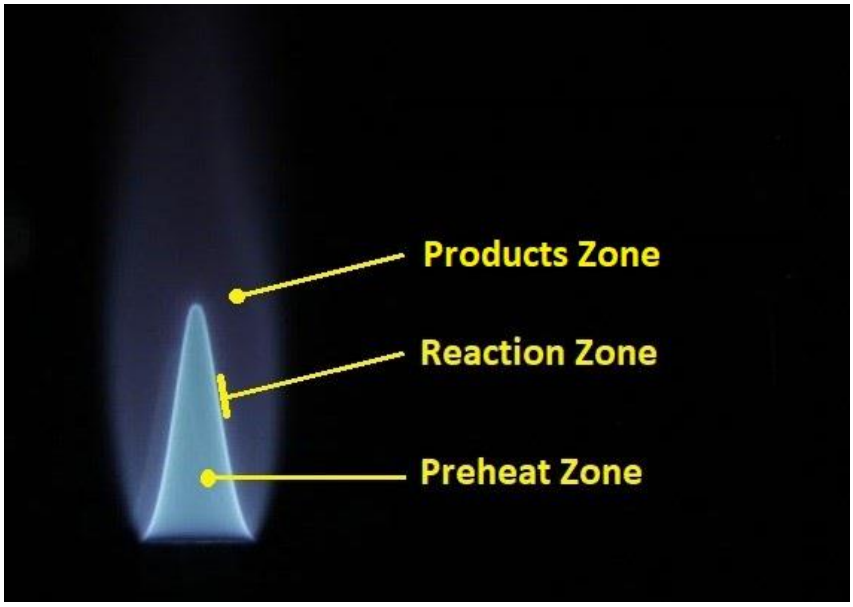

Figure 3: Premixed laminar methane/air Bunsen flame recorded at the Aircraft Power and Propulsion Laboratory, TU Delft. (Equivalence ratio, ϕ=1.25)

A typical Bunsen-burner flame resembles a dual flame as shown in Fig.3 above, there exists a fuel rich premixed inner flame which is surrounded by a pale diffusion flame. The diffusion flame occurs as a result of the CH and OH species from the rich inner flame encountering the ambient air. Zeldovich and Frank-Kamenetzki had formulated the classical asymptotic representation about the structure of a premixed flame in 1938. The asymptotic representation is shown below in Fig.4.

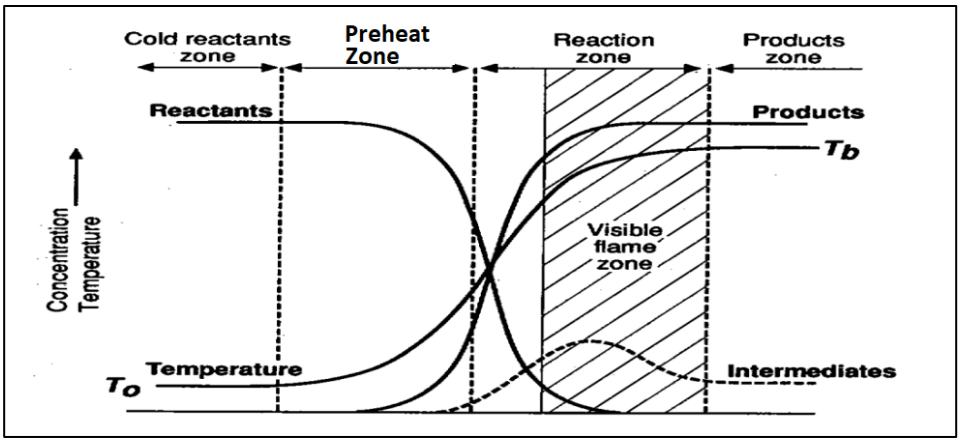

Figure 4: Asymptotic representation of flame zones

A typical premixed laminar Bunsen flame consists of the three major zones as shown in Fig.4

- **The Preheat Zone** is where the unburnt cold reactants enter the combustion zone, here the heat release is almost negligible, the fuel decomposes, and an intermediate radical formation is initiated.
- **The reaction Zone** is the site of all the major reactions, it is very luminous and very thin compared to the other zones. Here the temperature gradient and species concentration gradient is high. Combustion is sustained by the diffusion of heat energy and radicals from the reaction zone to the preheat zone.
- **The Products Zone** is where the end products such as CO_2 and H_2O are formed. The heat energy released here is again negligible as in the preheat zone.

2.2 Thickness of the chemiluminescent zone

The flame reaction zone can be further subdivided into two characteristics zones :

- A fast reaction zone, which is a very thin zone where decomposition reactions of the fuel occur and many intermediates such as the C_2 radicals are created. This region is dominated by bimolecular reactions leading to the formation of CO [13].
- A slow reaction zone, which is a relatively wider zone, which is dominated by recombination reactions of radicals and the final burnout of CO to form CO_2, by the reaction of CO with OH radicals.

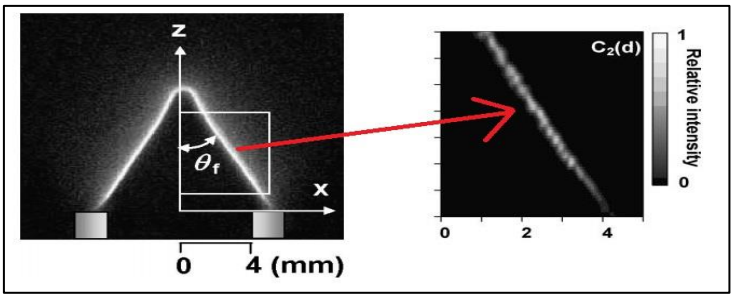

Figure 5: Direct photograph of a CH4–air laminar premixed flame (φ = 1.1). θf is the interior angle between a flame front and z axis. Time-averaged two-dimensional spatial distribution of $C_2(d)$ chemiluminescence in a CH4–air premixed flame (φ = 1.1). The "imaging" area is marked.(enclosed with a white-line square). The intensity for each "image" is normalized by its maximum intensity [13].

The reaction zone appears more bluish in case of lean combustion from excited CH radicals, and more blue-green in case of rich combustion from the C_2 radiations. From both the experimental and simulated results it has been found that the luminous zone thickness of all the radicals is wider in case of fuel-rich combustion and thinner in lean combustion. It is clear that C_2 radical has the thinnest emission zone among the three excited species, with an experimental thickness of about 190 µm at equivalence ratio, φ = 1.1 and 280 µm at φ = 1.5.

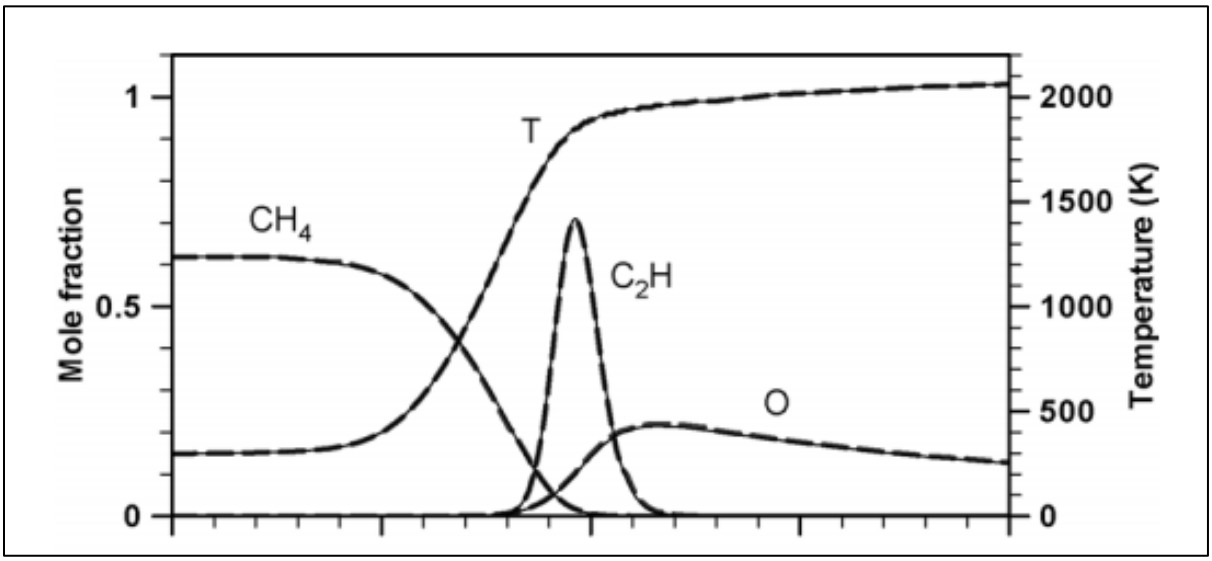

Figure 6: Laminar flame simulation, temperature and species concentrations [13].

Chapter 3. Background on Spectroscopy and the Swan band system

This chapter gives a basic understanding of spectroscopy, chemiluminescence and the Swan band system. Spectroscopy is the scientific study that involves analysis of matter from electromagnetic radiations pertaining to that matter. The main concept behind spectroscopy is resonance and corresponding resonant frequencies. It is based on the phenomenon that matter when energized by any means, might re-emit the energy as electromagnetic radiations. These emitted radiations have a frequency that is a unique characteristic of the species undergoing the energy loss. The amount of energy lost is directly proportional to the number of particles of the species undergoing the transition by going from a higher to a lower energy state. In quantum mechanics, the coupling of two different quantum energy states of an atom/molecule via an oscillatory energy source(example photon) represents the analogous resonance. The energy of a photon is related to its frequency by Planck's law, $E = h\nu$, and so the corresponding spectrum will peak at the resonant frequency. The spectra of different atoms and molecules consists of spectral lines and spectral bands respectively, representing the resonance between two quantum energy levels of their existence.

In the visible range of the spectra emitted by sources containing Carbon, there are several C_2 band systems that have been identified. The strongest among these band systems are the Swan bands identified by William Swan[14], who first studied the spectral analysis of radical Diatomic carbon C_2 in 1856.

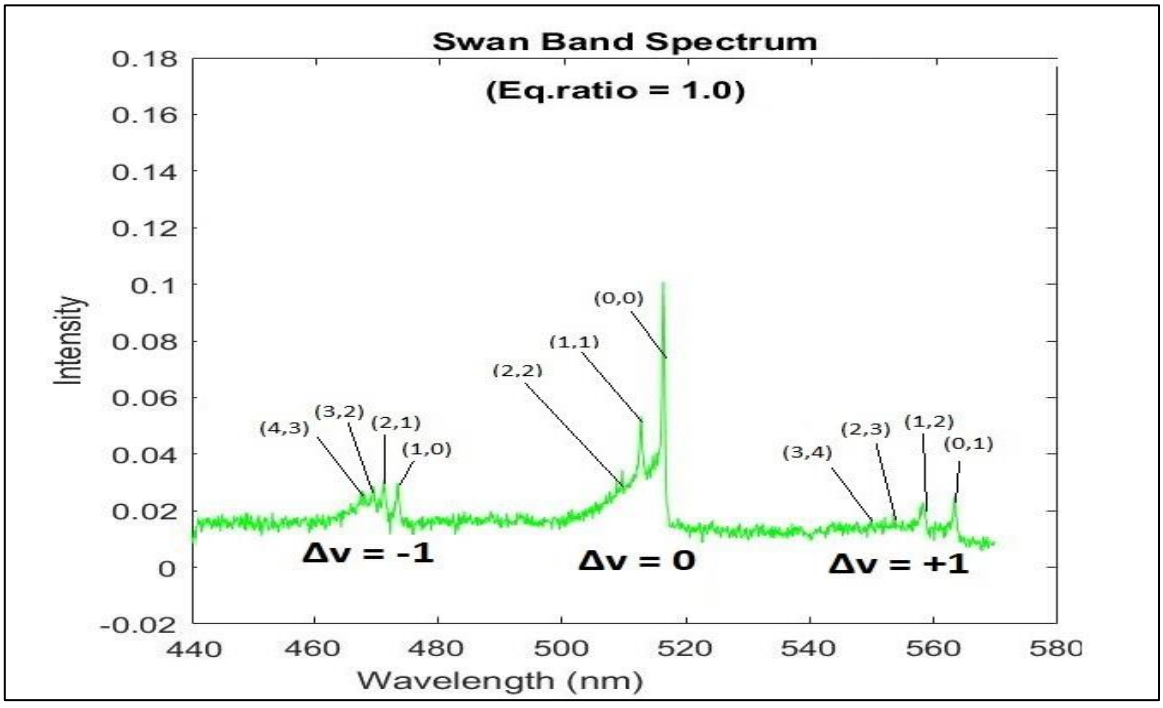

Figure 7: Emission spectrum from the reaction zone of a laminar premixed methane-air flame spectrum of the "Swan bands" captured experimentally.

The swan band spectrum obtained from a point on the reaction zone of a methane-air flame having an equivalence ratio of 1.0 is shown in Fig.7. The Swan band systems, seen between 410-580nm, are frequently encountered with sources containing carbon and they degrade towards the violet region of the spectrum with the band intensity dropping more slowly in that direction, but dropping sharply in the opposite direction. An emission spectrum in the visible wavelength range is emitted by excited C_2* radicals when it returns to a lower state, undergoing an electronic transition. C_2* undergoes many such electronic transitions to form different set of bands such as Philips bands, Bernath Bands, Duck Bands in different processes as shown below in Fig.8; one such electronic transition, namely, the the $d^3\Pi_g \rightarrow a^3\Pi_u$ transition results in the blue-green swan bands observed between 410-580nm wavelength, called the swan band system.

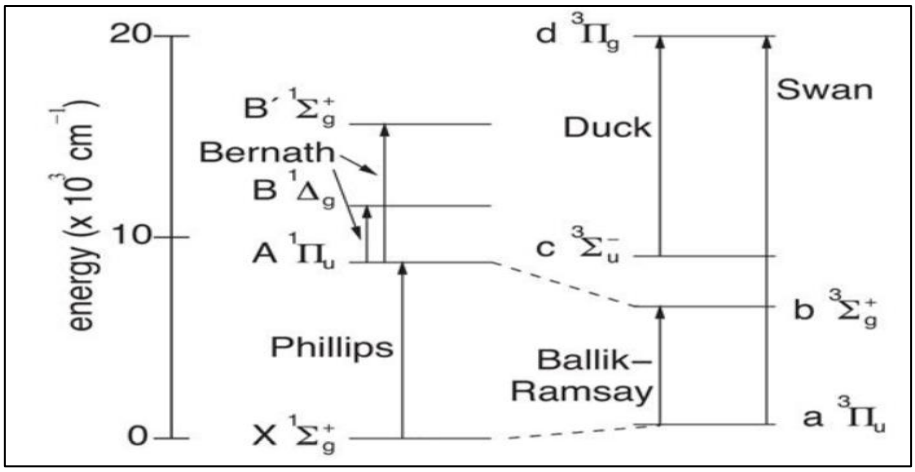

*Figure 8: Several different electronic bands of C_2**

The Swan system has been investigated extensively. The following Fig.9 can be used to explain the swan band transitions in a deeper perspective.

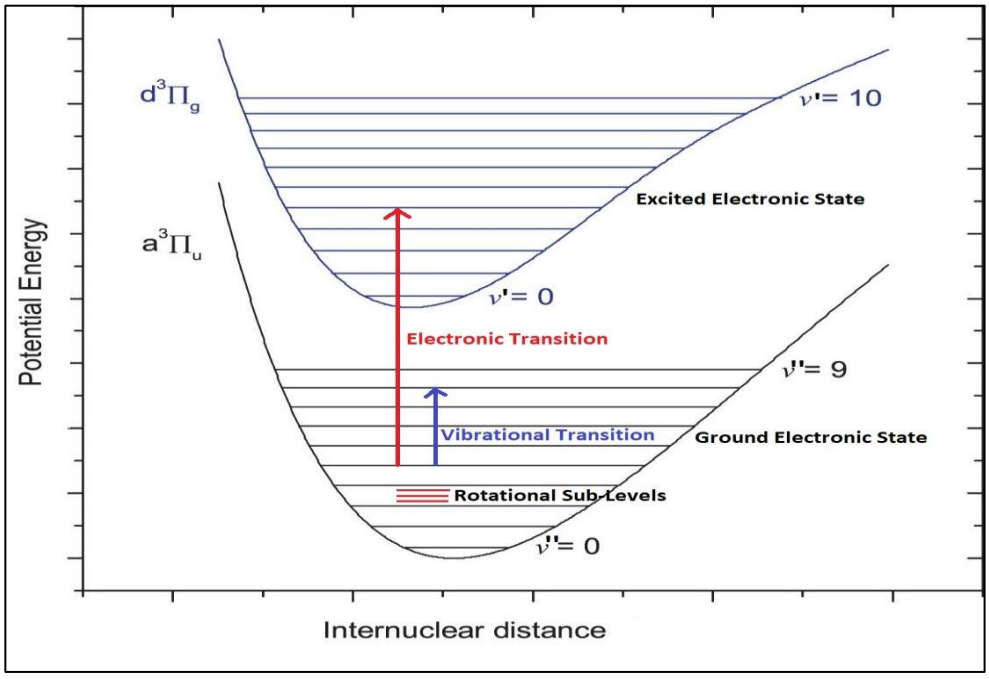

Figure 9: Swan Band Transitions

Each band system pertains to a fixed electronic transition. In case of swan bands, the electronic transition of C_2* from an excited state called $d^3\Pi_g$ to a ground state called $a^3\Pi_u$ is responsible. These transitions results in energy release in the form of electromagnetic radiations, which in case of swan bands lies in the visible green light region of the spectrum. So, each electronic transition is composed of a vibrational and rotational transition as well. For a given band system, the electronic transition is fixed. Every band corresponds to a fixed vibrational level in the upper and lower electronic states. The upper and lower vibrational quantum numbers ν' and ν" involved in the electronic transition, enables us to classify the bands into different progressions and sequences. Among the **progressions**, bands are further classified into ν' progressions and ν" progressions. In the ν' progressions, ν" is a constant having the same lower state post transition; in the ν" progressions, ν' is a constant having the same upper state before transition. **Sequences** on the other hand are formed by transitions having the same Δν, such as Δν = 0, ±1 and +2 bands. For example, Δν = -1 sequence consists of 4 different vibrational transitions as shown in Fig.7. These individual vibrational transitions within a sequence are denoted in round brackets with the initial vibrational state followed by the final vibrational state separated by a comma. The transitions in the Δν = -1 sequence are (4,3), (3,2), (2,1) and (1,0). The following Fig.10 shows different vibrational bands of the C_2 swan band system as recorded on a photographic plate.

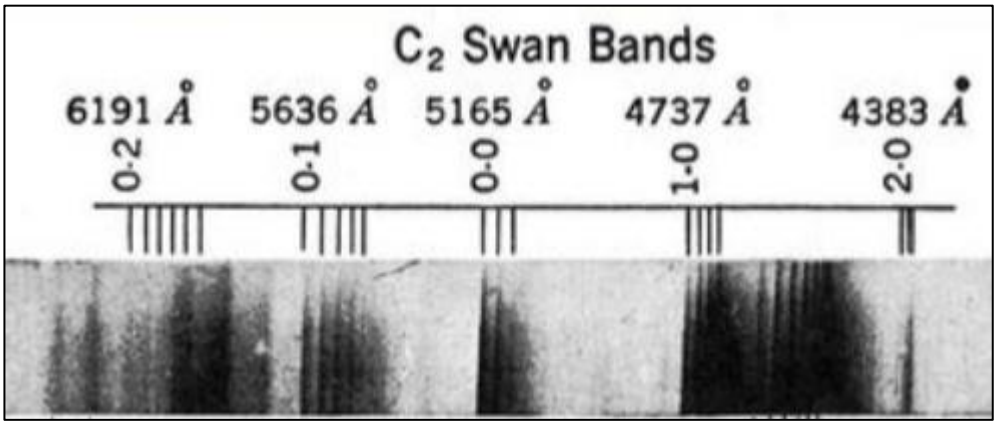

Figure 10: C_2 swan bands recorded on a photographic plate.

Each of these vibrational band heads from individual vibrational transitions are then further resolved into fine lines which indicate the rotational transitions within the corresponding vibrational transition.

3.1 Molecular spectra of diatomic molecules

Swan band emissions are a result of diatomic molecular energy transitions of the C_2 molecule. The molecular energy changes give rise to band spectra, wherein the spectral term of a molecule T, depends on the sum of three terms: the electronic term T_e, the vibrational term T_v and the rotational term T_r.

The general relation between the spectral terms and energy is given by eqn.1 :

$$T = \frac{\nu}{c} = \frac{1}{\lambda} = \frac{E}{hc} \qquad \text{(eq.1)}$$

where, $E = E_e + E_r + E_v$ (eq.2)

Here E_e is the energy of the valence electrons of the molecule, E_r is the energy of rotation of the molecule about a fixed axis and E_v is the energy of vibration of the molecule due to an oscillatory motion. Eqn.2 does not include the translational energy of the molecule E_t as a part of the total energy of the molecule because it is not quantized, and it is not directly involved in the transition frequencies. From wave mechanics, it has been justified by the Born-Oppenheimer approximation [17] that the total energy is divisible into electronic, vibrational and rotational energies. The total energy emitted in a transition can be given by :

$$E = [T_{el} + G(\nu) + F_\nu(J)] * h * c \qquad \text{(eq.3)}$$

where T_{el} , $G(\nu)$ and $F(J)$ are the electronic, vibrational and rotational spectral terms. The following sections explain the meaning and derivation of these spectral terms in detail.

3.1.1 Rotational spectroscopy

Consider a diatomic molecule such as the C_2 molecule, whose two nuclei are at a fixed distance(rigid rotor), and assume their electronic angular momentum is absent. Its rotational energy is given by the following equation [18] :

$$E_r = \frac{1}{2}\frac{R^2}{I} \qquad \text{(eq.4)}$$

where **R** is the angular momentum of the molecule taken parallel to the axis of rotation and *I* is the moment of inertia of the diatomic system. Now, the angular momentum **R** is quantized to make it valid in the quantum world:

$$\text{length of vector } \mathbf{R} = R = \sqrt{J(J+1)}\frac{h}{2\pi} \qquad \text{(eq.5)}$$

where J is an integer positive number or null. Now, substituting eqn.5 in 4 yields the term for rotational energy as:

$$E_r = \frac{h^2}{8I\pi^2}J(J+1) \qquad \text{(eq.6)}$$

Now these are the rotational energy levels of a diatomic molecule in state $^1\Sigma_0$. The rotation terms can be written as a function of J:

$$F(J) = \frac{E_r}{hc} = \frac{h}{8Ic\pi^2}J(J+1) \qquad \text{(eq.7)}$$

$$F(J) = BJ(J+1) \qquad \text{(eq.8)}$$

$$B = \frac{h}{8Ic\pi^2} \qquad \text{(eq.9)}$$

where B is called the rotational constant. When the effect of centrifugal stretching is taken into account the rotational constant is expressed as *B - DJ(J+1)*, where D is another constant which is about six orders of magnitude smaller compared to B; making B a decreasing function as J increases. Centrifugal stretching happens because the molecule is not a rigid rotor, the internuclear distance *r* increases due to the centrifugal effect of rotation, which increases when the speed of rotation increases, in other words when J increases. This explains the reason why the rotation spectrum is not perfectly equidistant, *B* diminishes with increasing *J*. Example of rotational spectra is shown in Fig.11.

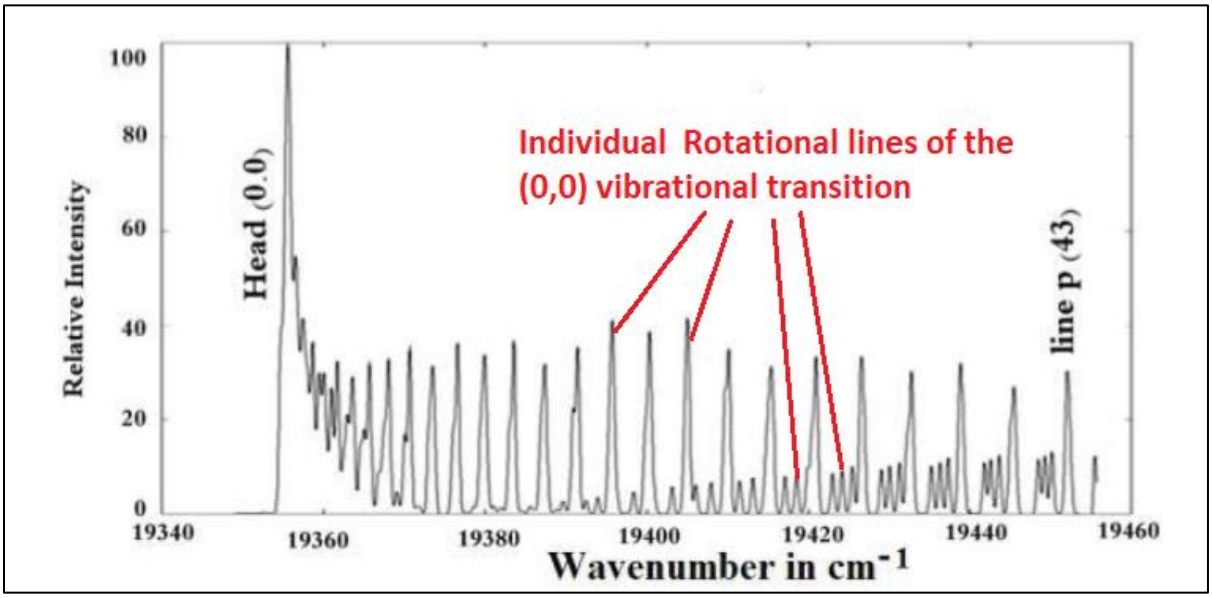

Figure 11: The rotational emission spectrum resolved finely showing individual rotational lines of C_2(0,0) transition [15].

3.1.2 Vibrational spectroscopy

Consider a diatomic molecule with atomic masses m_1 and m_2. Let the molecule have no rotational movement [18] and only the vibrational movement is taken into account. Let r_e be the equilibrium internuclear distance. When the molecule undergoes vibration, the internuclear distance becomes r and a restoring force F brings it back to the equilibrium distance r_e.

$$F = -k(r - r_e) \qquad \text{(eq.10)}$$

The oscillation frequency of the Vibrational movement is given by :

$$\nu_{osc} = \frac{1}{2\pi}\sqrt{(\frac{1}{m_1} + \frac{1}{m_2})k} \qquad \text{(eq.11)}$$

The quantized Vibrational energy levels, which is the sum of the Kinetic and Potential energies of the vibrating diatomic molecule is given by:

$$E_v = h\nu_{osc}(v + \frac{1}{2}) \qquad \text{(eq.12)}$$

where v is the vibrational quantum number. Here, even at the lowest vibrational level, $v = 0$, the molecule possesses a non-null energy:

$$E_0 = \frac{1}{2}h\nu_{osc} \qquad \text{(eq.13)}$$

The vibrational spectral terms of the harmonic oscillator can be written as:

$$G(v) = \frac{E_v}{hc} = \frac{\nu_{osc}}{c}\left(v + \frac{1}{2}\right) = \omega_e\left(v + \frac{1}{2}\right) \qquad \text{(eq.14)}$$

where, $\omega_e = \frac{\nu_{osc}}{c}$ is the wave number related to the classic vibrational frequency. Transitions between these energy levels are governed by the selection rule, $\Delta v = \pm 1$. If v' and v", which correspond to the upper and lower levels, be it absorption or emission, then the only allowed transition is v' - v" = 1. The wave number of the absorbed or emitted radiation is written as:

$\sigma = G(v') - G(v) = \omega_e(v' - v")$ and $\Delta v = \pm 1$ always, so:

$\sigma = \omega_e$ (eq.15)

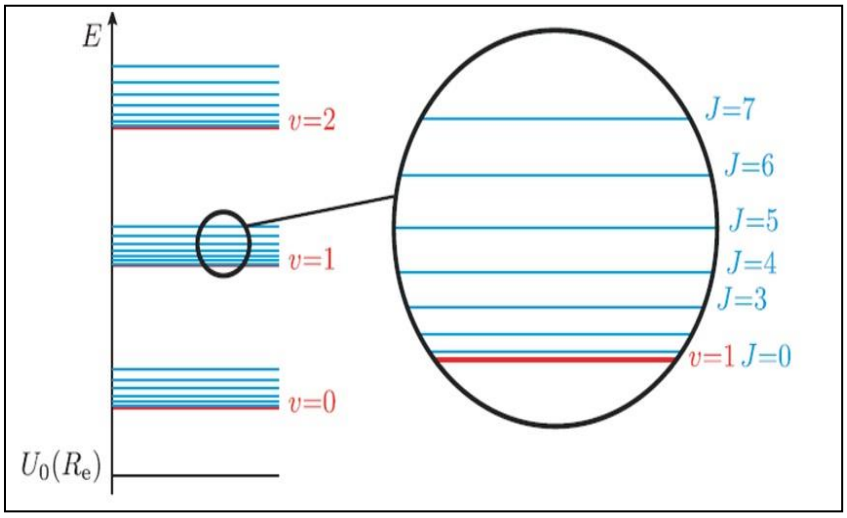

Figure 12: Schematic of the rovibronic energy levels of a diatomic molecule [20].

Hence there is a strong vibrational line formed at $\sigma = \omega_e$, usually seen in the infrared region, predicted by the theory of harmonic oscillator. When investigated experimentally more lines of decreasing intensity are seen at $2\omega_e$, $3\omega_e$, $4\omega_e$ and so on; these lines are known as the overtones of the vibrational line ω_e, which shows the ideal harmonic oscillator approximation is inaccurate. Each of these lines is composed of a large number of finer lines (as shown in Fig.12) which can be attributed to superposition of rotational transitions on the vibrational transitions, formed by "rovibronic" energy levels [20].

3.1.3 Morse potential curve - the Anharmonic oscillator

The curve of potential energy Vs Internuclear distance is not a perfect parabola, the oscillator is said to be anharmonic. The Morse potential, named after physicist Philip M. Morse [21], is a convenient interatomic interaction model for the potential energy of a diatomic molecule. As shown in the Fig.13, in the Morse curve the energy levels are unequally spaced as the energy approaches the dissociation energy, which is contrary to the evenly spaced energy levels in a harmonic oscillator. As r decreases from r_e, the potential energy increases with a steeper slope on the left side of the Morse curve, because the nuclei are impenetrable and the internuclear distance cannot become zero. Conversely, when the nuclei are pulled away from each other, as the internuclear distance increases, the potential energy increases, with a relatively gradual slope, then at a point when the energy approaches the dissociation energy D_e the molecule dissociates into atoms. The dissociation energy D_e required is marginally greater than the true energy necessary for the molecular dissociation due to the zero-point energy D_0, of the lowest (ν = 0) vibrational level, as inferred from eqn.13.

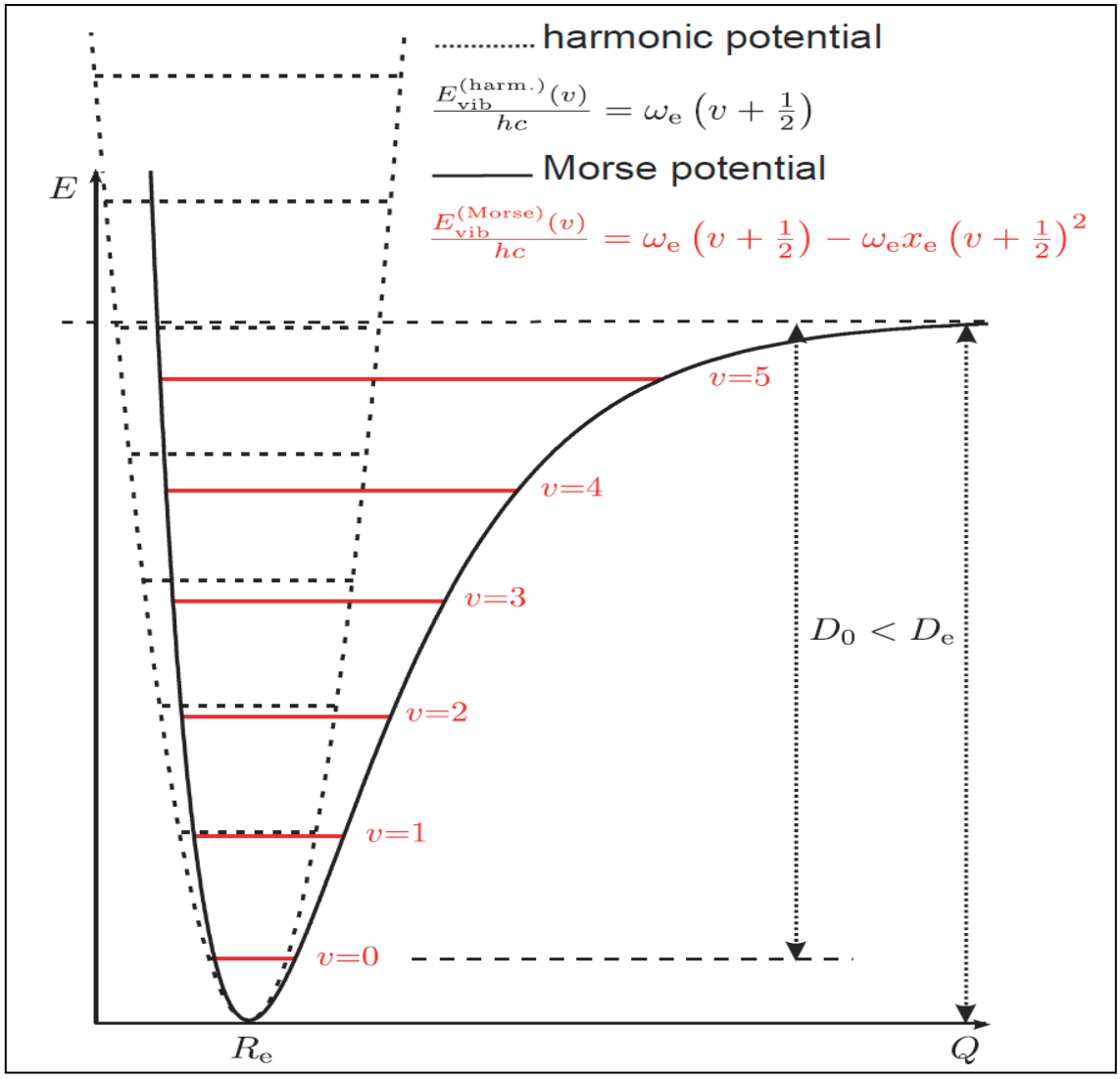

Figure 13: Comparison of the Morse potential and its vibrational eigenstates with those of a harmonic potential [21].

The potential energy of an anharmonic oscillator represented by the Morse function [21] is given by:

$$V = D_e(1 - \exp[-\beta(r - r_e)])^2 \qquad \text{(eq.16)}$$

where β is a constant given by:

$$\beta = \omega_e\sqrt{\frac{2\pi^2 c\mu}{hD_e}} \qquad \text{(eq.17)}$$

The vibrational energy levels hence formed [17] are:

$$E = hc\omega_e\left(v + \frac{1}{2}\right) - hcx_e\omega_e(v + 1/2)^2 \qquad \text{(eq.18)}$$

So, the vibrational spectral terms become:

$$G(v) = \frac{E}{hc} = \omega_e\left(v + \frac{1}{2}\right) - x_e\omega_e\left(v + \frac{1}{2}\right)^2 \qquad \text{(eq.19)}$$

where, $x_e\omega_e\left(v + \frac{1}{2}\right)^2$ is a corrective term to represent the Morse potential, which makes the energy levels to be unequally spaced as the energy approaches the dissociation energy, contrary to the evenly spaced energy levels in a harmonic oscillator.

3.1.4 The interaction of molecular rotation and vibration

When the fine structure of the molecular spectral bands are resolved, it can be seen that, the structure accounts for both vibration energy and rotation energy simultaneously, there is nothing known to exist as pure vibrational motion. The energy levels of such a system expressed as a 'vibrating rotator' have been diligently calculated and formulated by Dunham [22]. The vibrational frequency($c\omega_e$) is always much higher compared to the rotational frequency(*2BcJ*). By the time a molecule undergoes one rotation, it has undergone numerous vibrations, thus the internuclear distance *r* has varied numerous times between the limits of the Morse potential curve. The rotational constant ($B = \frac{h}{8Ic\pi^2}$) is no longer a constant because the moment of inertia *I* varies numerous times in a single rotation due to the periodical change in *r*, so B is averaged as B_v, this value B_v decreases as the vibrational energy increases, more precisely, as the vibrational quantum number v increases(as v increases, the limits of *r* increases as we move upwards in the Morse curve, hence moment of inertia I increases, and so B decreases). This can be written as:

$$B_v = B_e - \alpha_e\left(v + \frac{1}{2}\right) + \gamma_e\left(v + \frac{1}{2}\right)^2 - \cdots \text{(eq.20)}$$

here B_e would be the rotational constant of a non-rotating molecule and α_e, γ_e… are rotational constants. Similarly, the centrifugal constant D is replaced by D_v after averaging the same way:

$$D_v = D_e - \beta_e \left(v + \frac{1}{2}\right) + \ldots \qquad \text{(eq.21)}$$

Consequently, the rotational term of the 'vibrating rotator' becomes:

$$F_v(J) = B_v J(J+1) - D_v J^2 (J+1)^2 \qquad \text{(eq.22)}$$

This variation of $F_v(J)$ with the vibrational quantum number through rotational constants dependent on vibrational quantum numbers, expresses the rotation-vibration interaction. The constants used to compute B_v and D_v: α_e, D_e and β_e are given by Pekeris' relation [23], Kratzer's relation [24] and Dunham's relation [22].

The energies of rotation are so much smaller than those of vibrational or electronic excitations of a molecule, molecular rotation shows up in molecular spectra as a fine-structure splitting of the spectral lines. When the fine structure is not resolved, the spectrum appears as bands. Close inspection of these bands reveals that they have a fine structure due to the rotational energy levels as shown in Fig.11. [25]. All allowed transitions (v', J') ↔ (v", J") between two rotational-vibrational levels in the same electronic state for v' ≠ v", will have the vibrational-rotational spectrum of the molecule in the infrared spectral region between λ = 2−20μm. For v' = v" there are pure rotational transitions between rotational levels within the same vibrational state, which form the rotational spectrum. [26].

It is also to be noted that Homonuclear diatomic molecules have no dipole allowed vibrational-rotational spectra since the electric dipole moment of these molecules is zero. This means they do not absorb or emit radiation on transitions within the same electronic state. They may have very weak quadrupole transitions. The molecules N_2 and O_2, which represent the major constituents of our atmosphere, cannot absorb the infrared radiation emitted by the earth. Other molecules, such as CO_2, H_2O and CH_4 do have an electric dipole moment and absorb infrared rad

3.1.5 Electronic spectroscopy

The electronic spectrum consists of a system of vibrational bands. Each vibrational band includes many rotational lines. Only rotational transitions with ΔJ = 0; ±1 are allowed. The intensity of a rotational transition depends on the Ho¨nl-London factors giving a dependence on the rotational quantum numbers [28]. In case of the different vibrational bands, the intensities are determined by the intrinsic strength of electronic transitions, population of the vibrational levels and the square of the two vibrational wavefunctions overlap integral which is expressed as Franck-Condon factors based on the Frank-Condon Principle [29].

The total energy of a molecular level can be written as the sum $E = E_{el} + E_{vib} + E_{rot}$; this approximation, called the adiabatic or Born–Oppenheimer approximation [17], neglects the coupling between nuclear rotation and electron motion. It accounts for the orbital and spin angular momenta, **L** and **S**, through their projections **Λ** and **Σ** on the internuclear axis.

When the electronic state of a molecule changes, its basic architecture changes largely; the equilibrium internuclear distance r_e changes and the elastic force constant k also changes. So the vibrational constants $\omega_e x_e$, y_e…, which are used to define the vibrational energy will vary with the change in electronic states. Consequently, the rotational constants B_v and D_v, which depend on the vibrational quantum number v will also change with a change in the electronic states. The electronic spectral term T_e corresponding to the electronic energy E_{el} ($T_e = E_{el}/hc$) is summed up with the vibrational and rotational terms discussed previously to give the molecular term T [18].

$$T = T_e + G(v) + F_v(J) \qquad \text{(eq.23)}$$

When a molecule undergoes transition from one state to another, its wave number of emission or absorption is given by:

$$\sigma = T' - T'' = [T_e' + G'(v') + F_{v'}(J')] - [T_e'' + G''(v'') + F_{v''}(J'')] \qquad \text{(eq.24)}$$

$$\text{which implies, } \sigma = [T_e' - T_e''] + [G'(v') - G''(v'')] + [F_{v''}(J'') - F_{v''}(J'')] \qquad \text{(eq.25)}$$

In these equations., the single apostrophe is assigned to represent the upper energy state and the double apostrophe is used to represent the lower energy state.

3.2 Frank Condon principle

To explain the theory behind the intensity pattern of the bands formed in the C_2 emission spectrum the Frank Condon Principle is necessary. The intensity of the vibrational band structure in an electronic transition is governed by the Frank-Condon factors. In an electronic transition, the time interval for the emission or absorption of a photon is very small compared to the time interval taken to complete a vibrational movement, which implies that the internuclear distance r remains unchanged before and after the transition. Since the internuclear distance remains unchanged, in the potential energy diagram the transition is represented by a straight vertical line from a one electronic state to the other.

By the IUPAC Compendium of Chemical Terminology:

"Classically, the Franck–Condon principle is the approximation that an electronic transition is most likely to occur without changes in the positions of the nuclei in the molecular entity and its environment. The resulting state is called a Franck–Condon state, and the transition involved, a vertical transition. The quantum mechanical formulation of this principle is that the intensity of a vibrionic transition is proportional to the square of the

overlap integral between the vibrational wavefunctions of the two states that are involved in the transition."

Hence the intensity of the bands formed is directly proportional to degree of overlap between the initial and final vibrational wave functions. The favoured vibrational transitions in a given electronic transition are those wherein the change in the equilibrium internuclear distance is minimal as shown in Fig.14 [29].

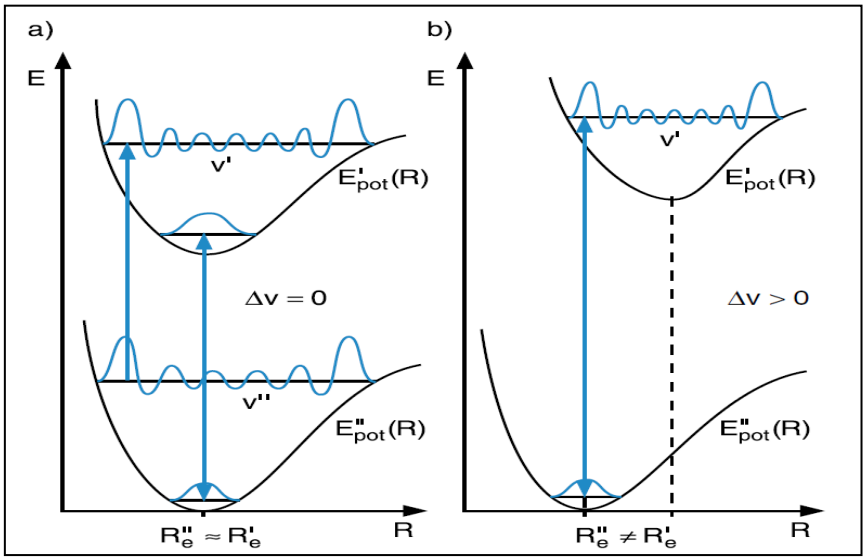

Figure 14: Illustration of the Franck-Condon principle for vertical transitions with Δv = 0 (a) and (b)Δv> 0 in case of potential curves with R"e = R'e and R"e<R'e [26].

As mentioned earlier, the quantum mechanical formulation of the Frank-Condon principle is that the intensity of a vibrionic transition is proportional to the square of the overlap integral between the vibrational wavefunctions of the two states, $\Psi_{V'}$ and $\Psi_{V''}$ that are involved in the electronic transition is depicted in Fig.15 shown below.

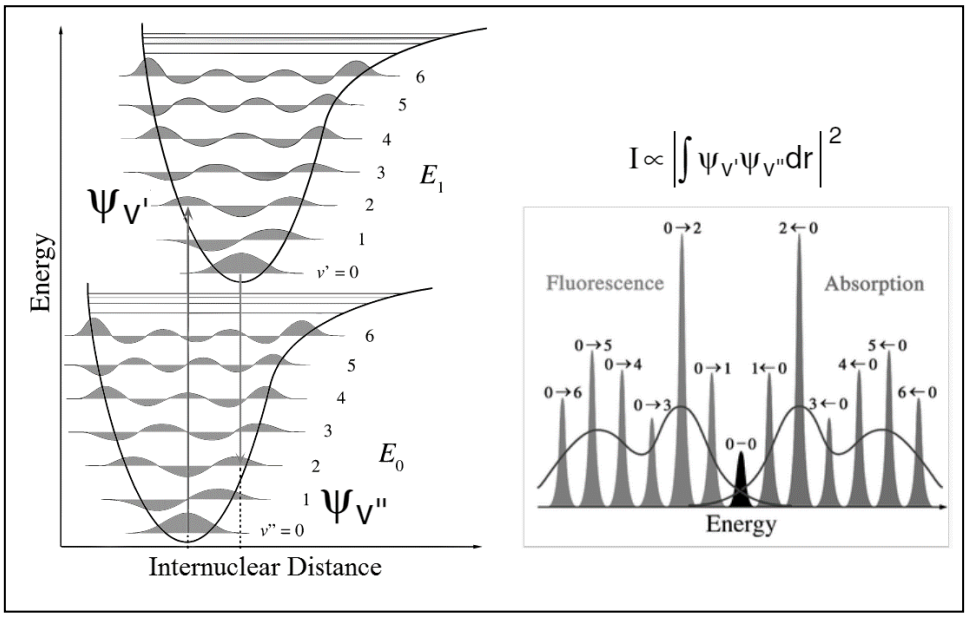

Figure 15: Vibrational overlap of wave functions and the corresponding line intensities obtained by the Franck-Condon Principle [31].

Chapter 4. Background on the Boltzmann Law and Spectroscopic Thermometry

The Boltzmann Law is the basic principle behind the technique of spectroscopic thermometry; in this chapter the Boltzmann law is discussed in detail. Then the method in which the law is applied to diatomic molecules such as C_2 for spectroscopic determination of the vibrational and rotational temperature of a system in equilibrium is discussed in the later sections. The other necessary parameters in this procedure, such as Einstein's coefficients and Oscillator Strengths are also discussed upon.

4.1 The Boltzmann Law

Ludwig Boltzmann, in 1898 formulated the now familiar 'Boltzmann Distribution' in his research paper “On the Relationship between the Second Fundamental Theorem of the Mechanical Theory of Heat and Probability Calculations Regarding the Conditions for Thermal Equilibrium." when he was researching about statistical mechanics of gases in thermal equilibrium. The modern common "Boltzmann Distribution" is a refined adaptation after a deeper investigation by Gibbs in 1902. The Boltzmann law holds valid in a state of thermal equilibrium; it states that when a system attains thermal equilibrium at absolute temperature T, the average number of particles of a given chemical species n_i and n_j with energies E_i and E_j respectively, are present in the ratio

$$\frac{n_i}{n_j} = \exp\left[\frac{-(E_i - E_j)}{kT}\right] \qquad \text{(eq.26)}$$

where k is the Boltzmann Constant. One more important criterion for the law to be valid is that the energy levels under consideration in the equation have to be non-degenerate [16]; they should not possess the same energies. If the sublevels of an atom/molecule is non-degenerate, then eqn.26 holds true and consequently if the sublevels belong to the same energy level then they are equally populated. So, if $E_i = E_j$, then, $n_i = n_j$. If the energy level E_i is deemed to have g_i sublevels, then the number of particles in the energy level E_i is given by:

$$N_i = g_i n_i \qquad \text{(eq.27)}$$

and here, by statistical mechanics, g_i is termed as the statistical weight of the energy level E_i. Hence, the ratio of populations of N_i and N_j pertaining to two different energy levels E_i and E_j is written as:

$$\frac{N_i}{N_j} = \frac{g_i n_i}{g_j n_j} = \frac{g_i}{g_j}\left\{\exp\left[\frac{-(E_i - E_j)}{kT}\right]\right\} \qquad \text{(eq.28)}$$

Another form of expressing eqn.28 to relate the total number(N) of particles of the species considered, belonging to all energy levels is:

$$\frac{N_i}{N} = \left[\frac{g_i\left\{\exp\left(-\frac{E_i}{kT}\right)\right\}}{\sum_j g_j\left\{\exp\left(-\frac{E_j}{kT}\right)\right\}}\right] \quad \text{(eq.29)}$$

where, $\left[\sum_j g_j\left\{\exp\left(-\frac{E_j}{kT}\right)\right\}\right]$ is termed as the partition function, Q.

4.1.1 Application of the Boltzmann law to diatomic molecules

For practical applications of the Boltzmann law, only the relative populations are exploited:

- If the population of a given rotational energy level relative to the population of all the rotational levels belonging to the same vibrational and electronic state is taken into consideration, then such a distribution is termed *rotational distribution.*
- If the population of a given vibrational energy level relative to the population of all the vibrational levels belonging to the same electronic state is taken into consideration, then such a distribution is termed *vibrational distribution.*

4.1.2 Rotational distribution

When eqn.29 is applied only to rotational energies E_r = hcF(J) for Hund's case (a) or (c), as discussed in [32] wherein the nuclear spins are not taken into account, which is the case for heteronuclear molecules, then rotational distribution law between the population N' of rotational level J' and the whole population N pertaining to all the rotational levels in the same vibrational and electronic state is written as :

$$\frac{N'}{N} = \left[\frac{(2J'+1)\left\{\exp\left(-\frac{hcF(J')}{kT}\right)\right\}}{\sum(2J+1)\left\{\exp\left(-\frac{hcF(J)}{kT}\right)\right\}}\right] \quad \text{(eq.30)}$$

where 2J+1 is the statistical weight g_i for heteronuclear molecules. In case of homonuclear molecules the statistical weights also involve the nuclear spin I by a factor I(2I+1) or (I+1)(2I+1) depending on the parity of J, which in turn depends on the symmetry properties of the nuclear wave functions. [18]

4.1.3 Vibrational distribution

When eqn.29 is applied only to vibrational energies E_v = $hcG_0(v)$, where $G_0(v)$ is vibrational spectral term, then vibrational distribution law between the population N' of rotational level J' and the whole population N pertaining to all the rotational levels in the same vibrational and electronic state is written as :

$$\frac{N'}{N} = \left[\frac{\left\{\exp\left(-\frac{hcG_0(v)}{kT}\right)\right\}}{\sum_v\left\{\exp\left(-\frac{hcG_0(v)}{kT}\right)\right\}}\right] \quad \text{(eq.31)}$$

Here the statistical weights are g = 1, for all vibrational levels, since the vibrational levels of a diatomic molecule are never degenerate.

4.2 Intensity and shape of spectral lines

The presence of a well-defined relationship between number of particles involved in emission of radiation and the intensity of these radiations forms the basis of the spectral quantitative analytical procedure. The number of particles *N* which give out emissions is a function of the initial concentration *c* of the species involved.

$$N = g(c);$$

Consequently, the intensity of the radiation *I* emitted is a function of the number of particles N of the species involved in the emission process.

$$I = f(N).$$

4.2.1 Einstein Coefficients and Oscillator strengths

Consider an unit volume of a gas undergoing spontaneous emissions, which consists of N_i atoms or molecules in an excited energy state E_i. Let $dN_{i\to j}$ be the number of molecules undergoing transition from E_i to a lower energy state E_j in unit time. This transition happens through an emission of an equal number of photons of frequency $\nu_{ij} = (E_i - E_j)/h$. The number of molecules undergoing emission per unit time is proportional to the population of molecules present in the initial state:

$dN_{i\to j} \propto N_i$;

So,

$$dN_{i\to j} = A_{ij} N_i dt \qquad \text{(eq.32)}$$

The constant of proportionality A_{ij}, which accounts for the probability of a transition to occur with photon emission, termed *Einstein transition probability of spontaneous emission* was put forward by Einstein [33]. The intensity of the emission hence produced I_{em} is the energy emitted per unit time. The energy of a single photon is $h\nu$, and so the intensity of the is given by:

$$I = h\nu dN_{i\to j} = A_{ij} N_i h\nu \qquad \text{(eq.33)}$$

Consequently, when an electromagnetic radiation of frequency ν is passed through a medium having a spectral volume density ρ(ν), some of the molecules in the lower energy level undergo a transition from a lower energy state to a higher energy state by absorbing the radiation. The no of molecules undergoing transition $dN_{j\to i}$ is directly proportional to the

spectral volume density of the medium and the total number of molecules in the lower energy state N_j.

$$dN_{j\to i} = B_{ji} N_j \rho(\nu) \qquad \text{(eq.34)}$$

where the constant of proportionality B_{ji} is called *Einstein transition probability of absorption*. But as an implication of the principle of detailed balance that at equilibrium: the rate of excitation of particles of a species A by collisions with particles of a species B is equal to the rate of deactivation of particles A by collisions with particles B, an emission is stimulated by the incident radiation. This phenomenon gives rise to a third coefficient B_{ij}, *Einstein transition probability of stimulated emission.* The number of atoms or molecules $dN'_{i\to j}$ undergoing transitions from E_i to state E_j due to stimulation by incident radiation is given by:

$$dN'_{i\to j} = B_{ij} N_i \rho(\nu) \qquad \text{(eq.35)}$$

Now the effective number of photons lost by absorption is $(dN_{j\to i} - dN'_{i\to j})$, and the fraction of energy absorbed by the medium is:

$$\frac{dI}{I_0} = \frac{h\nu}{c}(B_{ji} N_j - B_{ij} N_i) \qquad \text{(eq.36)}$$

The knowledge of the Einstein transition-probability coefficients of spontaneous emission for vibration-rotation transitions plays a crucial role in the determination of the internal energy distribution of the products of chemical reactions as measured by chemiluminescence spectroscopy [34]. Fig.16 depicts the coefficients involved in different processes.

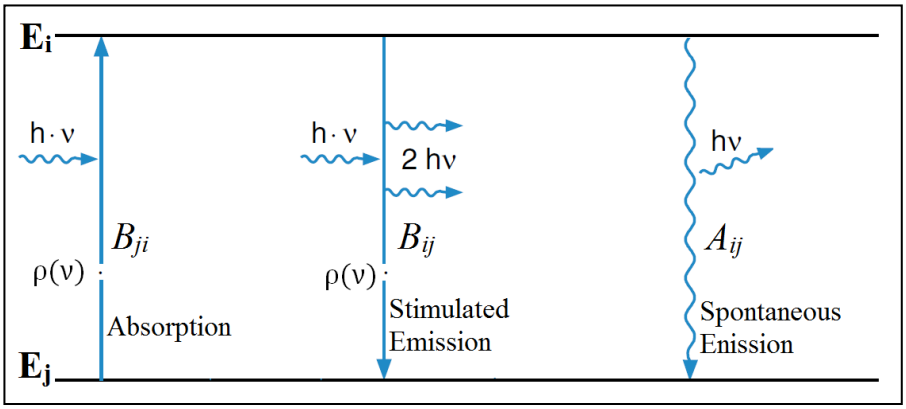

Figure 16: Depiction of Einstein Coefficients involved in different processes.

These Einstein coefficients A_{ij}, B_{ij} and B_{ji} are only dependent on the properties of molecules and not on the temperature or pressure of the system composed of the molecules. These coefficients are computed by the wave function of the involved states. They are also dependent on the statistical weight of the upper energy level and the strength of line S_{ij}.

$$A_{ij} = \frac{64\pi^2\nu^3}{3hc} . \frac{S_{ij}}{g_i} \qquad \text{(eq.37)}$$

Oscillator strength is a dimensionless quantity that expresses the probability of absorption or emission of electromagnetic radiation in transitions between energy levels of an atom or a molecule [35]. The intensity of an emission line involves this number termed oscillator strength, *f*. It is related to the Einstein transition probability coefficient by the relation:

$$A_{ij} = \frac{8\pi^2 e^2}{\lambda^2 mc} . f_{ij} \qquad \text{(eq.38)}$$

where λ is the wavelength of the radiation emitted when the atom/molecule undergoes transition from state i to j, e is the charge of an electron and m is the mass of an electron. In case of molecules, the transition probability, also called line strength in some research papers, can be approximated by the Born-Oppenheimer approximation as a product of three factors corresponding to a particular kind of transition: $N' \rightarrow N''$, $v' \rightarrow v''$, $m \rightarrow n$ resulting from rotational, vibrational and electronic transitions respectively. The resulting transition probability is given as:

$$A_{ij} = C\nu^3 . a_{N'N''} . a_{v'v''} . a_{mn} \qquad \text{(eq.39)}$$

where C is a constant factor. Substituting eqn.38 in eqn.33, intensity of emission is given by:

$$I_{em} = \frac{8\pi^2 e^2 h}{\lambda^3 m} . N_i f_{ij} \qquad \text{(eq.40)}$$

For all practical calculations, stimulated emissions could be ignored when compared to spontaneous emissions. For instance, at thermal equilibrium at 2500K, there is only one stimulated emission for every 22,000 spontaneous emissions. This is a common practice applicable to combustion flame temperatures and analysis in the visible or UV spectrum.

4.3 Spectroscopic determination of temperature

The thermodynamic temperature of a system is a measure of the average energy of the translational, vibrational, and rotational motions of the constituents of that system, which is a parameter which gives a definitive distribution of states among various energy levels. Only when all the degrees of freedom are equilibrated, it becomes strictly meaningful. Very often the degrees of freedom in a molecular system is separated into translational, electronic, vibrational and rotational with their corresponding temperature values. At equilibrium, each degree of freedom will have on average the same energy unless that degree of freedom is in the quantum regime. In most of the cases the thermodynamic temperature is specified by the average translational kinetic energy of the particles referred to as kinetic temperature. Rotations and translations take very few collisions to exchange energy and establish a state of local thermal equilibrium, and so they are often treated as having the same temperature. Due

to the larger amounts of energy exchanged vibrations take longer to equilibrate thermally with the rotations and translations, and so they are often tagged separately as vibrational temperature.

4.3.1 Spectroscopic determination of rotational temperatures

Rotational Temperatures are inferred from the rotational distribution of molecules. The temperature is deduced from the relative intensity of the rotational lines of the same vibrational band in a given vibrational and electronic state, which is a reflection of the relative populations present in different rotational levels. The following equation is used in general in the line-ratio method [36] or iso-intensity method for determination of population temperatures:

$$\ln\left[\frac{I_1}{A_1\nu_1 g_1}\right] - \ln\left[\frac{I_2}{A_2\nu_2 g_2}\right] = \frac{-(E_1-E_2)}{kT} \qquad \text{(eq.41)}$$

where the subscript 1 and 2 refers to two different lines, *A* is the transition probability, *ν* is the frequency and *g* is the statistical weight.

In case of rotational temperature T_r measurement, the general equations for rotational distribution and eqn.39 substituted in eqn.41 gives eqn.42. Here, in A_1 and A_2, the vibrational and electronic transition probabilities $a_{v'\to v''}$ and $a_{m\to n}$ cancel out since they are the same between the two transitions.

$$\ln\left[\frac{I_1}{a_1\nu_1^4(2N_1'+1)}\right] - \ln\left[\frac{I_2}{a_2\nu_2^4(2N_2'+1)}\right] = \frac{BN_2'(N_2'+1)-BN_1'(N_1'+1)}{kT} = constant \qquad \text{(eq.42)}$$

$$\text{which implies:} \quad \ln\left[\frac{I}{a\nu^4(N'+1)}\right] = -BN'(N'+1).\left(\frac{1}{kT}\right) + constant \qquad \text{(eq.43)}$$

Hence, from a set of rotational lines of a band, a plot of $\ln[I/(a\nu^4(2N'+1))]$ versus $BN'(N'+1)$ renders a straight line of slope (-1/kT) and so the rotational temperature is deduced from its slope. An experimental comparison of rotational temperatures determined from optical emission spectroscopy (OES) with the gas kinetic temperature is shown in Fig.17 [37]

4.3.2 Spectroscopic determination of vibrational temperature

A vibrational temperature can be inferred by the application of eqn.41 to different bands of a system for a given electronic state. When bands are not resolved well enough, the band heads are exploited in the determination process, with a compromise in accuracy [16]. The equation to determine vibrational temperature can be expressed as follows:

$$\ln\left[\frac{I}{g\nu^4 a_r a_v}\right] + \frac{E_r}{kT_r} + \frac{E_v}{kT_v} = constant \qquad \text{(eq.44)}$$

Here, a_r and a_v are rotational and vibrational transition probabilities respectively. The slope of the line($-1/kT_v$) plotted from eqn.44 is used to deduce the vibrational temperature from the emission spectrum.

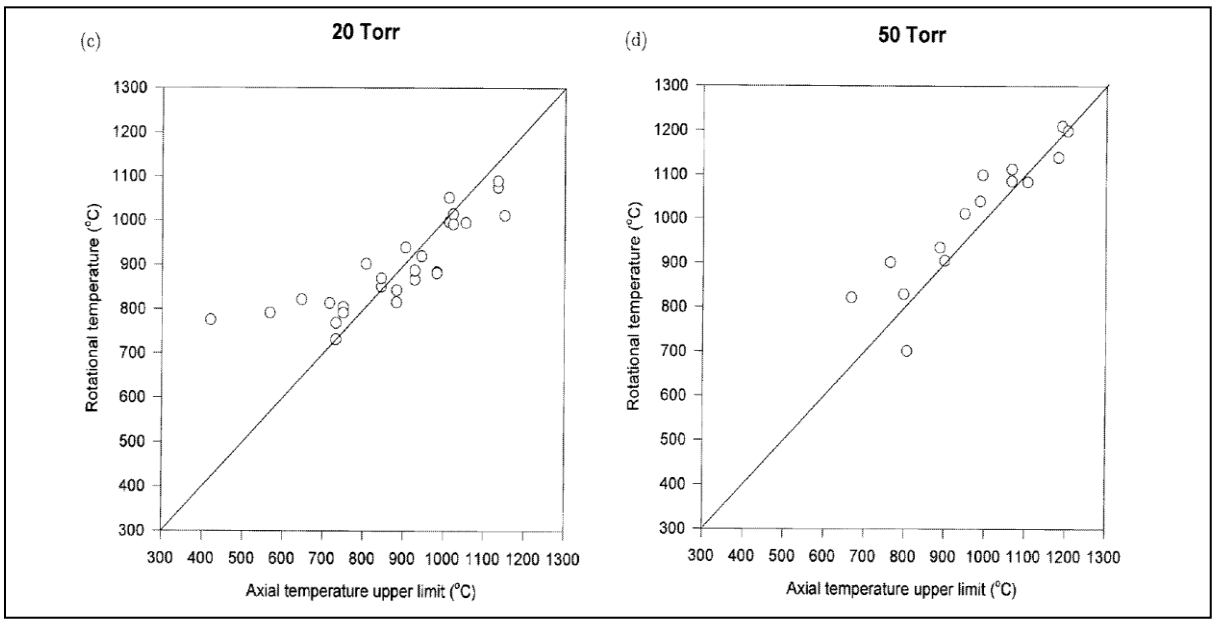

Figure 17: Plots of the rotational temperature versus the upper limit gas kinetic temperature for different pressure conditions [37] .

Chapter 5. Experimental Description

In this chapter the experimental setup with the list of apparatus used and the experimental procedure to record emission spectrum from a premixed laminar methane-air Bunsen flame is discussed.

5.1 Apparatus used in the experiment :

The set-up for capturing the optical emission spectra of the premixed hydrocarbon flame is shown below in Fig.18.

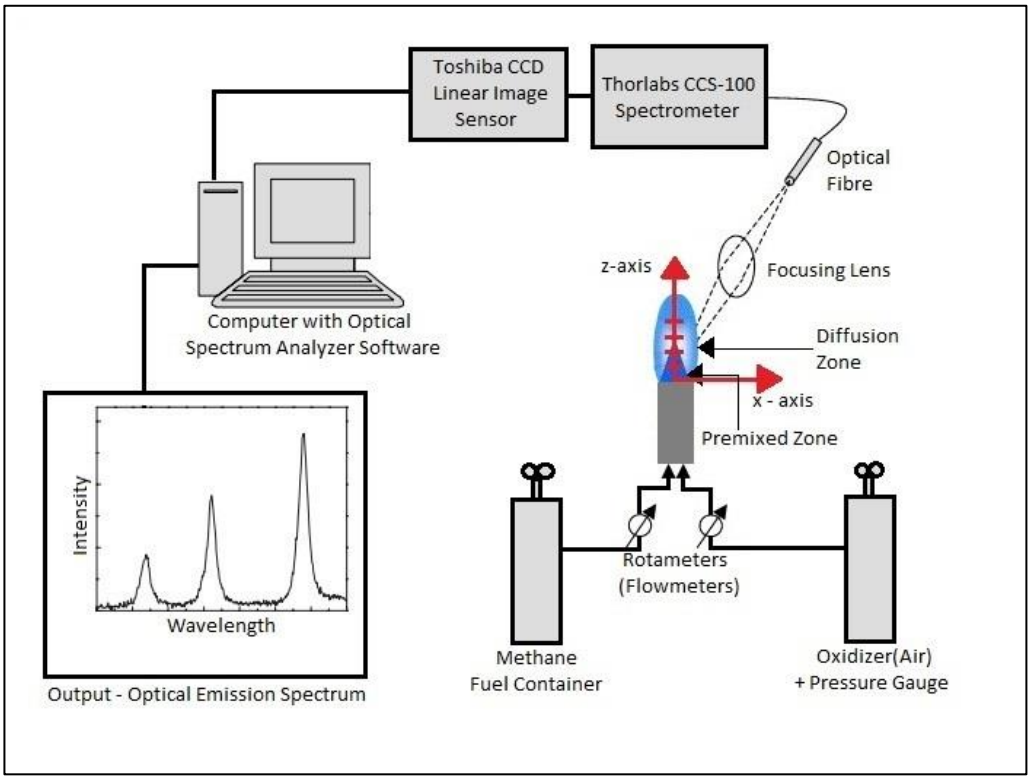

Figure 18: Schematic Layout of the experimental apparatus.

The details of the experiment set-up is as follows :

5.1.1 The hydrocarbon flame

Laminar premixed methane–air flames are stabilized on a stainless-steel Bunsen burner, having an outer diameter of 11 mm, an inner diameter of 8 mm and a length of about 1500 mm. The combustion occurs at standard atmospheric pressure conditions. The gaseous CH_4/air(containing 21% oxygen) mixture is supplied from separate channels and the flow rate of these constituents are separately regulated using calibrated variable area flow

meters(rotameters). Then they are premixed at a T-junction and channelled through a methane flame arrestor. The premixed gas then flows through a long stainless-steel pipe with a 1:100 - length to diameter ratio to suppress any vortex flows or irregularities in flow, thereby resulting in a smooth laminar flow at the burner exit. Two types of flames were used in this study, namely, the conventional conical Bunsen flame and a V-flame were used.

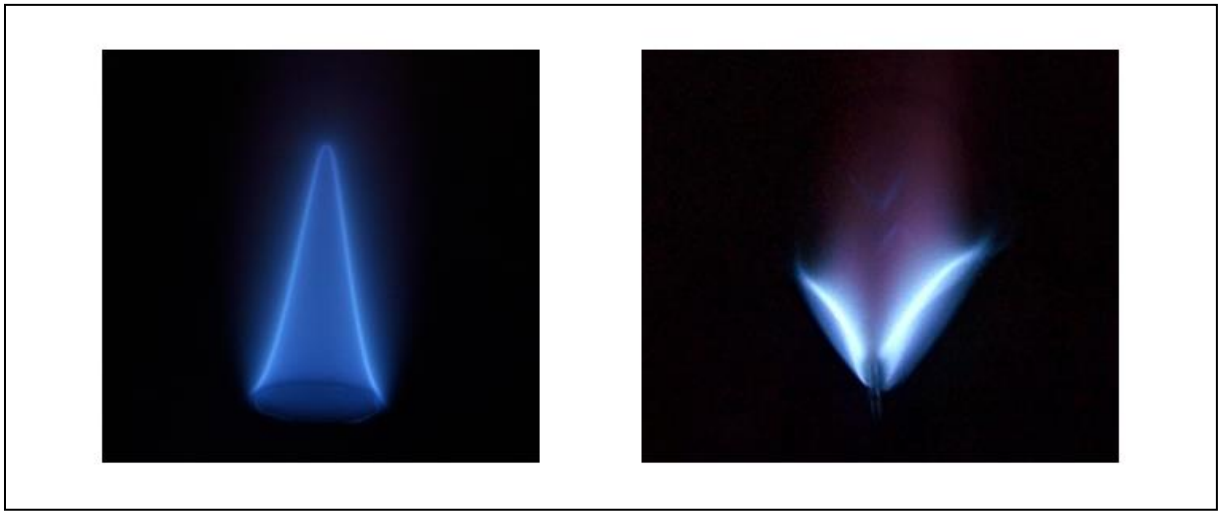

Figure 19: Premixed laminar Flames; a) Conical Bunsen Flame(Left) b) V-Flame(Right)

5.1.1.1 V Flame

The V flame is stabilized at about 6-8cm above the mouth of the Bunsen flame by placing a small steel rod of about 2mm diameter in the path of the unburnt gaseous discharge above the mouth of the Bunsen burner as shown in Fig.20. The purpose of using a V flame is to obtain a two-dimensional flame which in turn supresses the line of sight problem. The setup to stabilize a V flame over the mouth of the Bunsen flame is shown below:

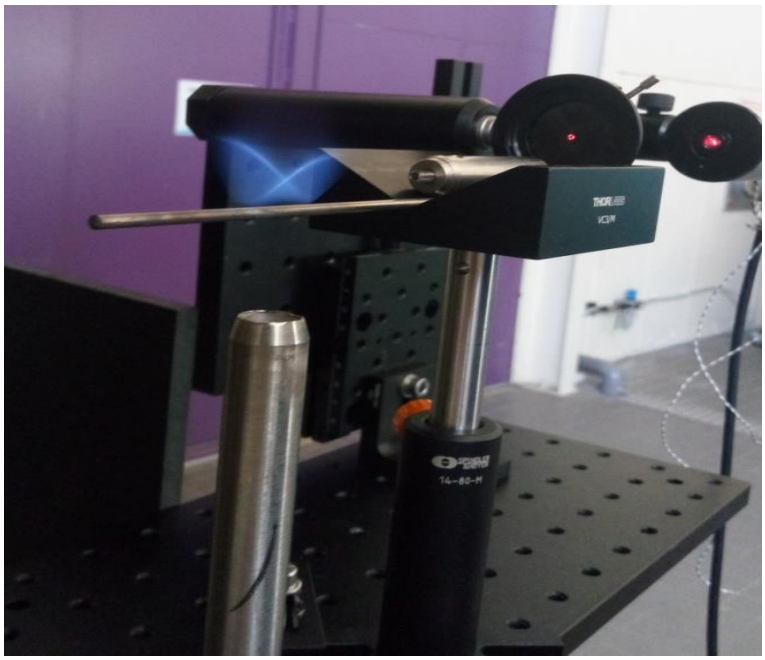

Figure 20: The setup to stabilize a V flame over the mouth of the Bunsen flame.

5.1.2 Helium Neon laser pointer

A He-Ne laser is used as a pointing device to identify the point of measurement across the flame front in a two-dimensional plane. The He-Ne laser operates at a wavelength of 632.8nm. An iris is placed in front of the laser beam to diminish the size of the laser beam, in order to get a very small point. This arrangement is mounted on a linear translation stage in order to translate the laser pointer across the flame front, as shown in Fig.21. This stage is translated simultaneously with the translational stage in which the fibre optic probe head of the spectrometer is mounted upon, such that the laser pointer is always pointing to the probe head. This gives an indication to map the location of the point on the flame being captured by the spectrometer probe.

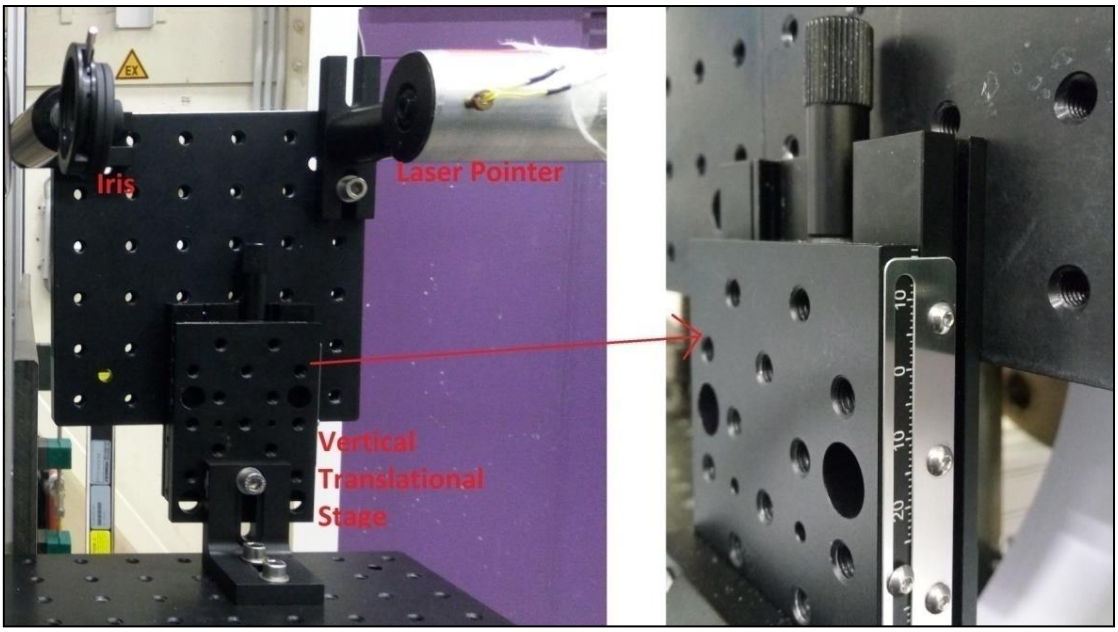

Figure 21: He-Ne laser coupled with an iris and mounted on a linear translation stage.

The usage of the laser pointer is shown in Fig.22 below. The figure shows the image of the flame and the laser pointer on the image plane (a graph paper), after passing through the focusing lens arrangement. Here a 1 mm^2 graph sheet is used to show the size of the laser pointer on the image plane. It can be seen that the size of the laser pointer is a small circular dot with a diameter of about 1 mm^2.

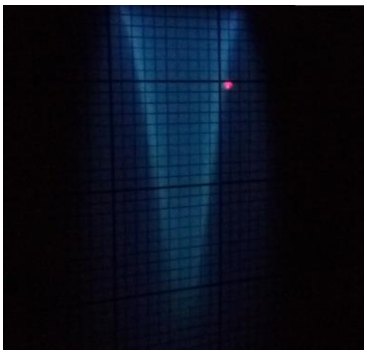

Figure 22: Laser pointer used to map the location of the point on the flame being captured by the spectrometer probe.

5.1.3 Focussing lens and fibre optic cable

The lens arrangement consists of a doublet, wherein two plano-convex lenses of focal lengths of 200mm are coupled together and held in position by means of a small fixture and hence the effective focal length of the doublet becomes 100mm. The object and the image are placed at 100mm from the centre of the doublet on either side of the doublet lens, hence there is supposedly no magnification. This is experimentally verified by measuring the diameter of the laser beam at the object plane and the image plane, it remains constant at 1mm diameter. This is first degree validation to show that there is no magnification of the object in the image plane. The image is an inverted two-dimensional projection of the object.

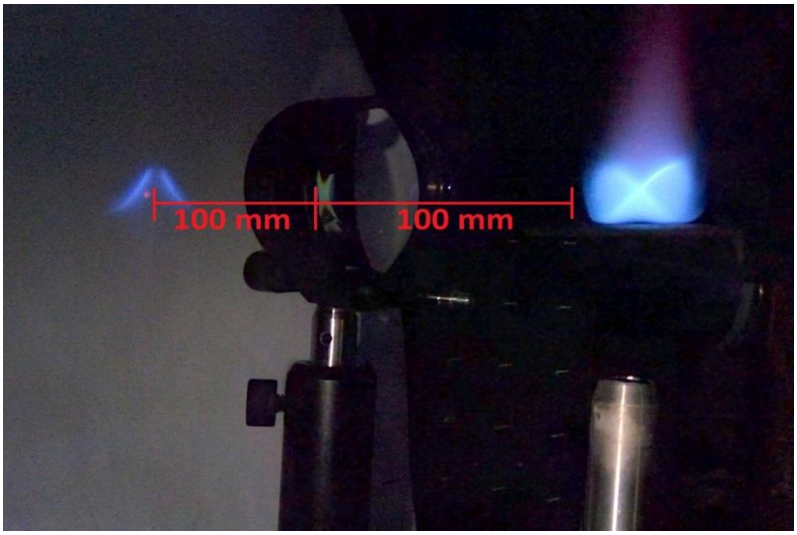

Figure 23: Lens Doublet showing the object(3-D V-flame in this picture) and its image(inverted 2D projection).

The photons of light emitted from the flame are focussed towards mechanical aperture of the bulkhead belonging to the fibre optic cable, which is placed at the image plane of the lens arrangement as shown in Fig.24. The fibre bundle, an M14L01 patch cable, with a length of 1m and a core diameter of 50 µm ± 2%, transmits the collected light signals to the CCS-100 spectrometer.

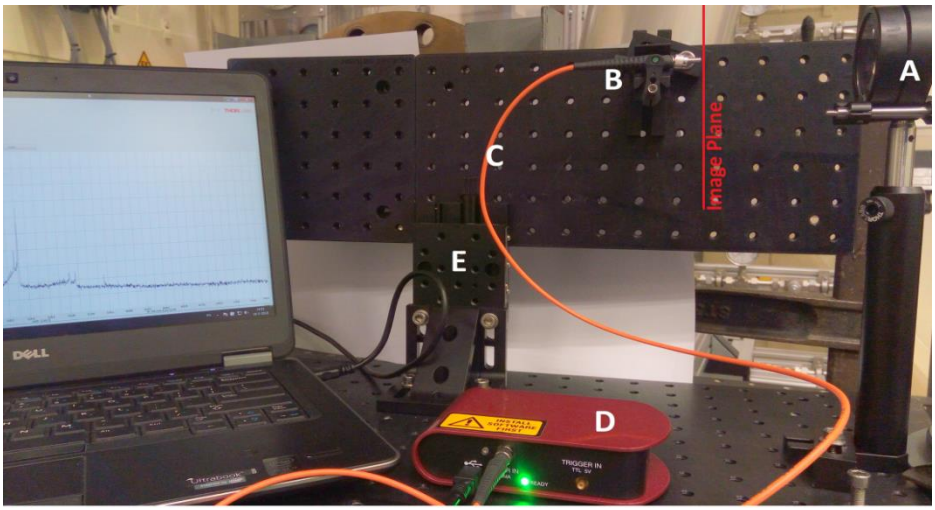

Figure 24: A.Lens Doublet B.Probe Head C.Fibre Optic Cable D.Spectrometer E.Translational Stage

This fibre bundle can transmit light signals between a range of 400 to 2400 nm wavelength. The spectrometer has an entrance slit dimension of 20 µm x 2 mm. But the mechanical aperture of the bulkhead of the fibre optic cable adjacent to the spectrometer slit only has a diameter of 1.2 mm. This in turn limits the effective slit dimension to 20 µm x 1.2 mm. These fibre optic bundles are optimized for use with spectrometers, so they consist of a linear fibre array on the spectrometer side of the cable. It is designed in a such a manner that it matches the spectrometer slit geometry.

5.1.4 The spectrometer and ccd detector

A CCS-100 spectrometer which is a Czerny-Turner spectrometer from Thorlabs is employed in the study. It can detect wavelengths between 350 - 700 nm. The spectrometer houses a grating of 1200 lines/mm, with a 500 nm blaze. The spectral resolution, which defines the ability to separate wavelengths is commonly expressed in terms of FWHM(Full Width Half Maximum). The FWHM of the spectrometer used is less than 0.5 nm @ 435 nm. The spectrometer is then coupled to a Toshiba CCD Linear Image Sensor. It consists of 3648 Pixel CCD Line Array. The integration time (or exposure time) of the CCD detector can be varied between 10 µs - 60 s.

5.2 Experimental procedure for recording of spectrum

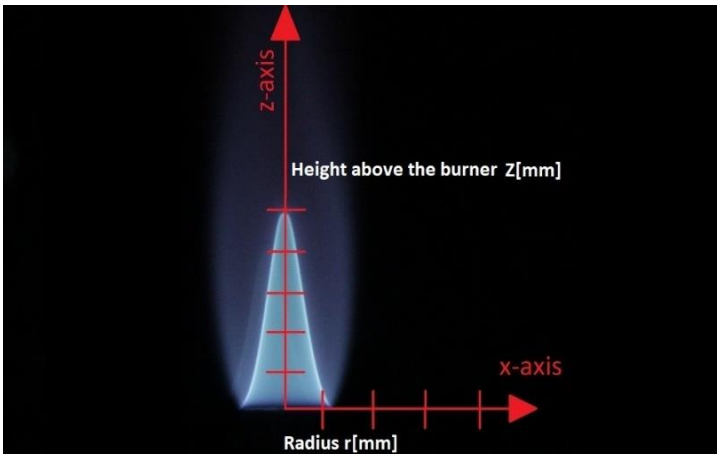

Figure 25: Premixed laminar methane/air Bunsen flame recorded at the Aircraft Power and Propulsion Laboratory, TU Delft. (Equivalence ratio, ϕ=1.25)

A two-dimensional translation of the fibre optic probe aperture is required to capture the intensity profiles of the C_2 radical at different points across the flame front, as obtained in linear scans. The linear intensity profile is recorded at different burner heights for the same flame conditions by translating the probe parallel to the z-axis, so that the axis of measurement cuts through the flame front, product zone and preheat zone as shown in Fig.26. The spatial intensity distributions of a given radical is directly proportional to the spatial concentration distribution of the radical in the flame. The target point on the flame front is recorded a number of times repeatedly for a given integration time and the average of the recorded spectrum data is considered to be a more reliable result.

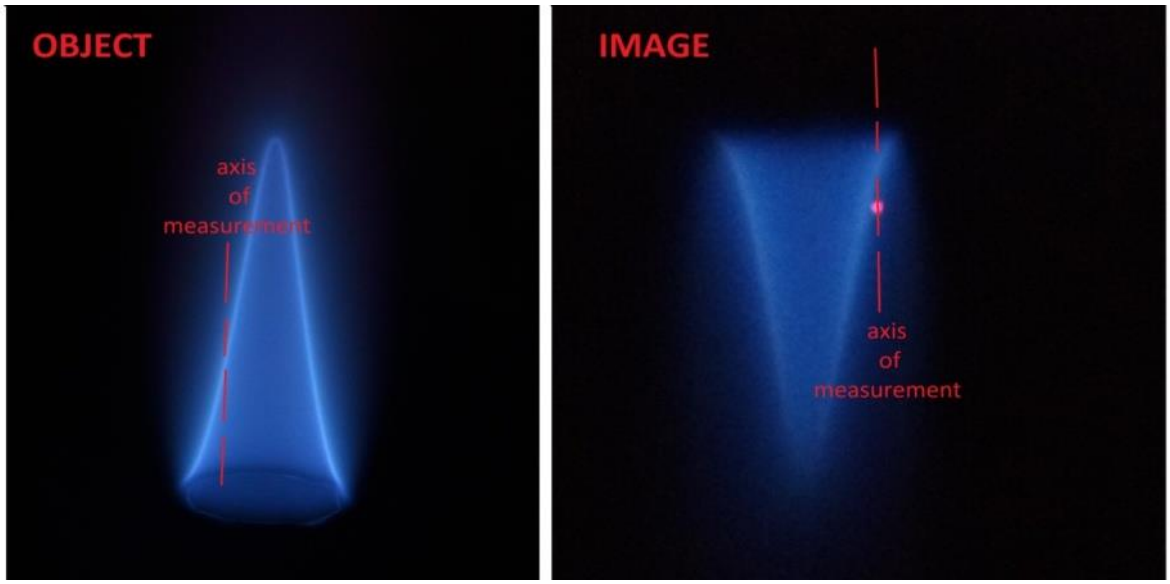

Figure 26: The axis of measurement along which the probe head is translated.

A millimeter translational stage has been used in this study. Using this millimeter translational stage shown in Fig.27, it was possible to translate the probe in steps of 0.5mm across the reaction zone, when required.

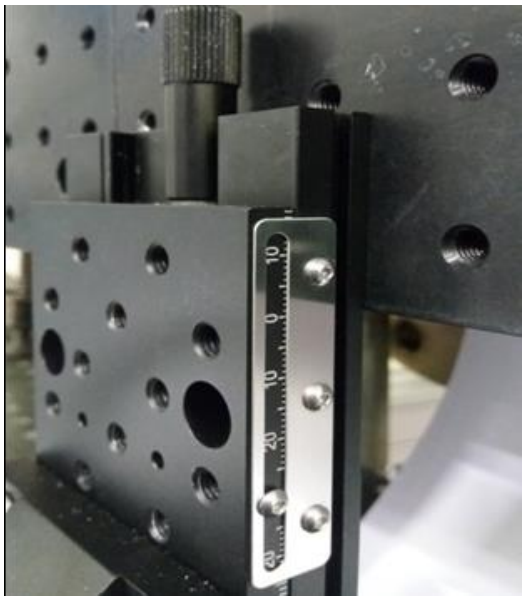

Figure 27: Thorlabs Travel Linear Translation Stage, Side Millimeter.

5.2.1 Optical Spectrum Analyzer software

The output of the CCS-100 spectrometer is analysed using software package provided by Thorlabs called OSA-SW(Optical Spectrum Analyzer Software). It provides a graphical User Interface to analyse the acquired optical emission spectra from the light source. It encompasses various useful features such as Wavelength Calibration, Normalized Y Axis, Peak Finder filters, Smoothing, Averaging, Polynomial or Gaussian Data Fitting and Integration Time adjustments.

5.2.2 Effect of integration time

The integration time in spectroscopy is analogous to the exposure time in photography. The longer the integration time greater is the intensity of the signal, as more photons of light are captured by the probe. Various studies have shown that the integration time varies non-linearly with the signal-to-noise intensity ratio and so this influence must be take into account by testing the quality of the spectra obtained for different integration times [44]. The Fig.28 below shows the spectrum for the methane-air flame with an equivalence ratio of 0.8, obtained for different integration times of 1000ms, 4000ms, 7000ms, 9000ms, 12000ms respectively.

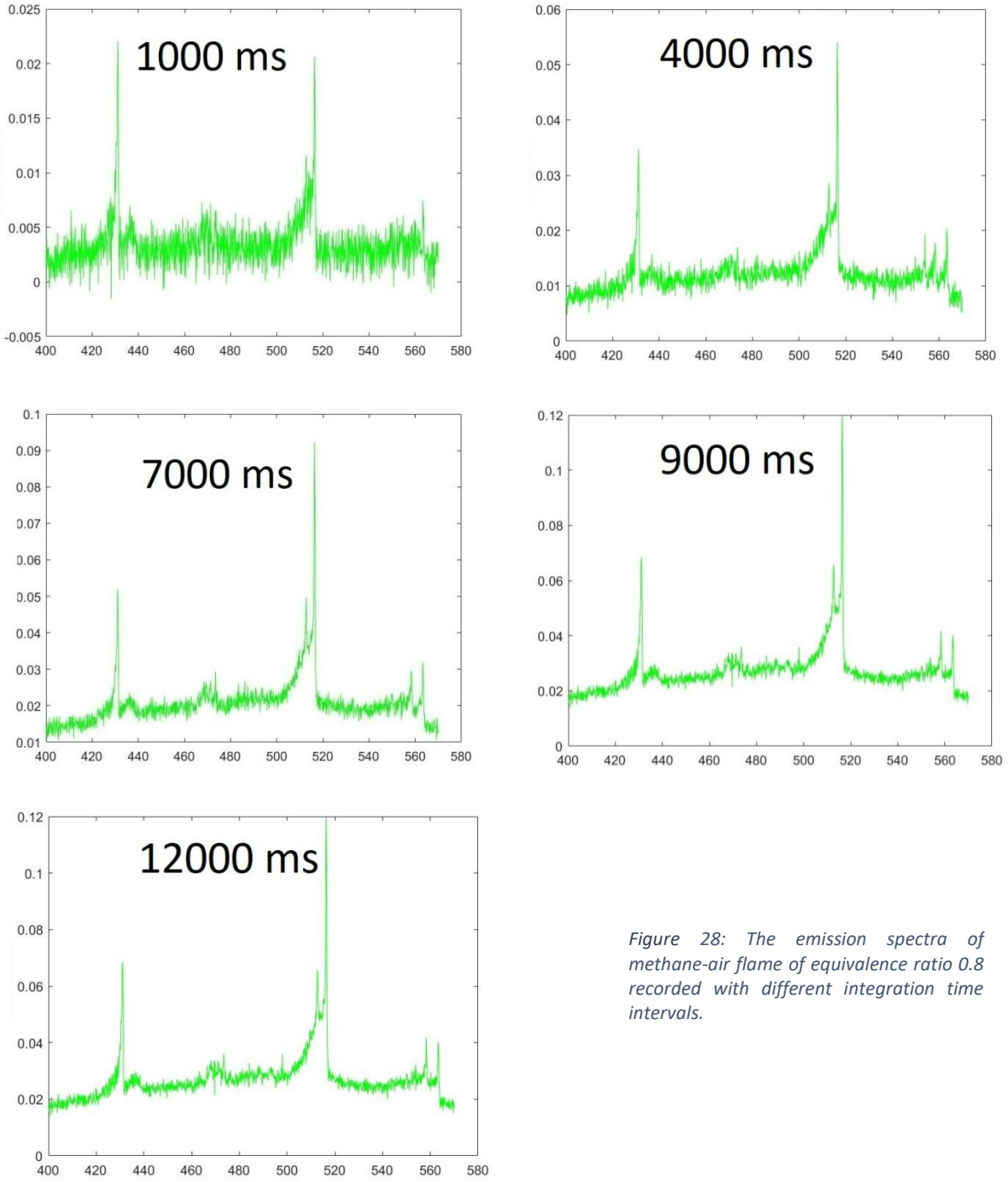

Figure 28: The emission spectra of methane-air flame of equivalence ratio 0.8 recorded with different integration time intervals.

Five different integration times were chosen for the study; 1000ms, 4000ms, 7000ms, 9000ms, 12000ms. It can be seen from the spectra in Fig.28 that as the integration time increases the intensity of the spectral signal increases and the signal-to-noise ratio increases. However, there is no difference seen between the signals captured using an integration time of 9000ms and 12000ms respectively. And so, an integration time of 9000ms has been used as the standard for this thesis work.

Chapter 6. The Concept of theoretical spectroscopic modelling and temperature computation using BESP - NMT.

The following flowchart gives a brief outlook about the steps involved in modelling of a theoretical spectrum using various input parameters corresponding to the emission spectrum :

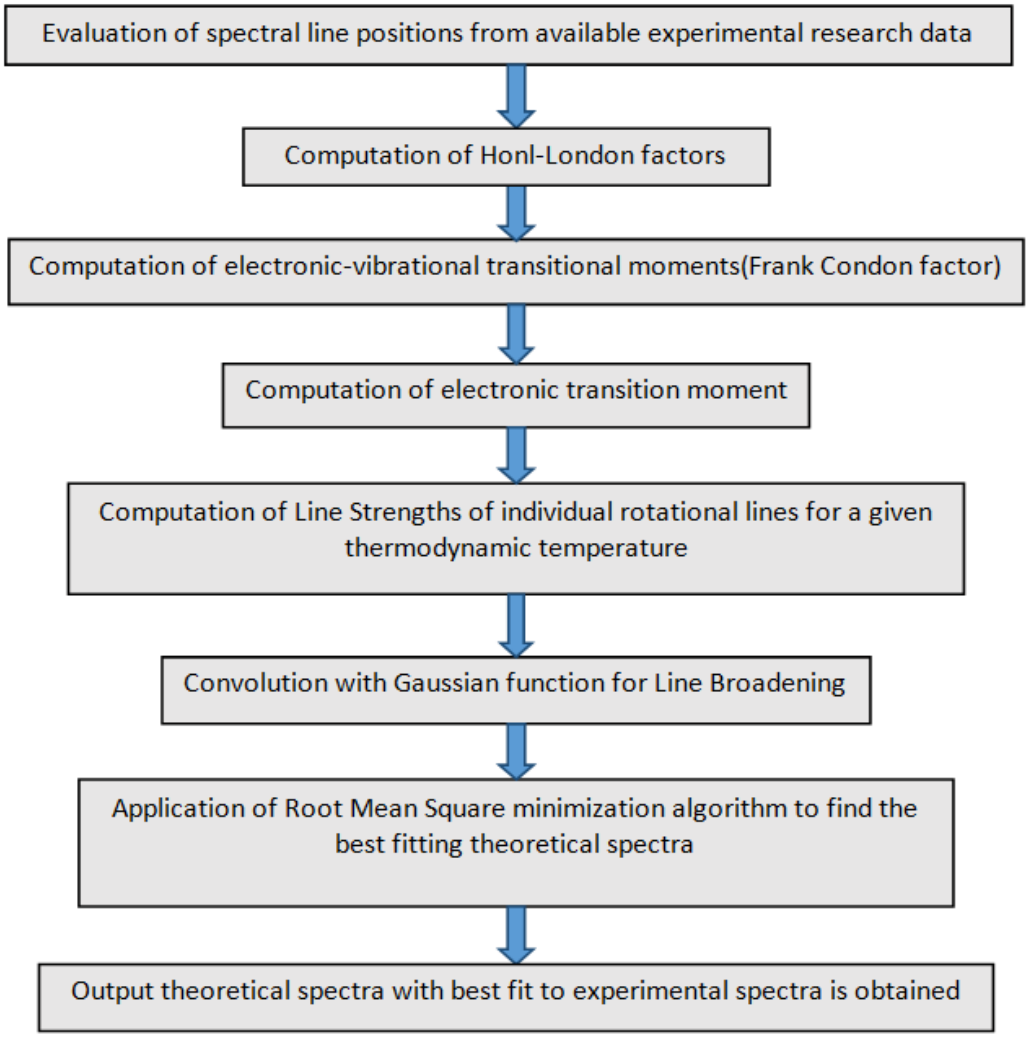

6.1 Computation of line strengths and line intensities

Molecular spectra in the visible range is formed as a result of electronic transitions. This gives rise to individual spectral lines across a range of wavelengths which is a characteristic of the

initial and final energy levels of the molecular species under observation. The emission spectra of a molecular species is a function of its thermodynamic temperature and the relative population of the species at different energy levels. The spectra can be computed by using the line strengths and line positions for a given thermodynamic temperature. Accurate and validated experimental data from years of research is used to establish the numerical values of parameters associated with the initial and final energy levels of each transition. These parameters associated with the transitions are used to predict the spectral line positions given by their corresponding frequencies denoted by v_{ul} (the subscript 'ul' refers to 'upper state to lower state'). Calculated line positions of the (0,0) Swan band, with their respective wavelengths are shown in Fig.29 below [45]. The Σ in Fig.29 corresponds to the combined rotational band spectrum output as seen in the emission spectrum.

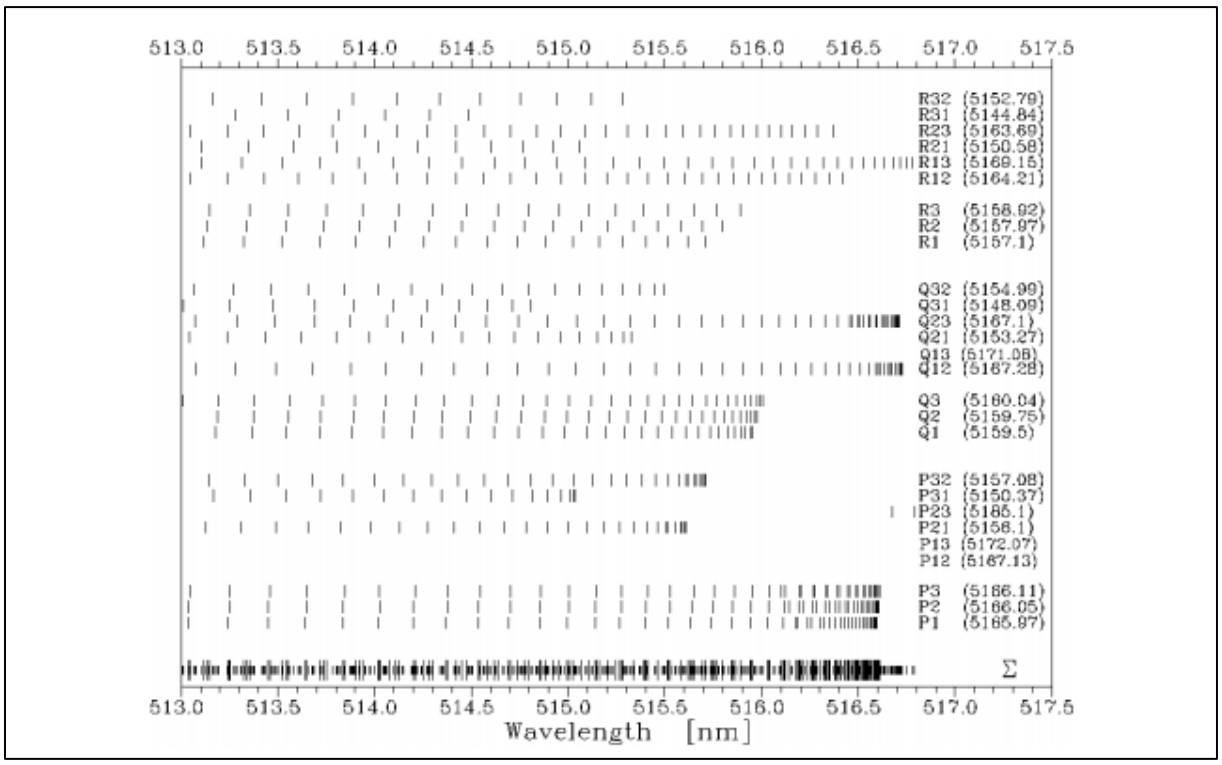

Figure 29: Calculated line positions of the (0,0)Swan band. [45]

These spectral lines are then used to compute the Honl-London factors which indicate the relative intensity distribution among the individual spectral lines involved in a rotational transition. In turn, the Diatomic Line strengths, S_{ul} are computed. The line strength is a product of the electronic transition moment, electronic-vibrational transitional moments(Frank Condon factor) and the Honl-London factor. The line strength is expressed as follows [46]:

$$S_{ul} = A_{ul} \frac{3h\lambda_{ul}^3 g_u}{64\pi^4} \qquad \text{(eq.45)}$$

where A_{ul} is the Einstein transition probability of spontaneous emission, h is the planck's constant, c is the velocity of light, g_u is the statistical weight of the upper energy level and λ_{ul}

is the transition wavelength given by the line position. Using the computed line strengths, S_{ul}, the individual line intensities, I_{ul}, are computed for each transition for a given absolute thermodynamic temperature, T, as follows [46] :

$$I_{ul} = C_0 \frac{64\pi^4 v_{ul}^4}{3c^3} N_0 \frac{e^{-hcF_u/k_BT}}{Q} S_{ul} \qquad \text{(eq.46)}$$

where c is the velocity of light of light, F_u is the term value of the upper energy level, N_0 is the total number of molecules of all the energy levels, v_{ul} is the transition frequency, k_B is the Boltzmann constant, Q is the partition function and C_0 is a constant of proportionality which encompasses experimental factors such as spectrometer-detector sensitivity. Using these line positions and line strengths, tables of spectral line lists are made, and these tables are fed as input to the computer program for computation of theoretical spectra.

6.2 Application of a Gaussian function for line broadening

The simulated theoretical spectrum profile is synthesised from the spectral lines belonging to different rotational transitions by convolving them with a Gaussian-type slit function [2] with the full width at half maximum(FWHM) value. It can be determined via measurement of the very narrow spectral line profiles emitted by low-pressure discharge lamps. Even at very high resolutions, the spectral lines emitted by molecular species are not separated but are spread over a range of wavelengths. This line broadening happens due to various phenomena like pressure broadening (collision broadening) and Doppler broadening. To account for this broadening a Gaussian function is used. The line shape function G_λ at FWHM(of the spectrometer) is expressed as [46]:

$$G_\lambda = \frac{1}{\sigma\sqrt{2\pi}} e^{-(\lambda-\lambda_0)^2/2\sigma^2}, \qquad \text{(eq.47)}$$

where the Gaussian standard deviation, σ is given by :

$$\sigma = \frac{\text{FWHM}}{2\sqrt{2ln2}}. \qquad \text{(eq.48)}$$

Here λ_0 is the wavelength of the peak intensity of the broadened spectral line.

6.3 RMSE minimization algorithm

The computation of a theoretical spectrum involves an iterative process to determine an optimum pair of temperature and resolution(FWHM) that minimizes the difference between the theoretical spectra and the experimental spectra in order to get the best fit. The absolute thermodynamic temperature input ascertains the relative spectral line intensities and the

resolution input ascertains the convolution of the lines, to fit the experimental spectrum. An initial guess of these two parameters, the line strength tables and the experimental spectrum data serve as user inputs. From these inputs, a theoretical spectrum is synthesized for each combination of temperature and resolution iteratively. Each of these synthesized spectra is then compared with the experimentally recorded spectra and the one that best matches with it is returned as output. A root mean square error (RMSE) is used to test the accuracy of the fit, which defines the quality of the synthesized theoretical spectrum. The best fit corresponds to the RMSE closest to zero, which is achieved by a mathematical least square minimization procedure as follows:

$$\chi^2(T^r, FWHM) = \frac{\sum_{i=1}^{N}[I_i^e - I_i^t(T^r, FWHM)]^2}{N(N-1)} \qquad \text{(eq.49)}$$

The χ^2 has to minimized iteratively as a function of the rotational temperature(T^r) and the spectral resolution expressed as Full Width at Half Maximum(FWHM). In the above equation, I_i^e and I_i^t are the experimental and theoretical intensities of the i_{th} pixel of a spectrum consisting of N number of points. The T^r value which corresponds to the least value of χ^2 is considered as the final output rotational temperature for a given experimental spectrum by means of a theoretical curve fitting procedure.

6.4 BESP-NMT

By the application of all the concepts discussed above, several commercial and open source software have been designed with a graphical user interface to analyse the experimental OES from various emitting species. Some examples of such software are NEQAIR (which is a NASA developed code for prediction and analysis of molecular spectra by utilizing standard molecular constants), SPECAIR, LIFBASE, BESP and NMT.

BESP and NMT will be made use for this thesis work as they are open source software. Using the concepts discussed in the previous sections, they were created by a team of researchers at The Center for Laser Applications, University of Tennessee Space Institute (UTSI), Tennessee, United States. BESP - Boltzmann Equilibrium Spectrum Program, is one such software tool which uses a table of line strengths for a specified diatomic transition band as input to compute the spectrum of spontaneous emissions from the diatomic gas in a state of thermal equilibrium. The Nelder Mead Temperature (NMT) program is another tool that exploits the Nelder–Mead minimization algorithm to minimize the value of χ^2, as discussed in section 6.3. The Nelder–Mead algorithm is numerical method which can be used for minimization or maximization of a function involving multiple parameters, for non-linear optimization problems. The NMT program uses BESP as a subroutine for acquiring the unprocessed theoretical spectra, yet to be convolved and fit.

6.4.1 The LSF file

This LSF file contains the parameters essential in determining the line intensities for each wavelength in the spectra to be modelled. An LSF file pertains to a particular molecular species. These parameters include the transition moments, electronic-vibrational transitional moments(Frank Condon factor), the Honl-London factors, Einstein transition probability of spontaneous emission, the statistical weights of the upper energy levels, the term values of the upper energy levels, the transition wavelengths given by the line position, the partition functions and constants of proportionality. In the current study a LSF file for the C_2 radical is used.

6.4.2 BESP

BESP is employed to just compute the diatomic spectra of a species for a given temperature and spectral resolution using a loaded input file consisting of a database of line strength tables. (C_2 line strength tables in this study). It is helpful in estimating visual appearance of spectra. BESP acts as a subroutine to NMT for acquiring the unprocessed theoretical spectra, yet to be convolved and fit.

6.4.3 Procedure for obtaining a theoretical spectrum using BESP

Fig.30 below is a screen shot of the BESP program with different user inputs which are discussed below.

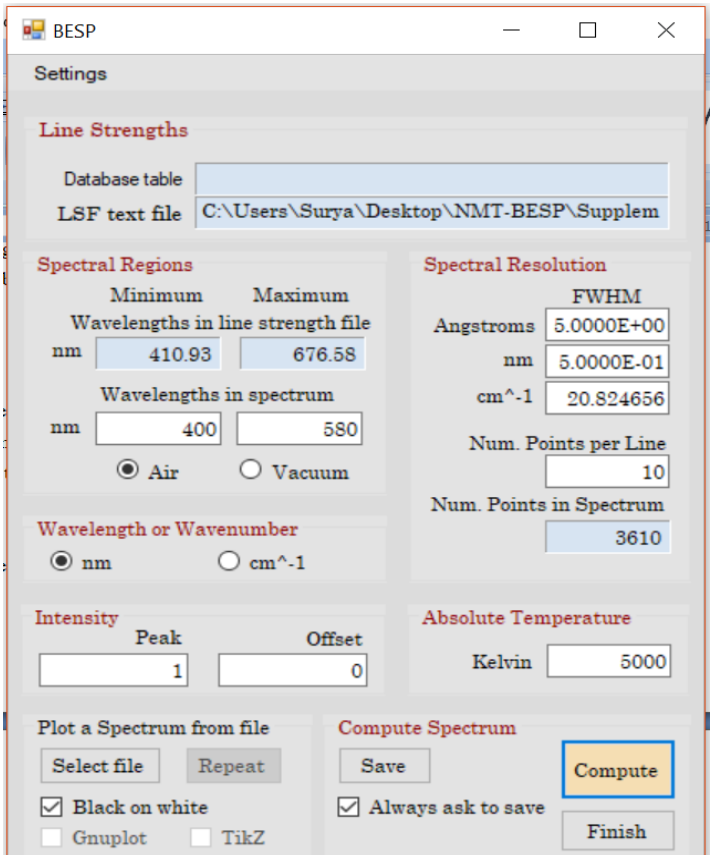

Figure 30: Screen shot of the BESP program with different user inputs.

In the BESP windows GUI as shown in Fig.38 z text file called the Line Strength File(LSF) is uploaded to the application as an input. The absolute temperature for which the theoretical spectra has to be synthesized is the user input parameter. The necessary spectral range to be modelled is specified and the required spectral resolution of the output is specified as well. The X-axis parameter of the spectra to be modelled can be chosen either in terms of wavelength (nm) or wavenumber(cm^{-1}) .Then the number of points to be plotted per line of the spectrum can be chosen. Finally, the spectra is computed and visualised. This can be saved in the required file format.

The C_2 swan spectra synthesized using BESP for different absolute temperatures between 500 K to 5000 K for a FWHM of 0.5 is shown below in Fig.39.

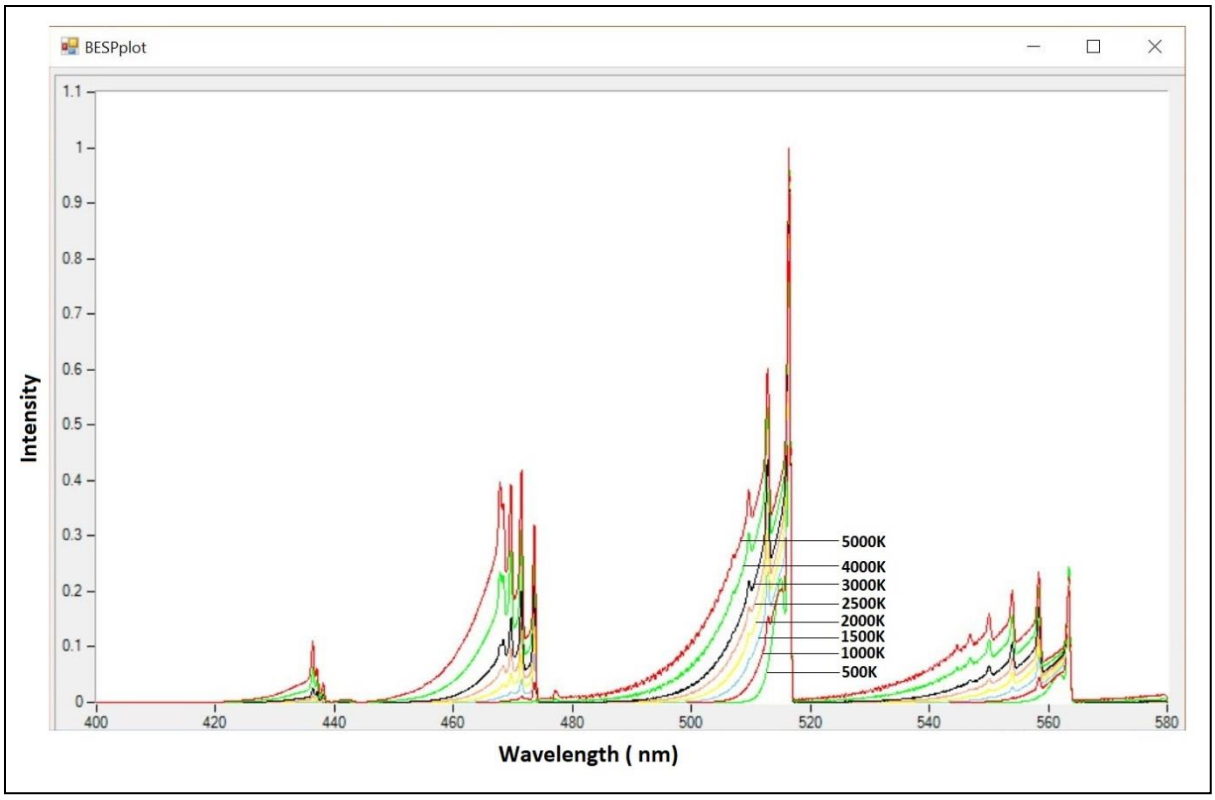

Figure 31: BESP output window displaying the synthesised theoretical spectra for different absolute temperatures.

From Fig.31 the temperature dependence of the emission spectrum of a flame can be clearly seen.

6.4.4 NMT

NMT plays the bigger role of synthesising a theoretical spectrum by means of convolution and a curve fitting procedure employing the Nelder–Mead algorithm. Input consists of the database of line strength tables, the measured experimental spectrum data file, the wavelength range under consideration, the initial guess temperature, the initial guess spectral resolution and tolerances for the curve fitting. Also, the user is given a choice to apply a baseline offset in case of need of a baseline correction. After an iterative procedure, the final output thermodynamic temperature and the best fitting FWHM resolution for a given experimental

spectrum is obtained. The experimental data file needs to be wavelength and sensitivity calibrated. The wavenumber resolution of the C_2 line strength tables used is typically better than 0.05 cm− 1 and so the wavelength spectral resolution, δλ, at about 400 nm is better than 0.001 nm, or better than 1 pico-meter (1 pm). Fig.32 below is a screen shot of the NMT program with different user inputs which are discussed below. When the NMT program runs , simultaneously, a visualization pop-up window displays the measured and real-time computed spectra in a separate window as shown in Fig.33.

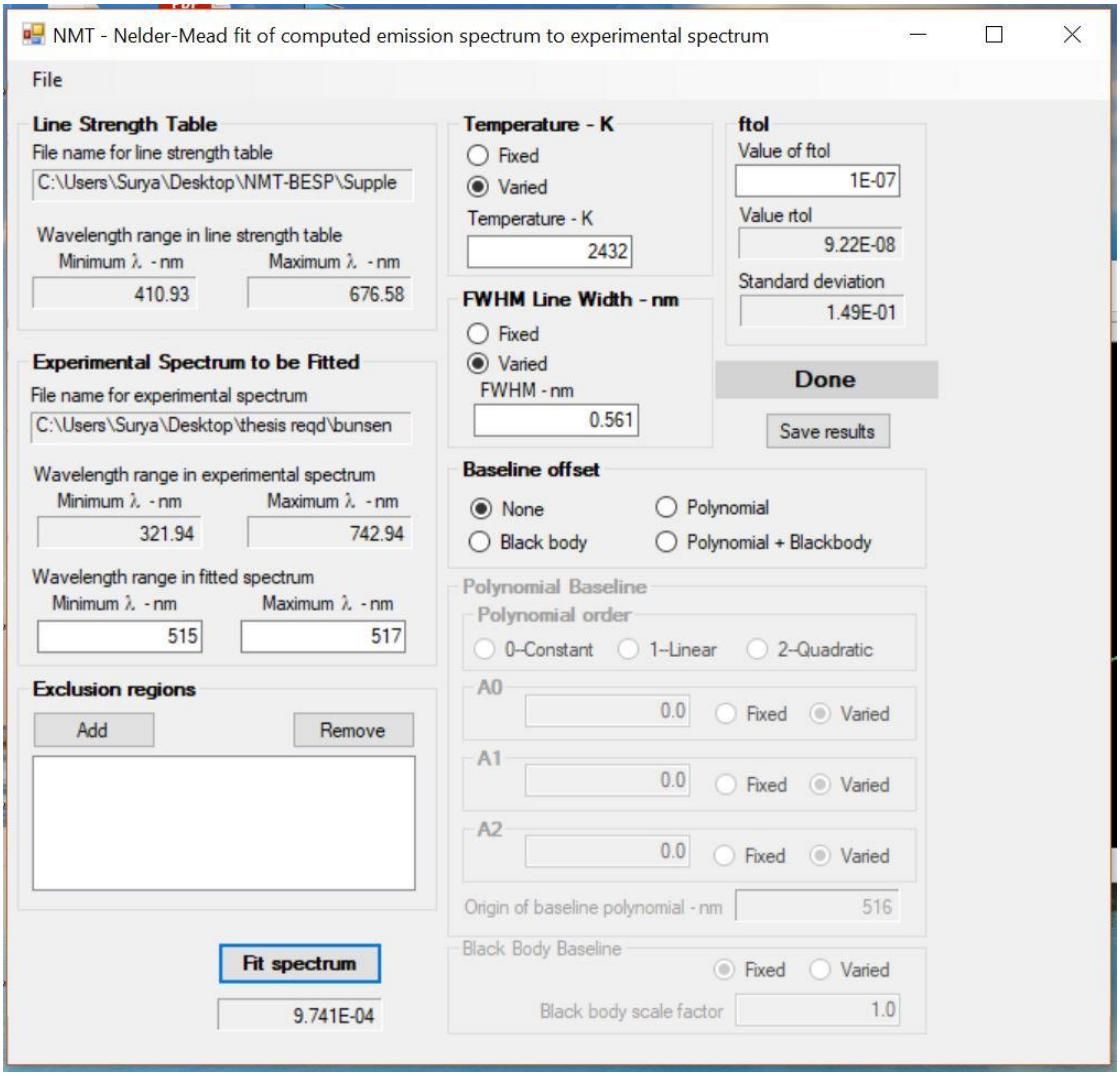

Figure 32: Screen shot of the NMT program with different user inputs.

6.4.5 Procedure for computation of temperature using NMT :

Similar to BESP, a text file called the Line Strength File(LSF), which contains a database of required input parameters is uploaded to the application. Additionally, here the experimental spectrum to be fitted to the theoretical one is also given as an input text file. Depending on the need the spectral range to be fit is chosen. For vibrational temperature computation, a set of bands are chosen and for rotational temperature computation, just one transition band is chosen. An initial guess temperature value and an initial guess FWHM value is given, this value gets rewritten iteratively until the best fit temperature for the and a

corresponding FWHM are obtained as output. The X-axis parameter of the spectra to be modelled can be chosen either in terms of wavelength (nm) or wavenumber(cm¬-1). Tolerance values and baseline offset values can be specified only if required. Finally, the spectra is computed and visualised. This can be saved in the required file format.

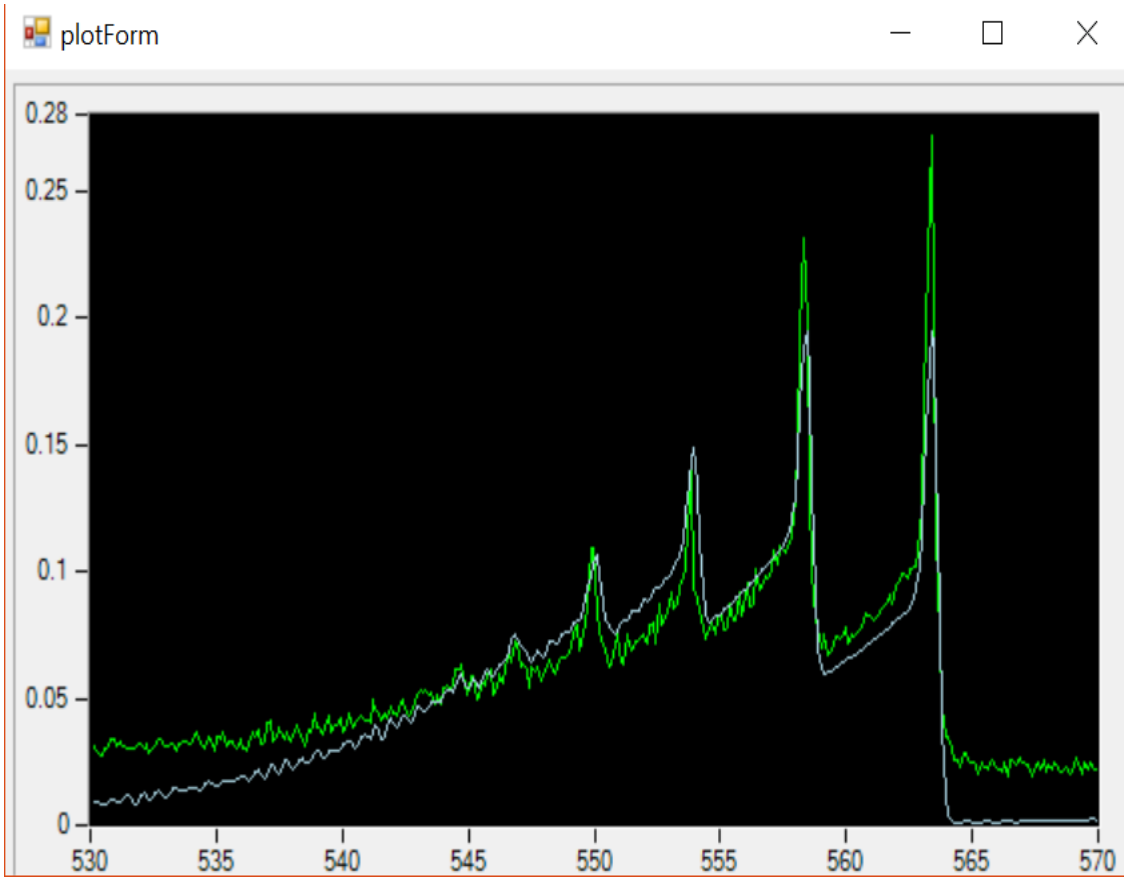

Figure 33: NMT pop-up window displaying the measured experimental spectrum(green line) and the fitted computed spectrum(white line)

6.5 Example: Temperature computation using NMT

In this thesis work, the computation of vibrational and rotational temperatures using the Swan band spectrum shall be performed with the help of NMT application. In this section two examples have been discussed to give the reader an insight into the computation process using NMT.

Fig.34 shows the experimental Spectra obtained in the reaction zone of a methane-air Bunsen flame having an equivalence ratio of 1.0, captured using the setup discussed in the previous chapter. This spectrum is uploaded to the NMT program for fitting it to the theoretical spectra which has been synthesized using a database of line strengths.

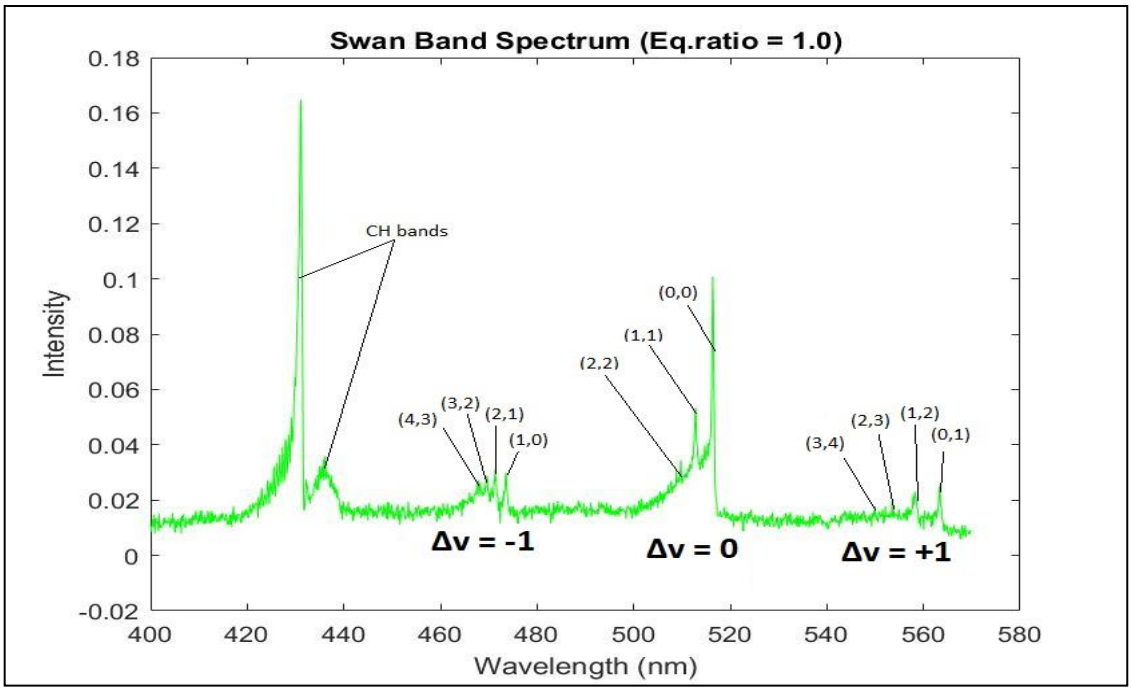

Figure 34: Experimental Spectra obtained in the reaction zone of a methane-air Bunsen flame having an equivalence ratio of 1.0

6.5.1 Case 1 : (0,0) Swan band rotational temperature computation

Commonly the (0, 0) Swan band peak spectrum between 513.5 -516 nm is used in the determination of rotational temperature because this range encompasses enough "thermometric peaks"(peaks whose relative intensities are more sensitive to changes in the rotational temperature). In this case, the rotational temperature of the (0,0) band has to be determined from the experimental spectrum, so only that spectral range which encompasses the rotational lines of the (0,0) band is chosen. The chosen range is between 515nm and 517nm as shown in Fig.35. An initial guess temperature of 2000K and spectral resolution of 0.1 is chosen. Once the 'Fit Spectrum' tab is clicked the NMT program iteratively finds the best fit temperature from the given spectrum, by exploiting the least square minimization algorithm. **The rotational temperature hence found is 2432K.**

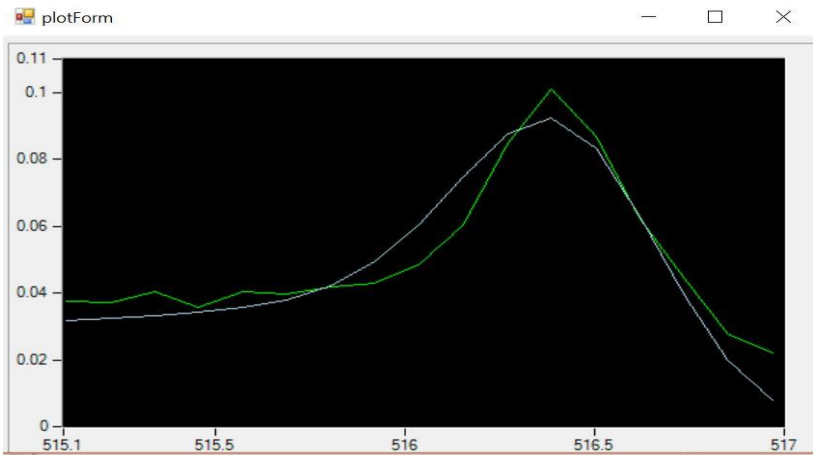

Figure 35: NMT pop-up window displaying the measured experimental spectrum(green line) and the fitted computed spectrum(white line), for computation of rotational temperature.

`

6.5.2 Case 2 : Vibrational temperature computation

In most cases only the $\Delta v = -1$ transitions of the C_2 molecule, observed between 460-475 nm, are used for the determination of vibrational temperature. This chosen range is between 465 nm and 475 nm as shown in Fig.36. This range encompasses all the bands of the $\Delta v = -1$ transitions. An initial guess temperature of 2000K and spectral resolution of 0.1 is chosen. Once the 'Fit Spectrum' tab is clicked the NMT program iteratively finds the best fit temperature from the given spectrum, by exploiting the least square minimization algorithm. **The vibrational temperature hence found is 3371K.**

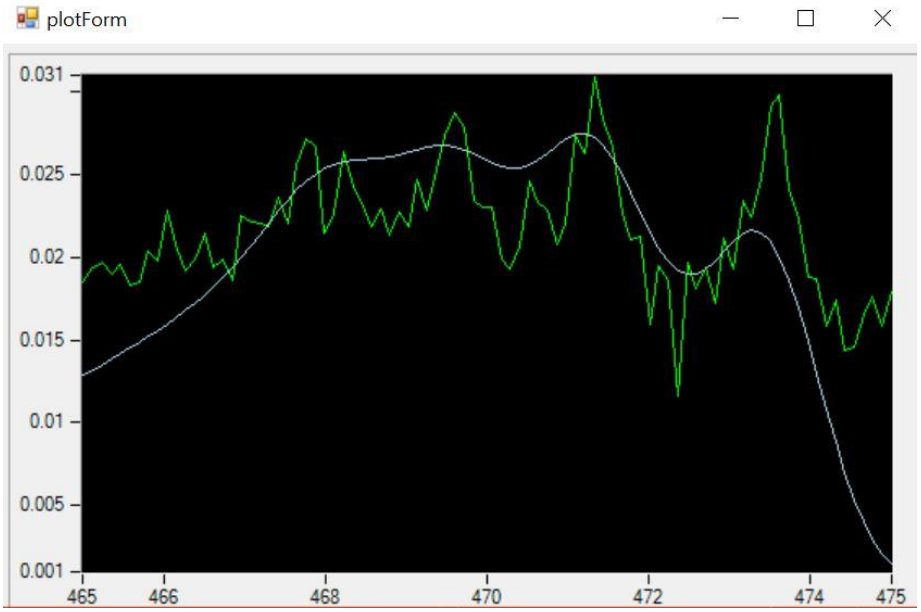

Figure 36: NMT pop-up window displaying the measured experimental spectrum(green line) and the fitted computed spectrum(white line), for computation of vibrational temperature.

BESP and NMT are open source programs. They can be found online as an appendix to this research article: *https://doi.org/10.1016/j.sab.2015.02.018* , authored by Christian G. Parigger et al, Center for Laser Applications, University of Tennessee Space Institute.

Chapter 7. Results and Analysis

In this chapter, the various results obtained using the experimental setup is discussed, inferences are drawn analytically and compared with some results taken from existing literature.

7.1 Spatial mapping of the distribution of C_2* radical

Spatially resolved measurements of relative concentration of the C_2* radical within the flame can be studied by mapping the spatial distribution of emission intensity at characteristic wavelengths. Horizontal and vertical emission intensity profiles for the C_2, OH and CH radicals in a hydrocarbon flame are obtained in linear scans, translating the fibre optic aperture along straight lines through the flame image using an x-y translational stage. The horizontal intensity profiles across the reaction zone at 1.05 mm above the burner head recorded with the point monitoring system is shown in Fig.37.

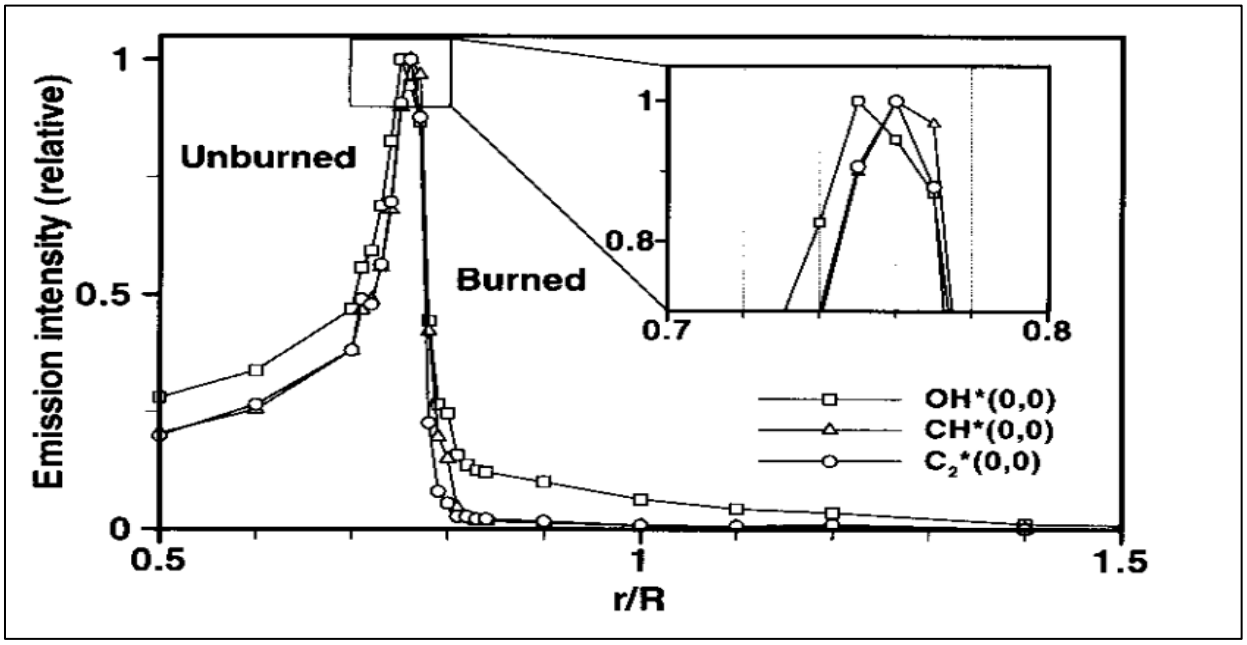

Figure 37: OH, CH*, and C_2* emission intensity distributions for the flame front. CH4-air; Φ = 1.1. [48]*

The Fig.37 above shows the radial distribution and emission intensities of excited radicals at the flame front. The OES was measured at different points along the radial axis (r/R = 0.5–1.5). Emissions were mainly occurring around r/R of 0.72–0.8, which is the location of the mean flame front. [48].

In this study, to measure the spatial distribution of the C_2 and CH radical concentration, the emission intensity has been captured across the reaction zone of a conical flame with an equivalence ratio of 1.0. The probe head of the fibre optic aperture is translated vertically in steps of 1mm so that it translates across the reaction zone of the flame. Over the

reaction zone, the probe is translated in steps of 0.5mm (the best possible resolution using a millimeter translation stage). The path in which the probe is translated over the reaction zone of a conical flame is shown schematically in Fig.38.

Initially the probe head is placed at the base of the cone such that it captures the spectrum in the cold gas region just before the preheat zone. Then the probe is gradually translated vertically towards the outer flame cone such that it traverses the preheat zone, the luminous reaction zone and the product zone. Within the reaction zone the probe is translated in steps of 0.5mm for a deeper insight in the reaction zone, which is the primary region of interest.

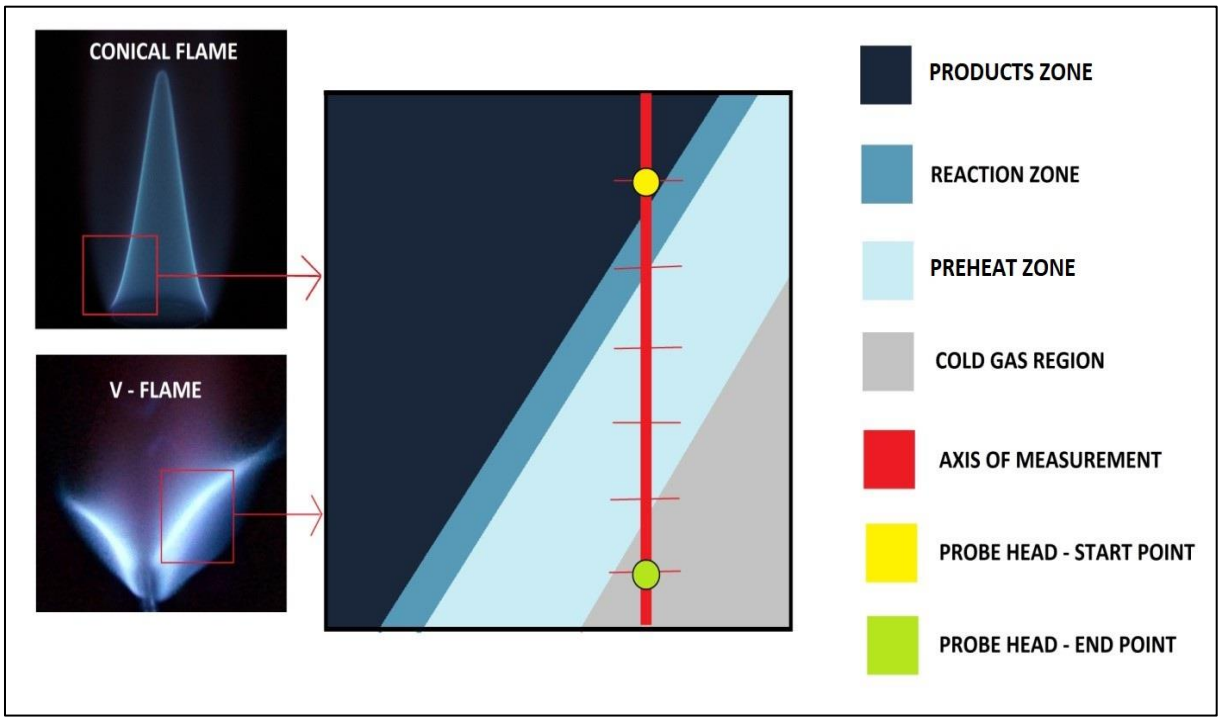

Figure 38: The path of translation of the fibre optic probe head across different zones of the flame.

The Fig.39 in the following page shows the image of the V-Flame as seen by the fibre optic probe head. The laser pointer is used as a guide to visualise the point on the flame captured by the fibre optic probe. The probe start point is marked as 0.0mm at the initial point of measurement, such that this point lies in the cold unburnt gas region as shown in the Figure. Gradually it is traversed linearly such that it cuts through all the flame zones as discussed above. Between 4mm and 8mm, the probe is traversed in steps of 0.5 mm, to get a deeper insight of the spectral emission in the reaction zone. The final point is at 9mm from the initial start point, this point lies in the product zone. The translation was not performed orthogonal to the flame front owing to difficulties involved in translating simultaneously in the x and y axis, instead the probe was traversed linearly along the y-axis such that it cuts through all the flame zones.

These images in Fig.39 were photographed by placing a white sheet on the image plane. The white sheet is printed with gridlines which form 1mm X 1mm squares.

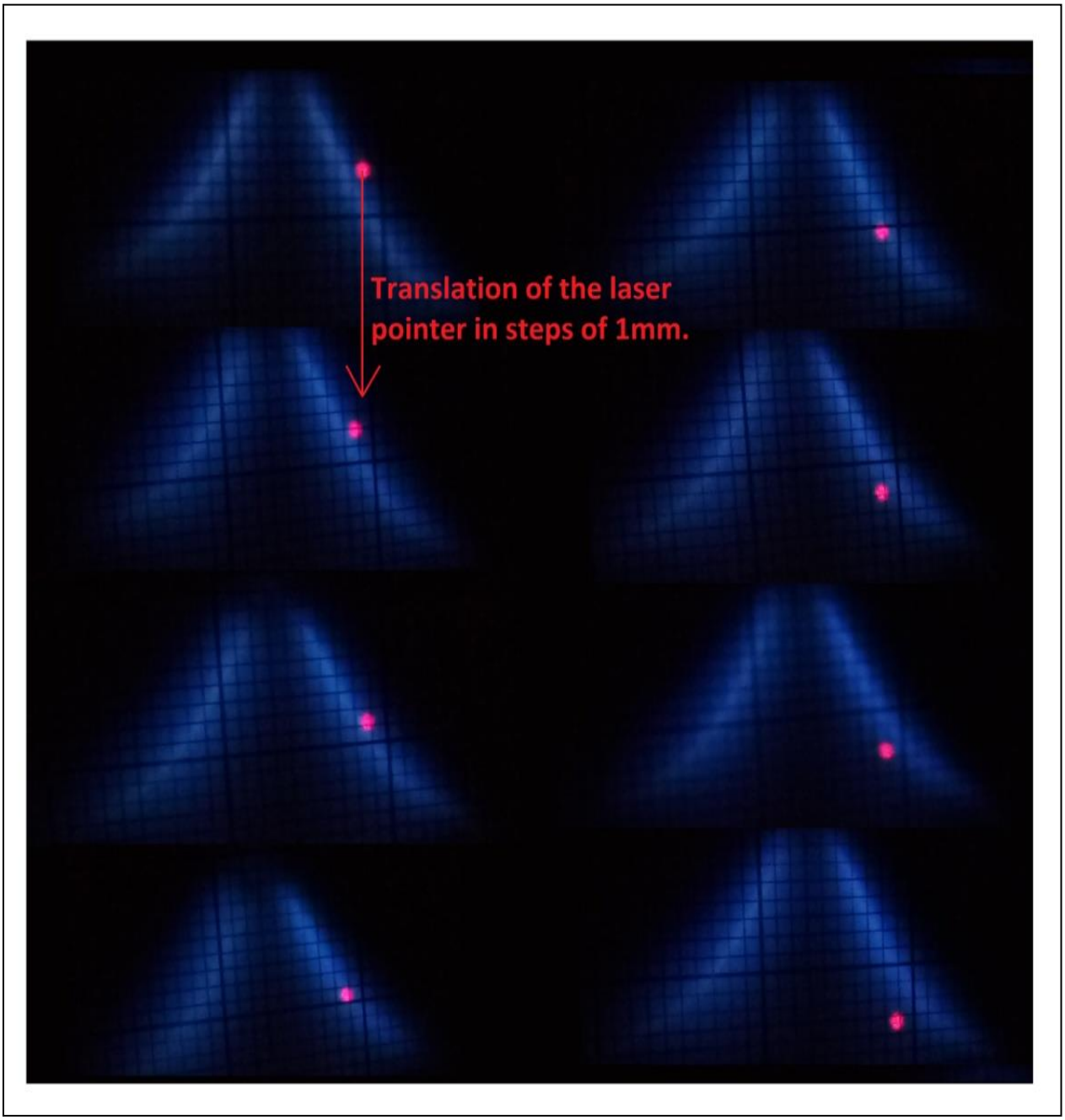

Figure 39: The image of the V-Flame as seen by the fibre optic probe head. The laser pointer indicates the point on the flame being captured by the probe head.

The following images, from Fig.40a-40n, show the change of the spectrum spatially as the probed is traversed over the flame front from the cold gas region towards the product zone region. The flame in this case is a V-flame having an equivalence ratio of 0.8.

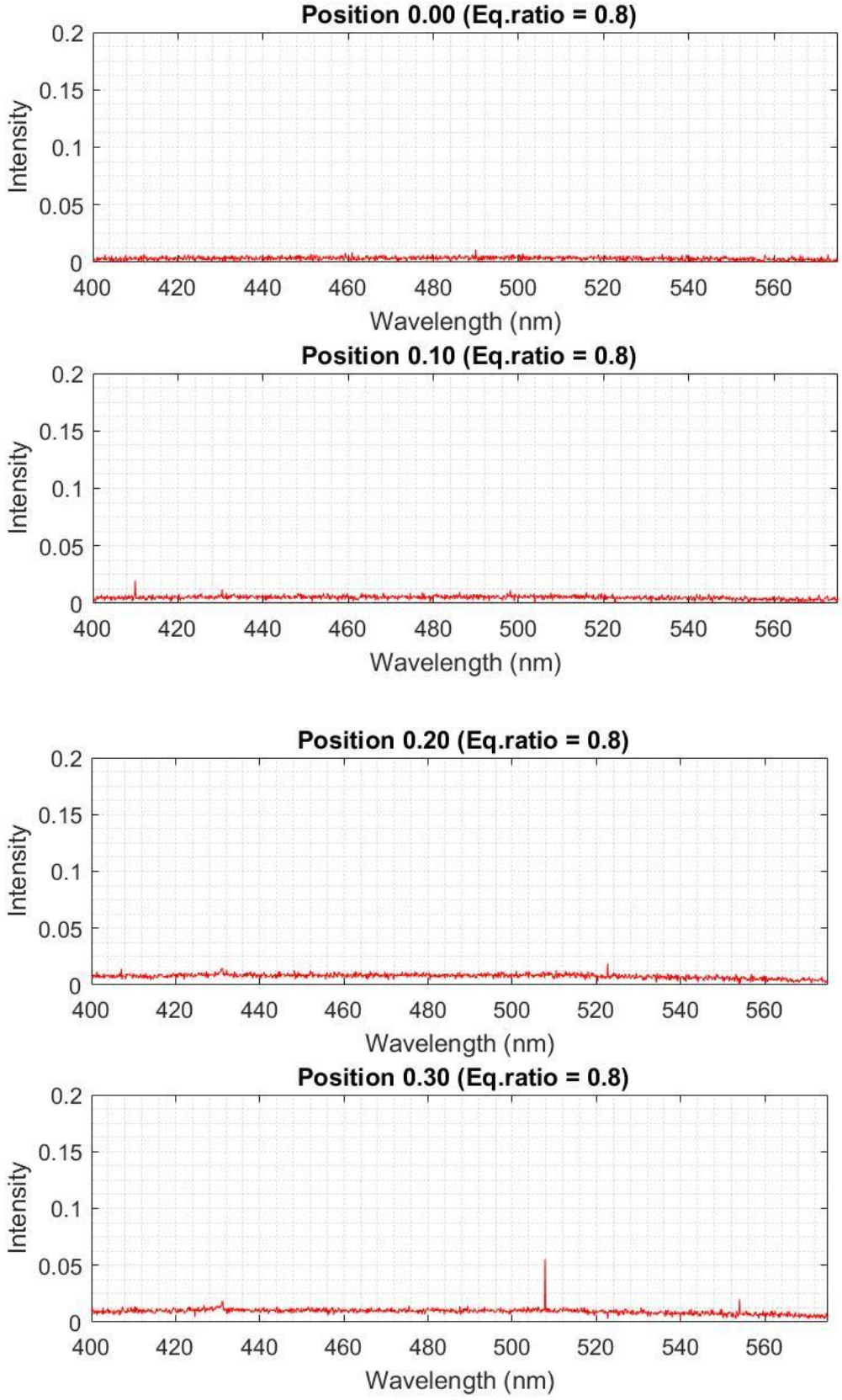

Figure 40:a,b,c,d - from top to bottom respectively; V-flame spectrum from a premixed laminar methane-air flame of equivalence ratio 0.8. Starting from Fig.48a, the laser probe head used to capture the spectrum is traversed gradually in steps of 1mm or 0.5mm across the flame front.

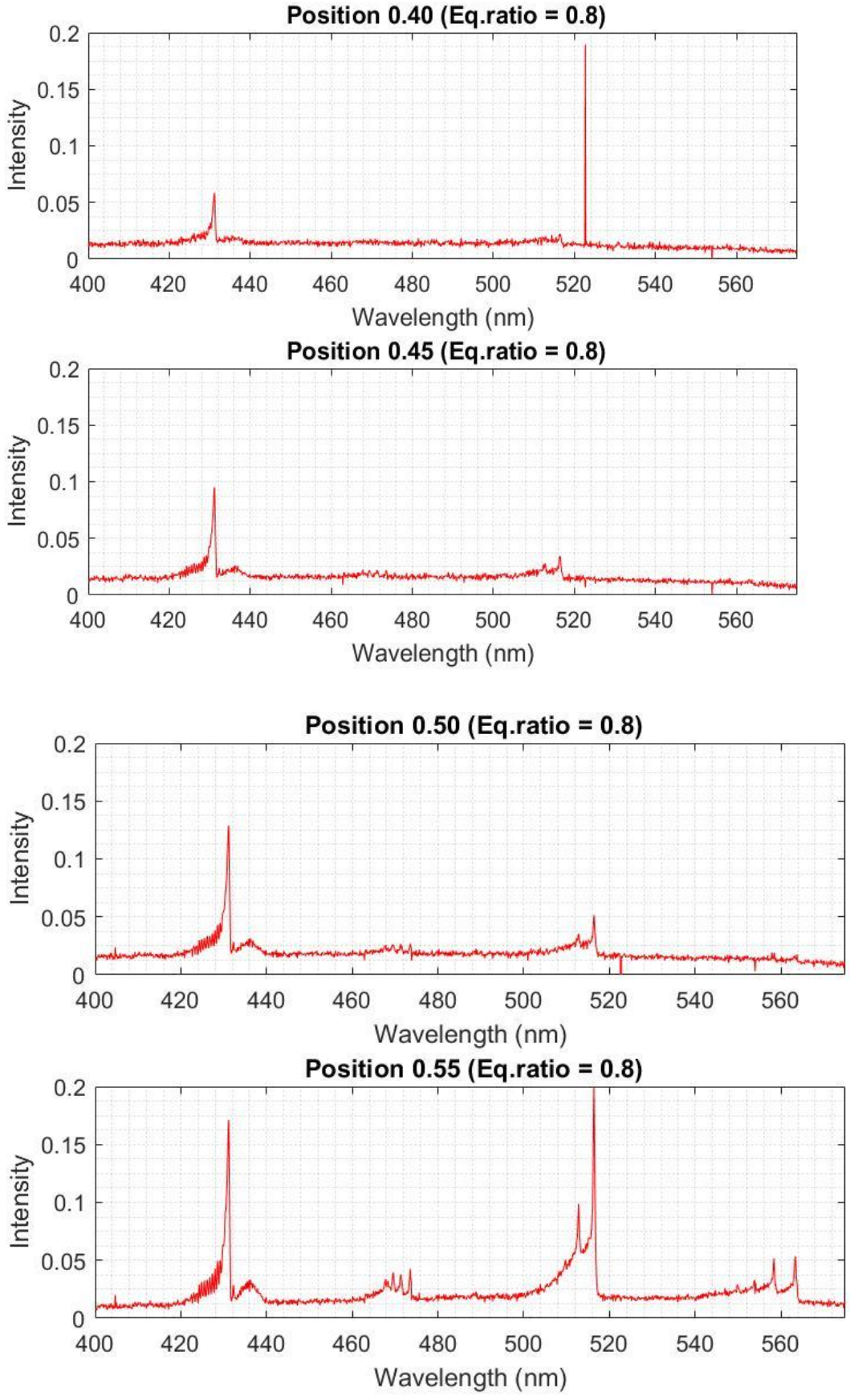

Figure 40:e,f,g,h - from top to bottom respectively; V-flame spectrum from a premixed laminar methane-air flame of equivalence ratio 0.8. Starting from Fig.48a, the laser probe head used to capture the spectrum is traversed gradually in steps of 1mm or 0.5mm across the flame front.

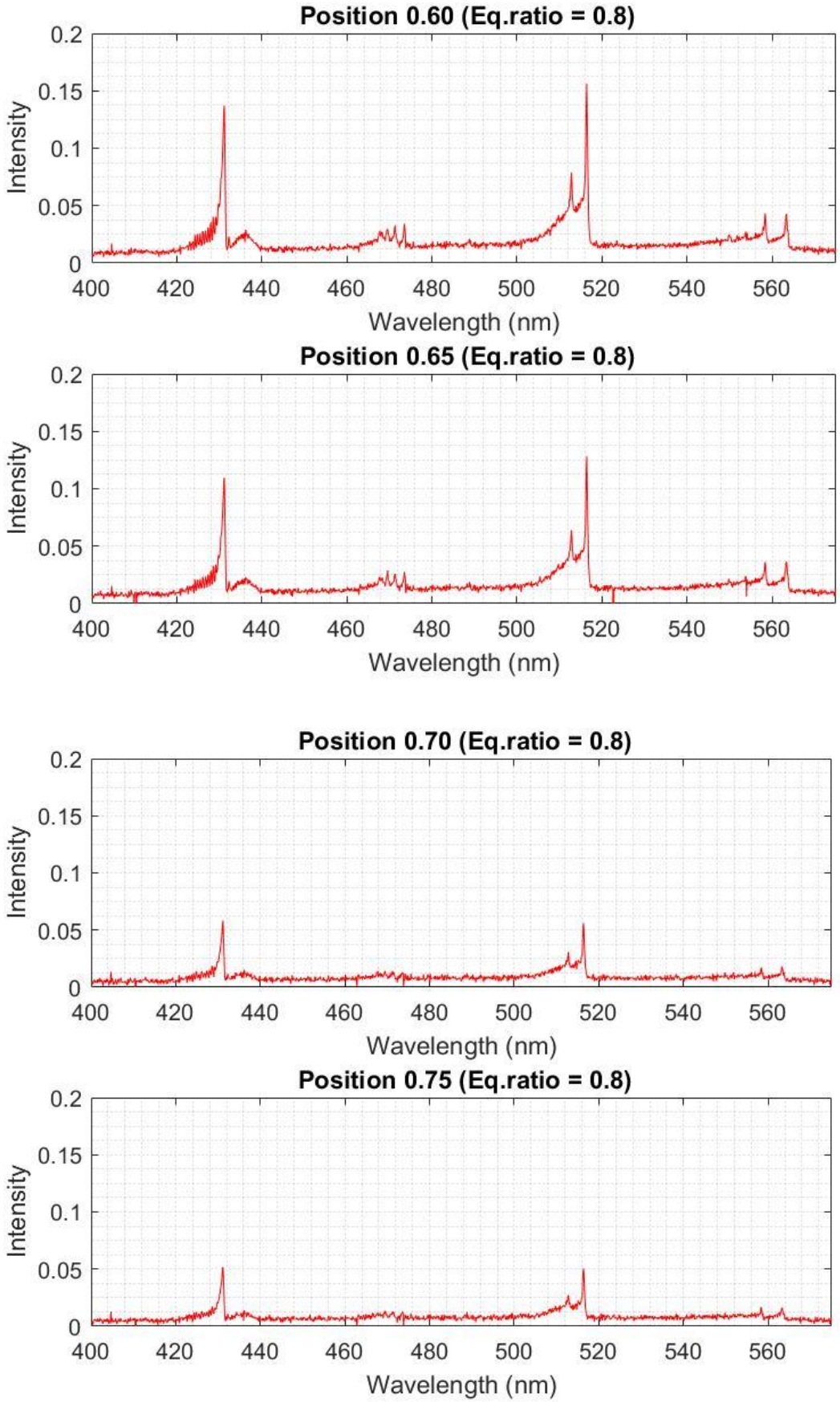

Figure 40:l,j,k,l - from top to bottom respectively; V-flame spectrum from a premixed laminar methane-air flame of equivalence ratio 0.8. Starting from Fig.48a, the laser probe head used to capture the spectrum is traversed gradually in steps of 1mm or 0.5mm across the flame front.

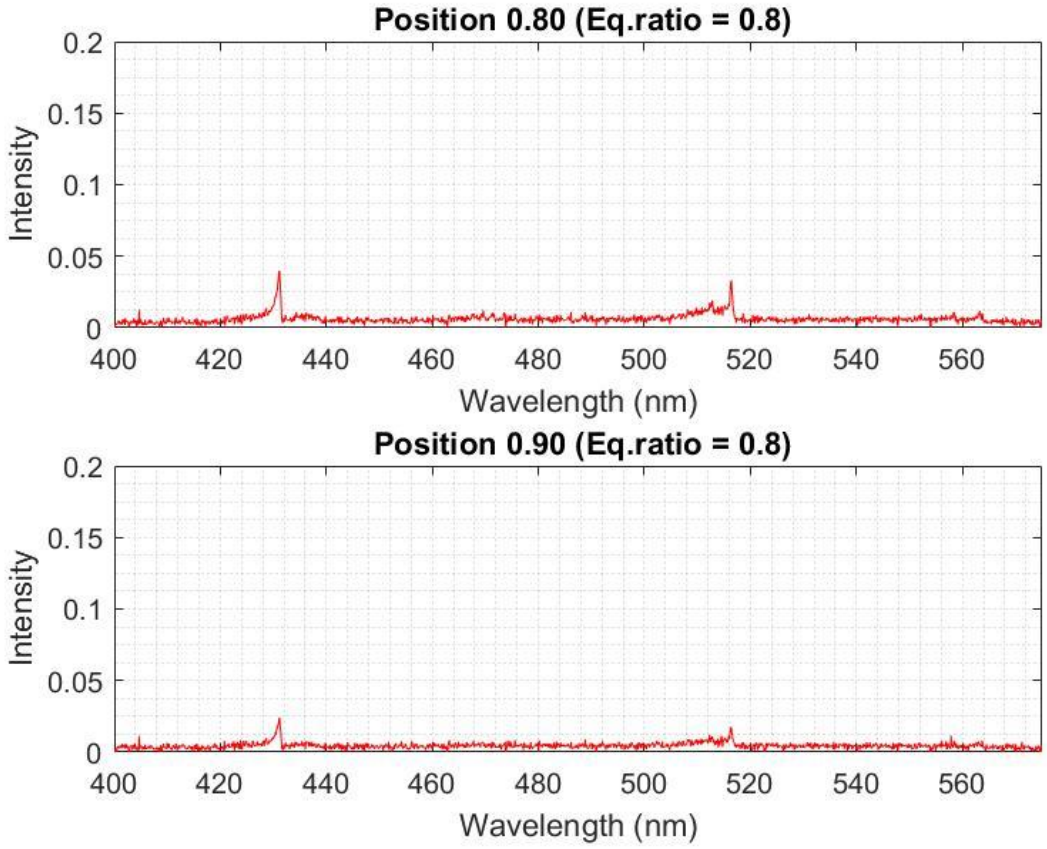

Figure 40:m,n - from top to bottom respectively; V-flame spectrum from a premixed laminar methane-air flame of equivalence ratio 0.8. Starting from Fig.48a, the laser probe head used to capture the spectrum is traversed gradually in steps of 1mm or 0.5mm across the flame front.

Fig.41 depicts the Spatially resolved measurements of relative concentration of the (0,0) transitioning CH* radical and the (0,0) transitioning C_2* radical across the flame front of the V-flame of equivalence ratio 0.8 discussed above.

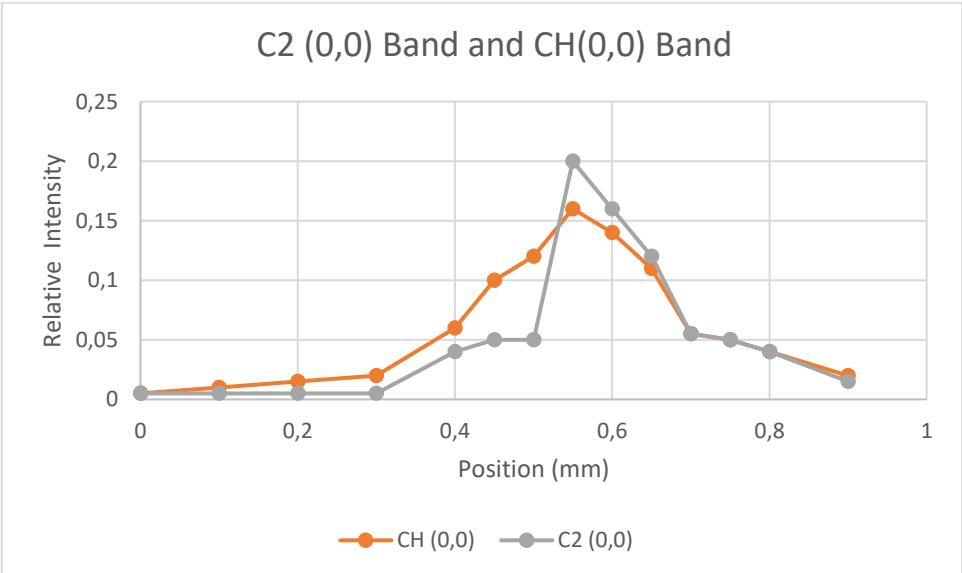

Figure 41: Spatially resolved measurements of relative concentration of the (0,0) transitioning CH radical and the (0,0) transitioning C_2* radical across the V-flame front of equivalence ratio 0.8.*

Fig.42 depicts the Spatially resolved measurements of relative concentration of the C_2* radicals belonging to the ΔV =0 sequence across the flame front of the V-flame of equivalence ratio 0.8 discussed above.

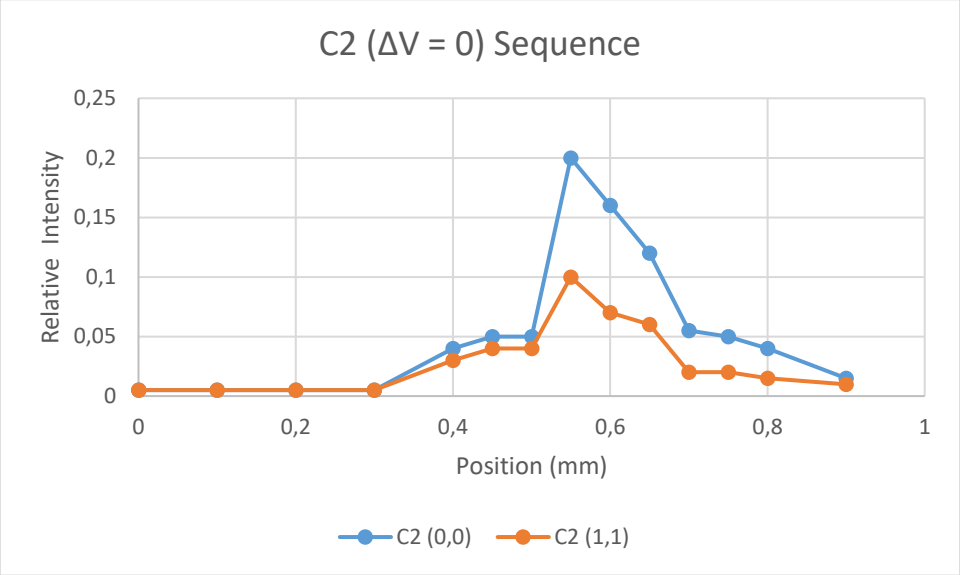

Figure 42: Spatially resolved measurements of relative concentration of the C_2 radicals belonging to the ΔV =0 sequence across the flame front of the V-flame of equivalence ratio 0.8.*

A similar procedure is repeated for a conical flame having an equivalence ratio of 1.0, as shown in Fig.43.

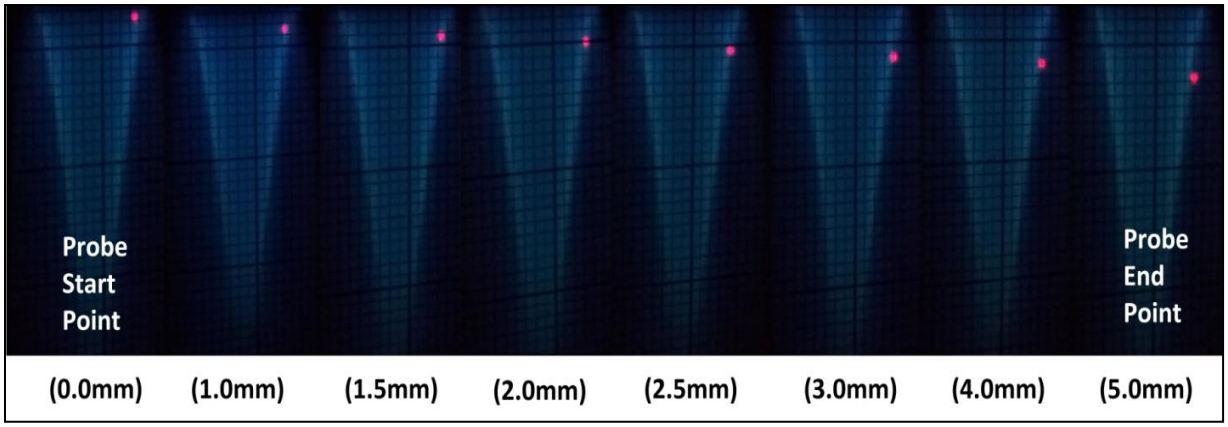

Figure 43: The image of the Conical Flame as seen by the fibre optic probe head. The laser pointer indicates the point on the flame being captured by the probe head.

The probe start point is at 0.0mm from the base of the flame cone, such that this point lies in the cold unburnt gas region. Gradually it is traversed linearly such that it cuts through all the flame zones as discussed above. Between 1mm and 3mm, the probe is traversed in steps of 0.5 mm. The final point is at 5mm from the cone base, this point lies in the product zone.

Fig.44 depicts the Spatially resolved measurements of relative concentration of the (0,0) transitioning CH* radical and the (0,0) transitioning C_2* radical across the flame front of the conical flame of equivalence ratio 1.0 discussed above

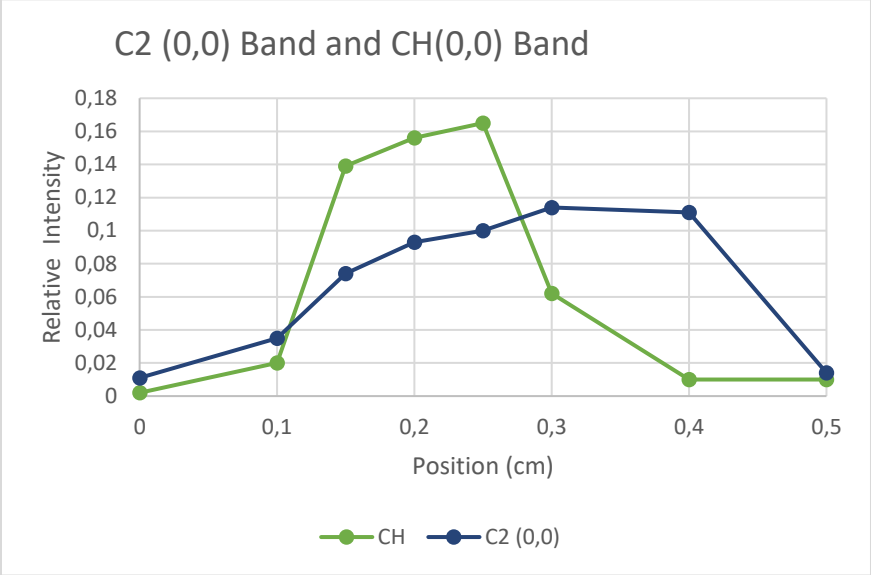

Figure 44: Spatially resolved measurements of relative concentration of the (0,0) transitioning CH radical and the (0,0) transitioning C_2* radical across the Bunsen flame front of equivalence ratio 1.0.*

The following images, Fig.45, 46 and 47 depict the Spatially resolved measurements of relative concentration of the C_2* radicals belonging to different sequences(ΔV = -1,0,+1), across the flame front of the conical flame of equivalence ratio 1.0 discussed above.

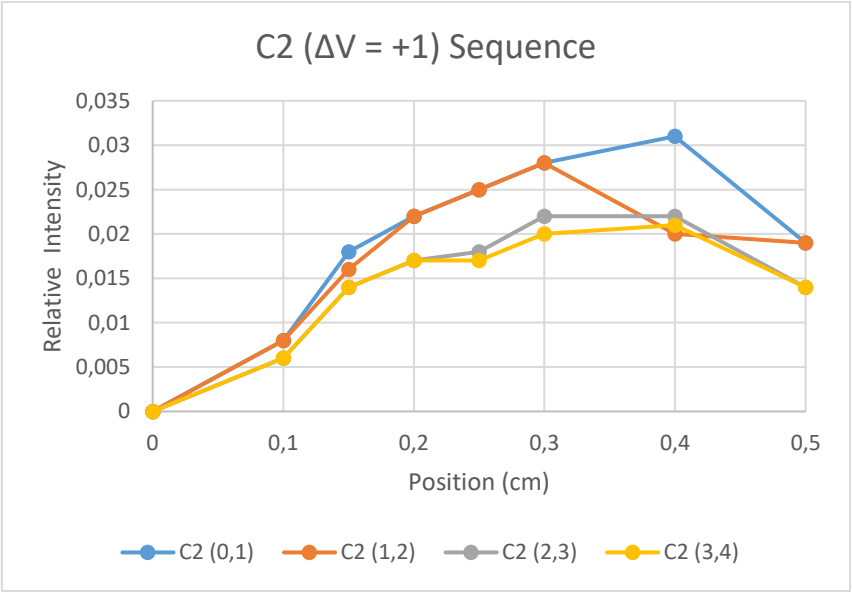

Figure 45: Spatially resolved measurements of relative concentration of the ΔV = +1 sequence of the C_2 radical across the flame front.*

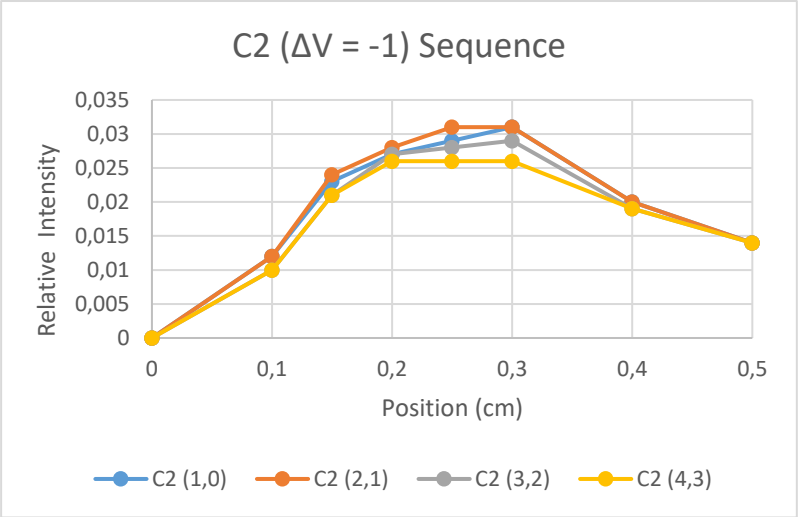

Figure 46: Spatially resolved measurements of relative concentration of the ΔV = -1 sequence of the C_2 radical across the flame front.*

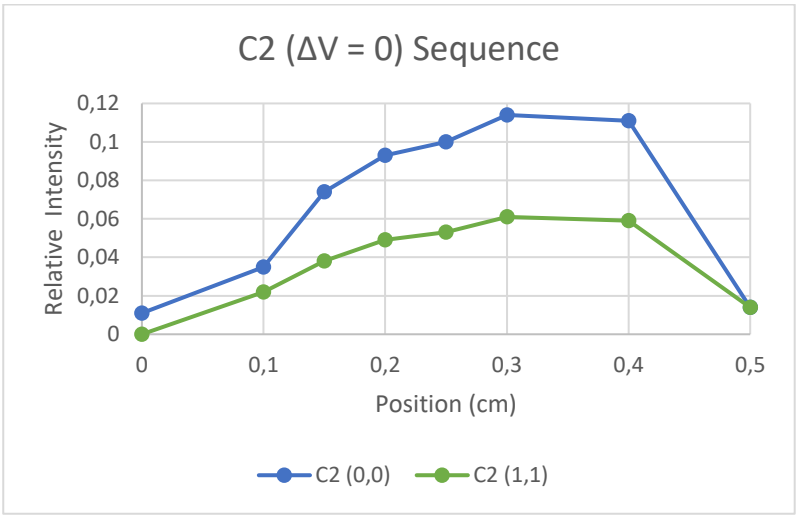

Figure 47: Spatially resolved measurements of relative concentration of the ΔV = 0 sequence of the C_2 radical across the flame front.*

The following inferences are made from the results obtained in Section 7.1 :

- There is almost zero spectral emissions in the visible wavelength from the cold gas zone.

- Just at the beginning of the preheat zone slight emissions from the CH radical is seen and this grows until the mid-reaction zone. The emission from the C_2 radical in this zone is almost zero.

- Post this zone, the emission intensity from the C_2 radical is more dominant and peaks higher than the CH radical throughout.

- After the reaction zone ends, once again in the product zone, the radical emissions start subsiding gradually and reach zero finally.

7.2 Thermometry using the recorded experimental spectrum

In a combustion process the existence of a thermal equilibrium results in a dependence of the number density of different species formed during combustion on the flame temperature. The relative spectral line intensities observed from flame emission spectrum is a representative of the relative number density of different species formed in the combustion process. Hence using this correlation, the flame temperature can be inferred by making use of the Boltzmann law which connects the thermodynamic temperature(rotational/vibrational temperature) and the relative number density of different chemical species formed in the reaction. The thermodynamic temperatures of such combustion flames are determined by making spectroscopic quantitative measurements on the relative line intensities of spectra emitted by the C_2 radical.

In this study, temperature measurements will be made by comparing the theoretically modelled spectra with the experimentally recorded spectra, using the Nelder-Mead Temperature(NMT) Program discussed in Section 6.4. An example of such a comparison to estimate rotational temperature is shown below in Fig.48.

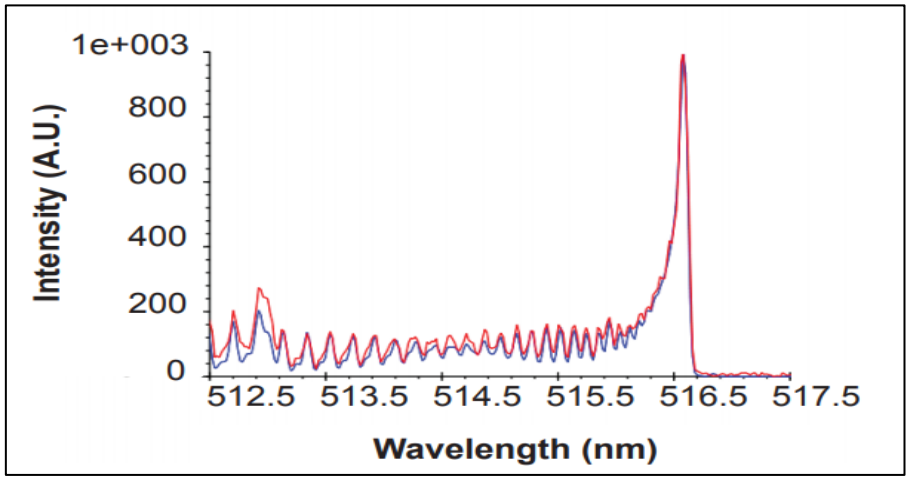

Figure 48: Experimental C_2 spectrum(red line) with instrumental resolution of 0.061 nm superimposed to a synthesized spectrum computed(blue line) with rotational temperature of 1850 K and spectral resolution of 0.061 nm after the matching operation. [2]*

7.2.1 Spectral sensitivity of the results

For accurate estimation of different thermodynamic temperatures, the spectral region sensitive to the required temperature(rotational/vibrational) has to be selected for computation.

- The **vibrational temperature, T_v**, is a function of the relative heights/integral intensities of two band heads with different initial vibrational quantum numbers.
- The band tails are due to sub-transitions between different rotational quantum numbers and are the small frequent overlapped peaks decaying to the left of the band head. The

-elative height of the individual spectral lines spread the between the band head to the band tail is sensitive to the **rotational temperature, T_r**.

7.2.2 Computation of vibrational temperature from spectrum

Some important points to be noted from past research in T_v computation:

- Within a single sequence, the band intensities are more a reflection of T_v [49].
- The vibrational temperature data of the C_2 molecules are also different depending on the sequence [50].

In this study, the vibrational temperature was measured from Δv=0 sequence transitions of the C_2 molecule, observed between 500-520 nm as shown in Fig.49

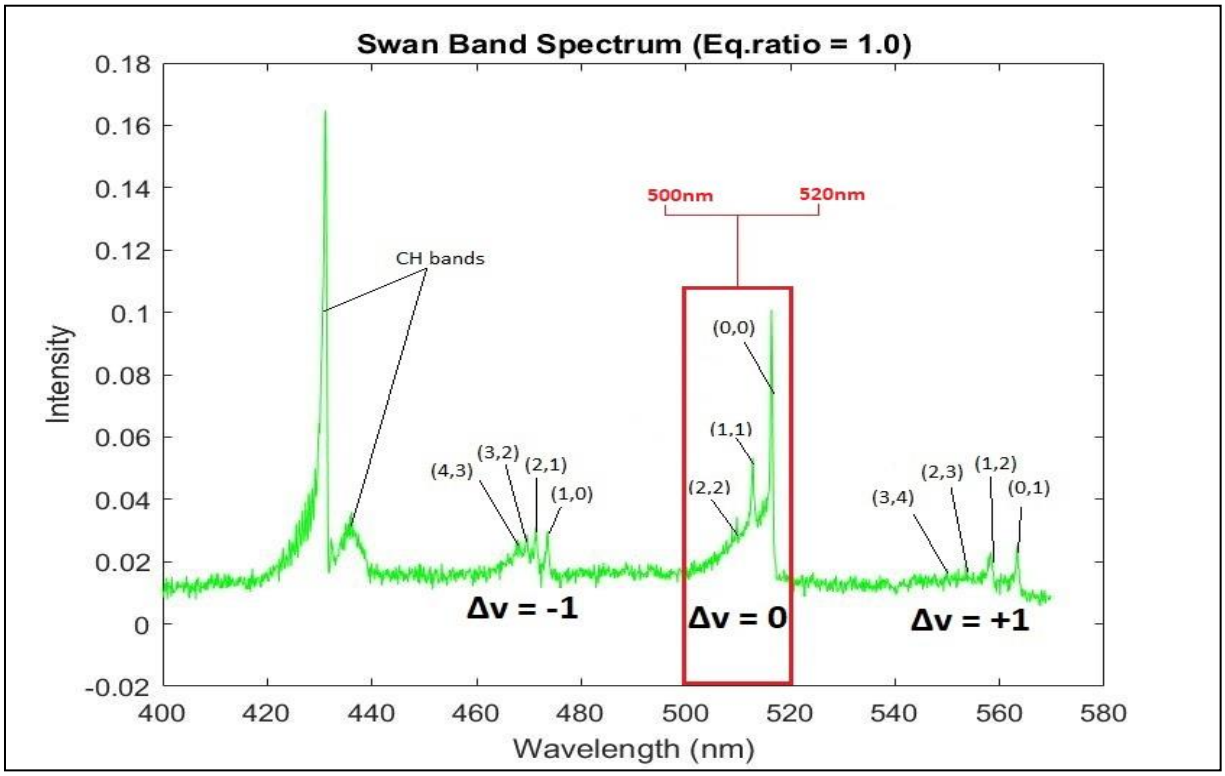

Figure 49: Swan Band Spectrum captured at the reaction zone of the flame. The square indicates the region of the spectrum sensitive to vibrational temperature.

The Δv=0 sequence transitions include the (0,0), (1,1) and (2,2) Vibrational transitions of the C_2 radical. The vibrational temperature is extracted for premixed laminar methane-air flames of a range of equivalence ratios between 0.9 and 1.35. This vibrational temperature is plotted against the equivalence ratio as shown in Fig.50.

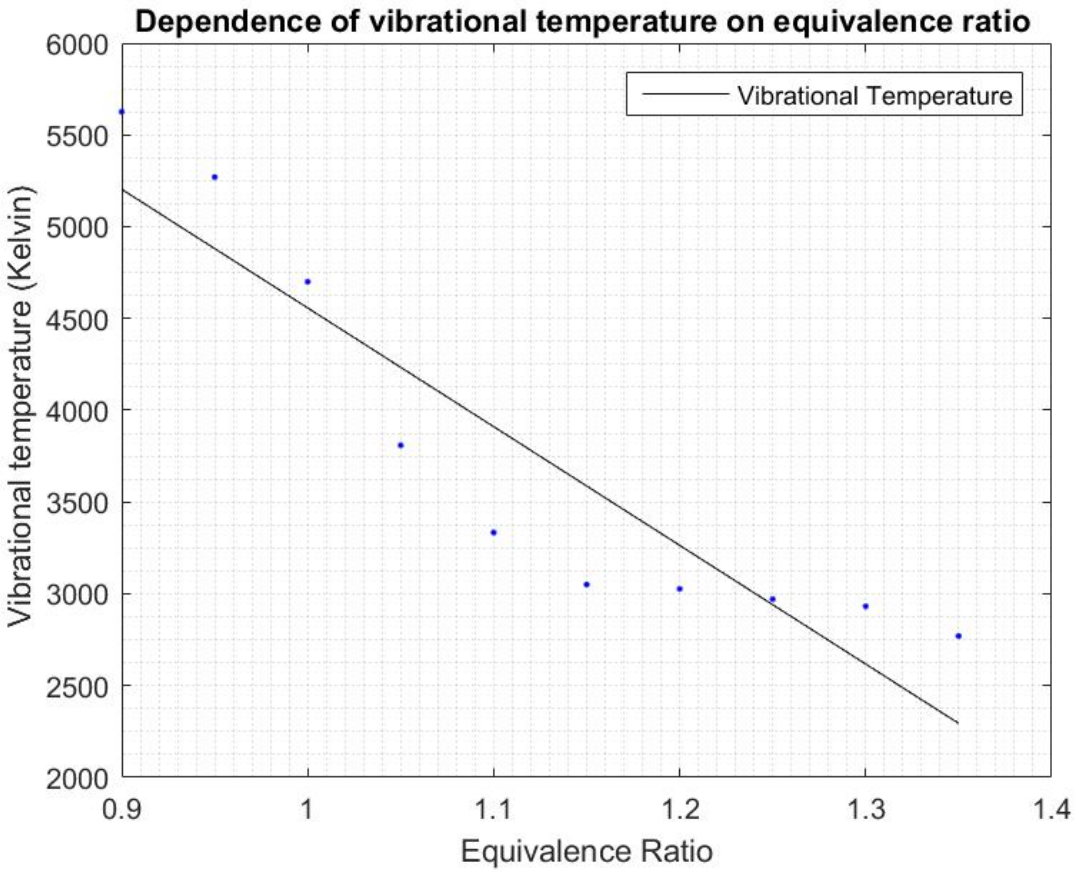

Figure 50:Dependence of vibrational temperature on the equivalence ratio. (The blue dots show the exact values obtained from the experimentally recorded spectrum, the black line is fitted to these dots as a linear polynomial)

7.2.3 Computation of rotational temperature from spectrum

The rotational temperature can be determined by exploiting the relative height of the individual spectral lines(which consists two different branches of lines called P and R lines) spread the between the band head to the band tail of a single band in a sequence.

Some important points to be noted from past research in T_r computation:

- The ratio (P/R) of the peak intensities of the P and R branches have strong dependence on the rotational temperature [49].
- Commonly the peaks of (0, 0) Swan band spectrum between 515 -517 nm as shown in Fig.51 are used in the determination of rotational temperature because this range encompasses enough "thermometric peaks"(peaks whose relative intensities are more sensitive to changes in the rotational temperature) [51].

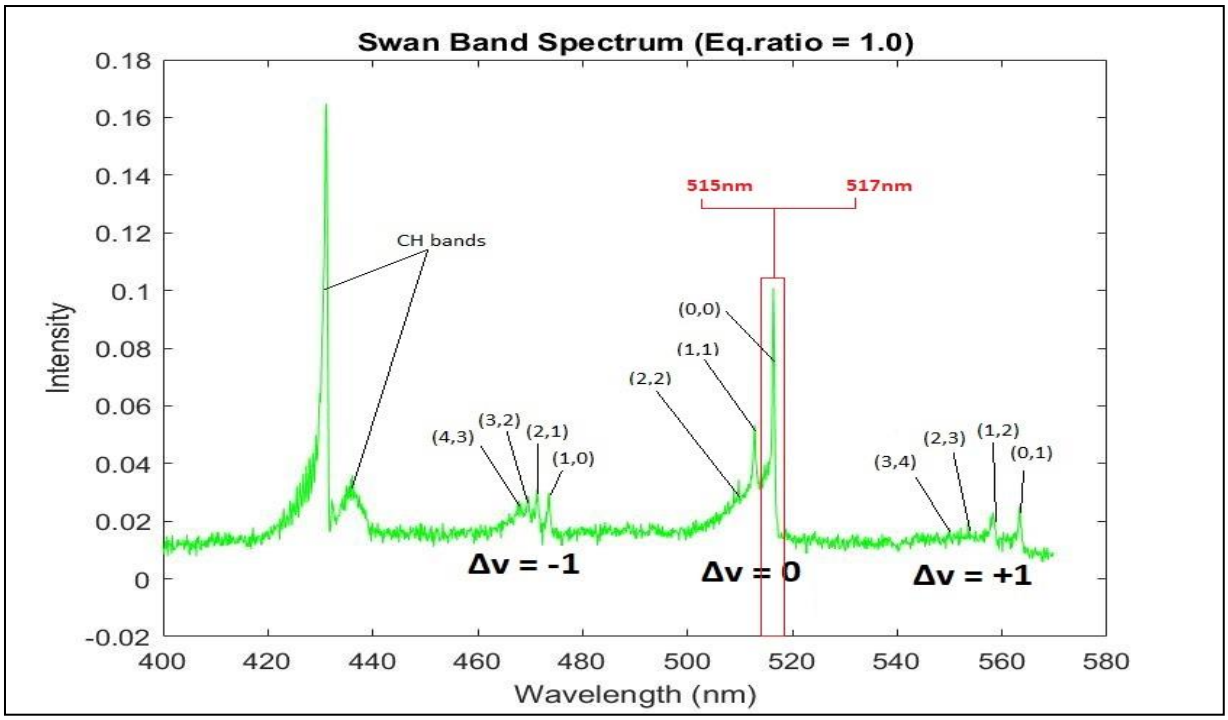

Figure 51: Swan Band Spectrum captured at the reaction zone of the flame. The square indicates the region of the spectrum sensitive to rotational temperature.

The rotational temperature is extracted for premixed laminar methane-air flames of a range of equivalence ratios between 0.9 and 1.35. This rotational temperature is plotted against the equivalence ratio as shown in the Fig.53 below.

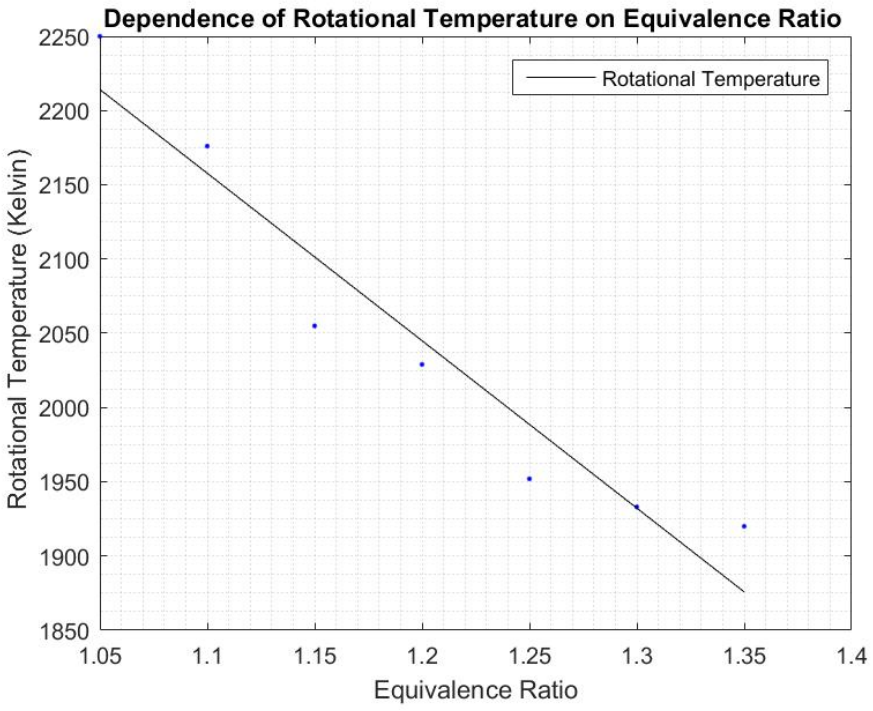

Figure 52: Dependence of rotational temperature on the equivalence ratio. (The blue dots show the exact values obtained from the experimentally recorded spectrum, the black line is fitted to these dots as a linear polynomial)

7.2.4 Relationship between the rotational temperature and the adiabatic flame temperature

It has been often proved by various research studies that there exists a strong coupling between the translational and rotational energy states of excited radicals in flames, since they take very few collisions to equilibrate. Hence, the rotational temperature deduced from experimental spectra can very often be regarded to be equal to the translational temperature(also called as gas kinetic temperature).

Determination of C_2* Rotational Temperature(T_r) for different equivalence ratios and analysing the degree of agreement with the adiabatic flame temperature(gas kinetic/translational temperature) at the respective spatial location, by fitting the recorded experimental spectrum to a simulated theoretical spectrum, would be of interest in this study. The temperature is extracted at the reaction zone of methane–air flames of different equivalence ratios and the degree of agreement with the adiabatic flame temperature is studied.

The right-hand side of Fig.53 shows the change of rotational temperature with equivalence ratio and the left-hand side of Fig.53 shows the Adiabatic flame temperature plotted as a function of the fuel equivalence ratio ϕ (taken from literature) [52].

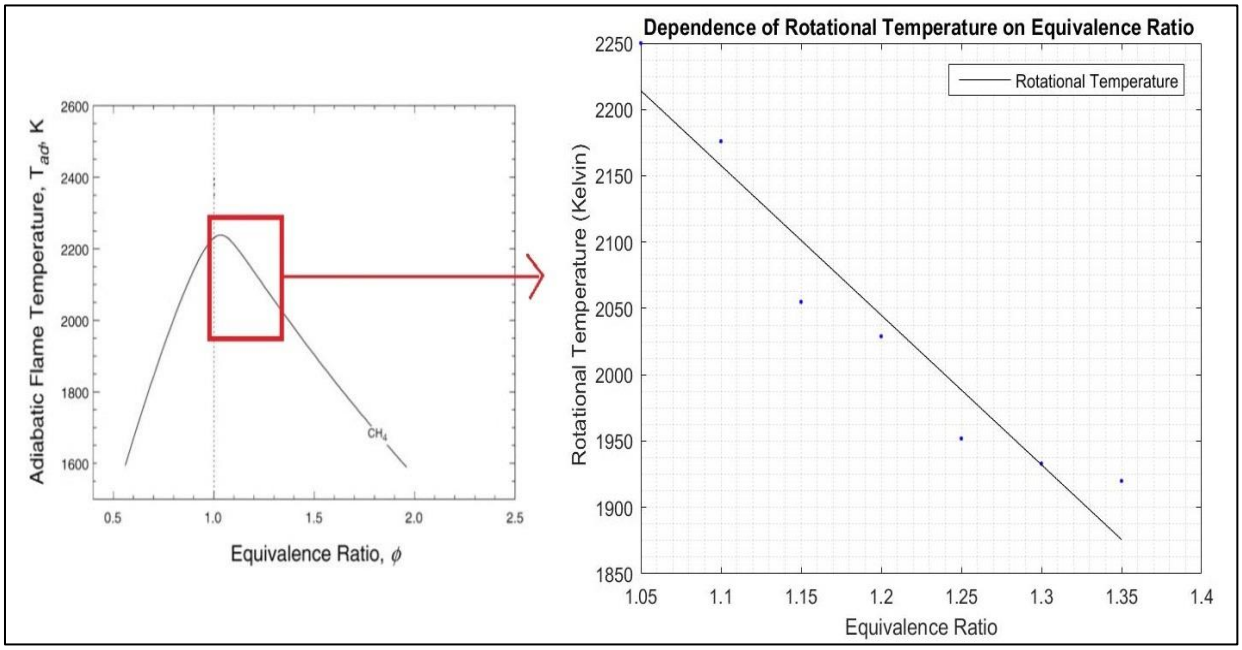

Figure 53: Left-Adiabatic flame temperature plotted as a function of the fuel equivalence ratio φ for several fuel/air mixtures at STP. Right-Rotational temperature plotted as a function of equivalence ratios between 0.95 and 1.35.

Fig.54 gives the reader an idea about the agreement of the adiabatic flame temperature with the rotational temperature.

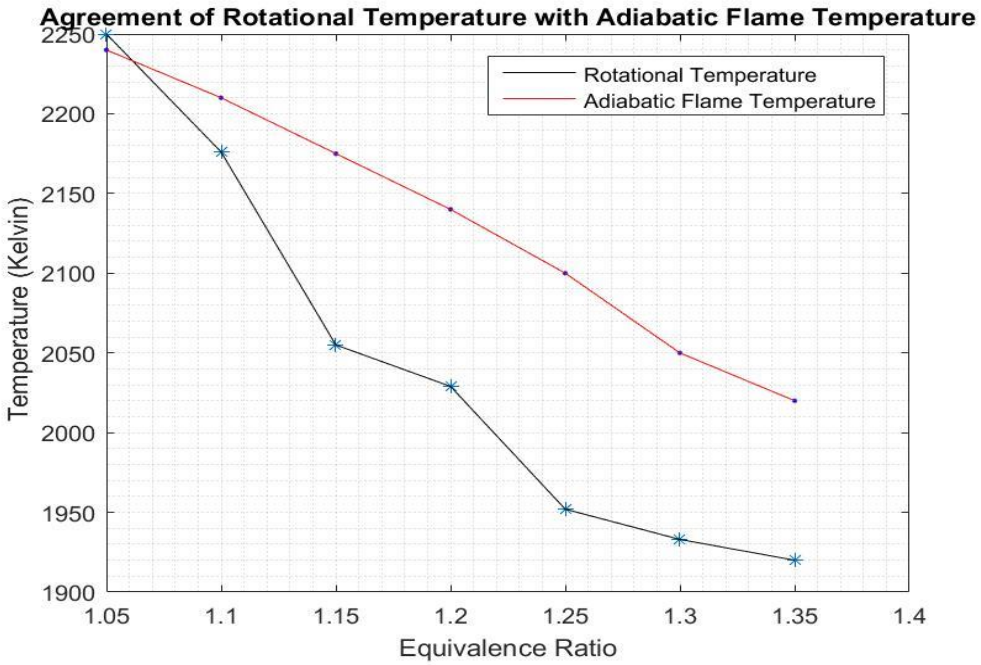

Figure 54: Agreement of the adiabatic flame temperature with the rotational temperature, plotted as a function of equivalence ratio.

Equivalence Ratio	Rotational Temperature (K)	Adiabatic Temperature (K)	Deviation of Rotational Temperature from Adiabatic Temperature	% Deviation
1.05	2250	2240	10	0.45
1.10	2176	2210	34	1.54
1.15	2055	2175	120	5.52
1.20	2029	2140	111	5.19
1.25	1952	2100	148	7.05
1.30	1933	2050	117	5.71
1.35	1920	2020	100	4.95
			Mean Percentage Deviation =	4.3 %

Table 1: Deviation of Rotational Temperature from Adiabatic Temperature.

The following inferences are made from the results obtained in Section 7.2 :

- There is a close agreement between rotational temperatures and adiabatic flame temperature in combustion processes. The mean deviation between the two temperature values is only about 4.3% for the entire range of equivalence ratios between 1.05 and 1.35. This range is the supposedly the rich combustion regime wherein the Swan band emission signal intensity is strong.

- The vibrational temperature is always much higher than the adiabatic flame temperature, since it takes much longer to equilibrate with the mean thermodynamic temperature.

- The computation of rotational temperature using chemiluminescent spectra is limited only to the flame reaction zone, as this is the only zone where intermediate radicals are formed in excited states, thereby emitting spectra when they undergo transition to lower energy levels.

7.3 Determination of equivalence ratio across the flame front

The spectrally resolved chemiluminescent spectra in the reaction zone of a laminar premixed methane/air flame can be used for investigating the stoichiometry at the flame front [48]. The peak intensity of each band spectrum is strongly correlated to the equivalence ratio. Calibration equations obtained from the laminar flame measurements can be exploited to ascertain the local equivalence ratio in premixed flames [53]. This behaviour can be attributed to the fact that the relative vibrational band peak intensities depends on the relative radical populations in the corresponding vibrational levels, which is a function of the flame zone temperature, wherein the flame temperature is a function of the equivalence ratio. This functional dependency can be represented as follows:

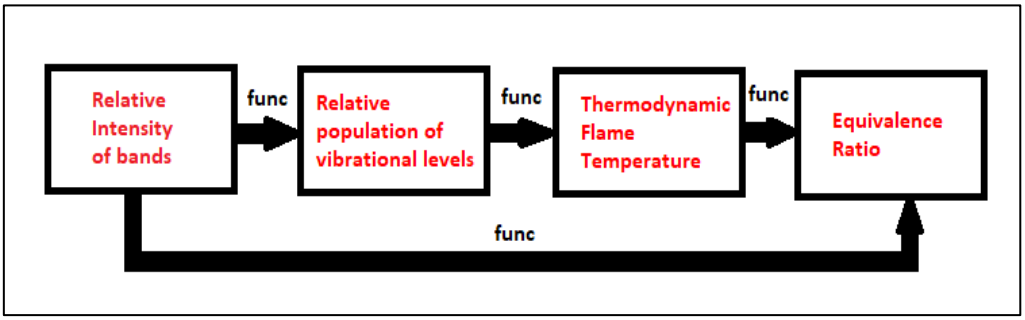

Figure 55: Dependency chain between relative band intensity and equivalence ratio

Fig.56 shows the premixed laminar methane-air flames of different equivalence ratios photographed during this study :

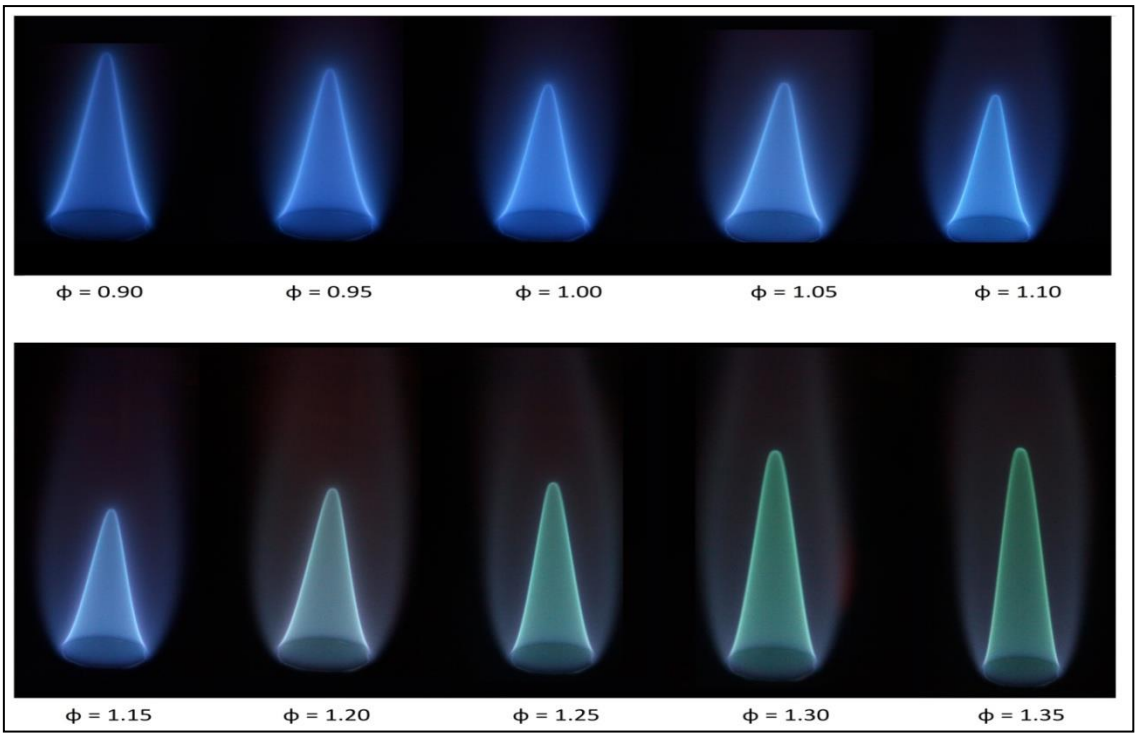

Figure 56: Premixed laminar methane-air flames of different equivalence ratios

The following Figures, Fig.57a) to Fig.57i) depicts the change of spectra with the equivalence ratio. This emission spectra was recorded at a point in the reaction zone.

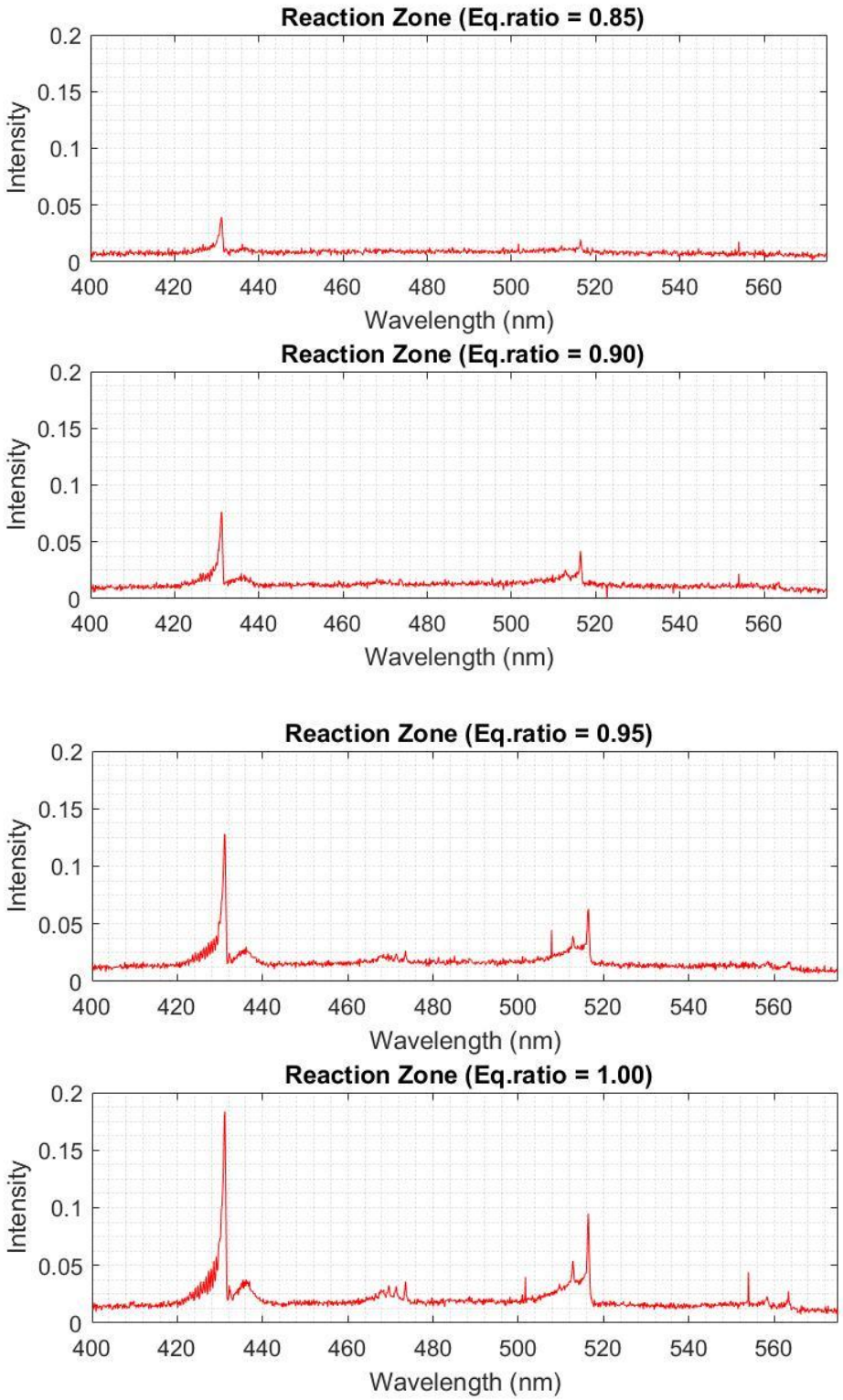

Figure 57: a),b),c),d) - Change of methane-air spectrum with equivalence ratio.

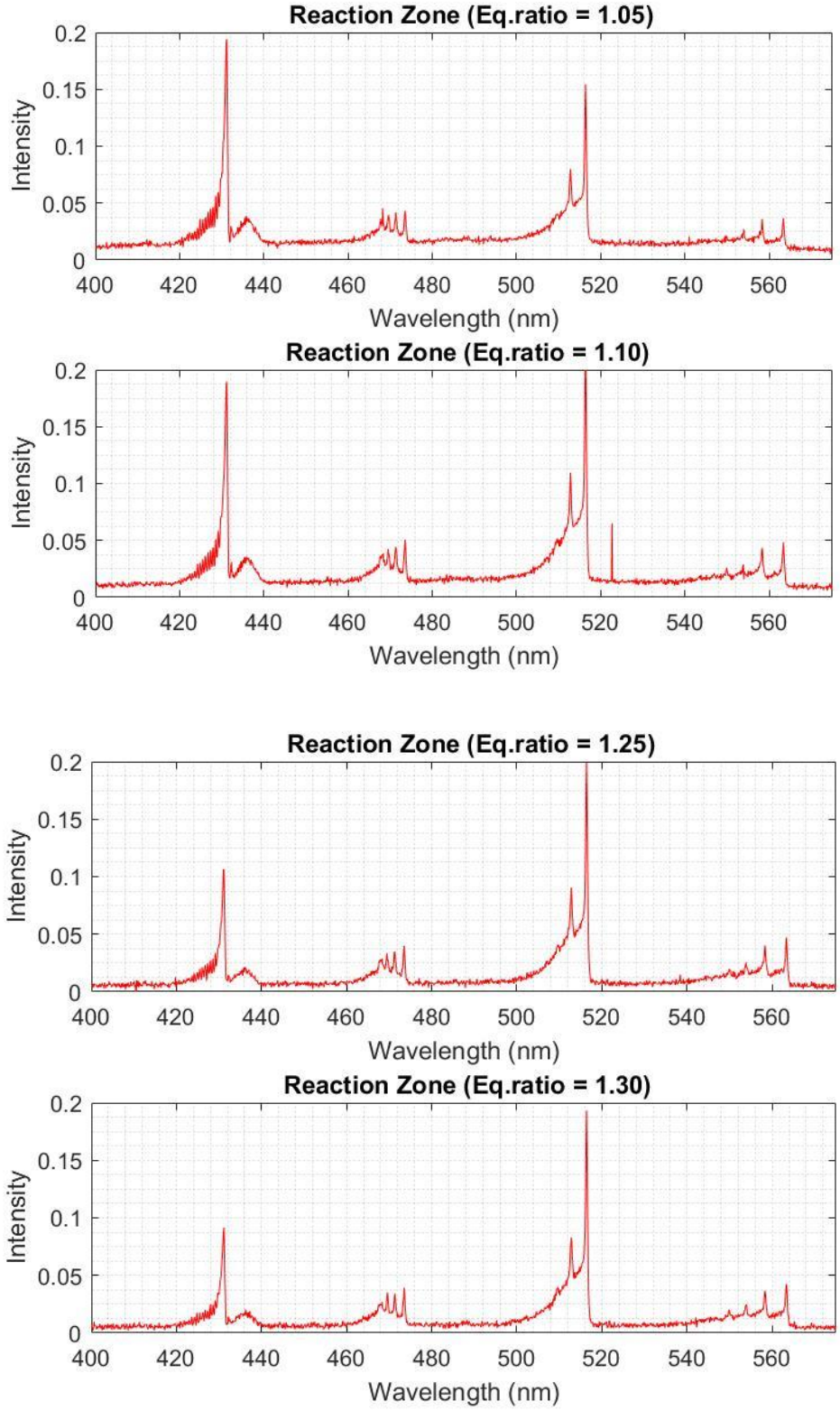

Figure 57: e),f),g),h) - Change of methane-air spectrum with equivalence ratio

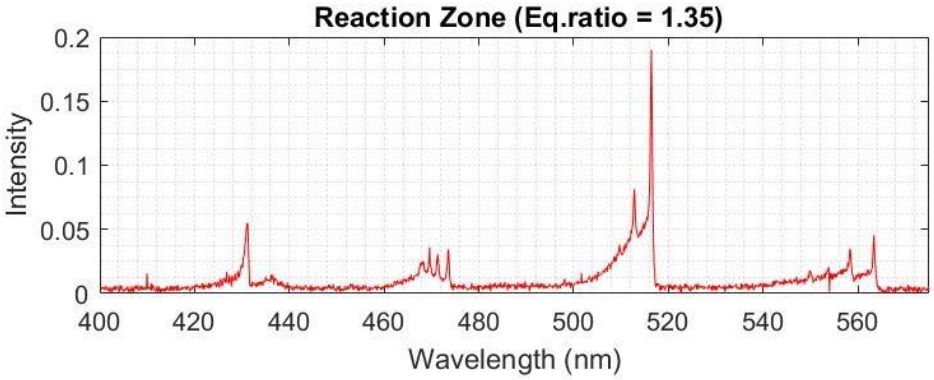

Figure 57: i) - Change of methane-air spectrum with equivalence ratio

7.3.1 C_2* peak and band intensity ratios versus local flame stoichiometry

The Fig.58 below, taken from literature, depicts the dependence of peak intensities of every C* vibrational band emission on the local equivalence ratio, this is of interest to this study, as the swan band transitions are under observation.

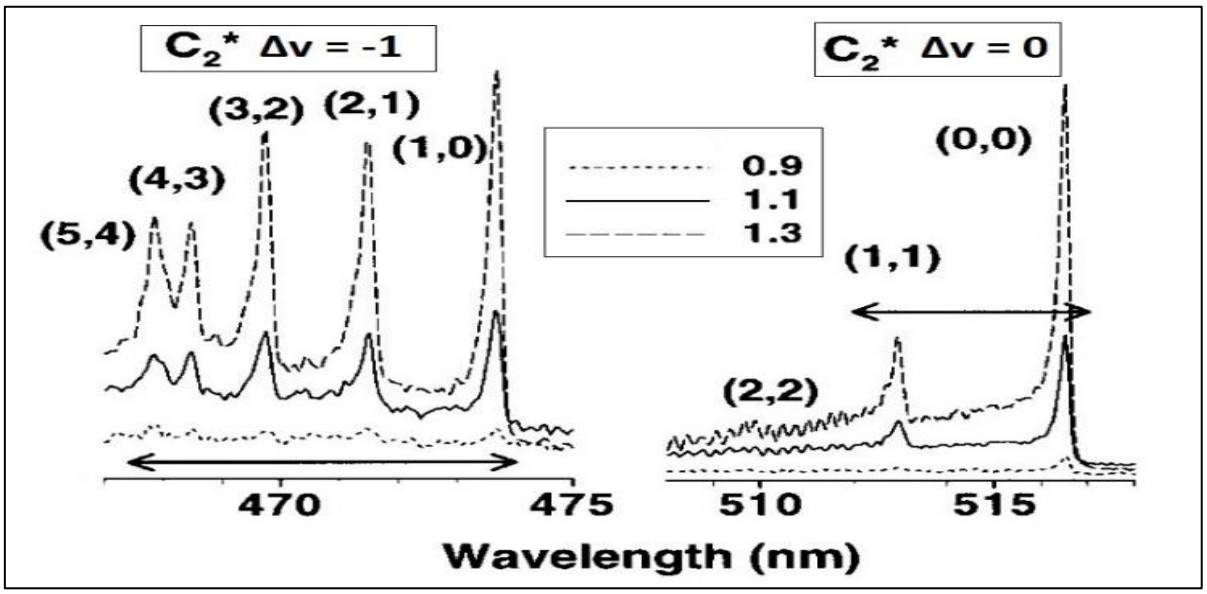

Figure 58: : Spectrally resolved flame spectra (1200 lines/mm) obtained within the reaction zone at different equivalence ratios of 0.9, 1.1 and 1.3. The arrows show the spectral integration range for each emission band, here denoted band [48].

In Fig.59 below, the (1, 1) swan band with spectrally integrated spectra intensity between 467.5 and 474.0 nm, and the (0, 0) swan band with spectrally integrated spectra intensity between 512.0 and 517.0 nm, are used to establish a relationship between their relative emission intensities and the local equivalence ratio.

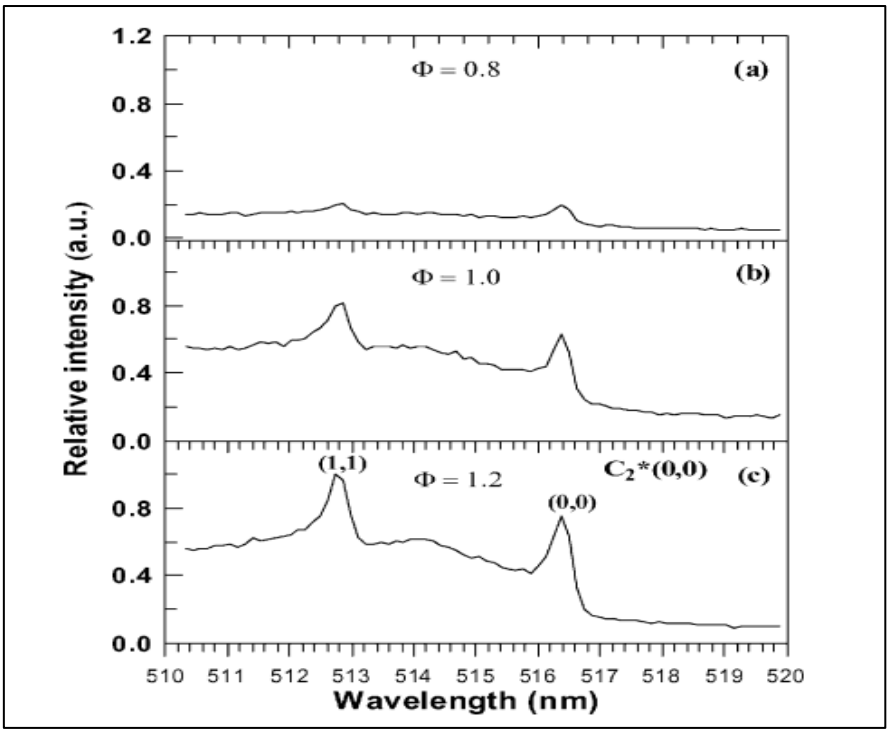

Figure 59: Flame emission spectra of C_2 (0, 0) and (1,1) band measured from laminar methane-air flames at (a) Φ = 0.8, (b) Φ = 1.0, (c) Φ = 1.2. [53]

In this study, a similar observation of the peak intensities of the (0,0) and (1,1) C_2 band, for different equivalence ratios was made and the peak intensity ratio data is tabulated below :

Equivalence Ratio	**C_2 (0,0) Peak Intensity**	**C_2 (1,1) Peak Intensity**	**C_2(0,0)/C_2(1,1) Peak Intensity Ratio**
0.85	0.019	0.013	1.52
0.90	0.042	0.025	1.68
0.95	0.062	0.039	1.58
1.00	0.095	0.053	1.79
1.05	0.154	0.080	1.92
1.10	0.225	0.110	2.04
1.15	0.245	0.112	2.18
1.20	0.223	0.101	2.20
1.25	0.198	0.091	2.17
1.30	0.194	0.082	2.36
1.35	0.189	0.079	2.39

Table 2: C_2(0,0)/C_2(1,1) Peak Intensity Ratio Data

The peak emission intensity ratio of (0,0) transition and the (1,1) transition of the C_2 radical is plotted against the equivalence ratio as shown in the Fig.60 below :

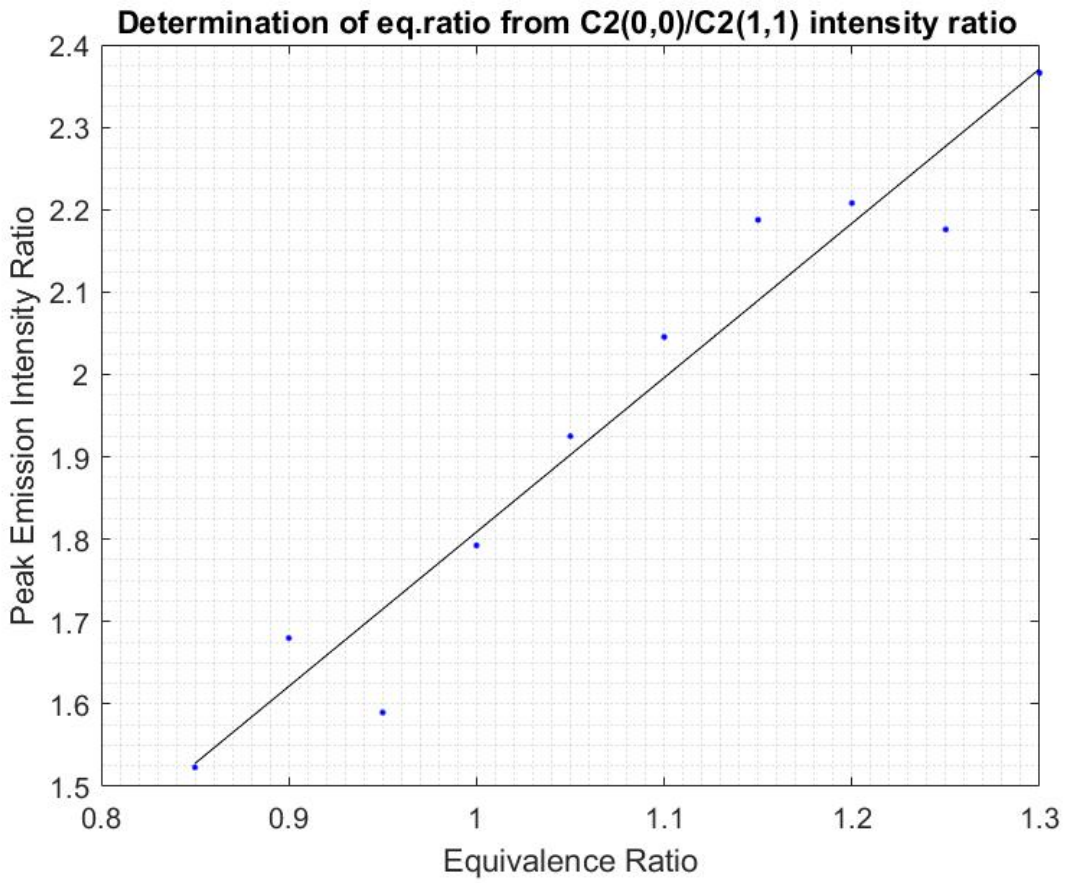

Figure 60: C_2(0,0)/C_2(1,1) peak intensity ratio vs equivalence ratio. (The blue dots show the exact values obtained from the experimentally recorded spectrum, the black line is fitted to these dots as a linear polynomial)

7.3.2 [C_2*/CH*] peak and band intensity ratios versus local flame stoichiometry

The Fig.61 below shows that the relation between the C_2*/CH* peak intensity ratio(represented by hollow shapes) to the equivalence ratio and the relation between the C_2*/CH* band integrated intensity ratio(represented by solid shapes) to the equivalence ratio. In this Figure peak ratios are represented by hollow shapes and spectrally integrated band intensity ratios are represented by solid shapes. There is not much difference observed between the usage of either method. A comparison of these correlations showed almost no difference between the peak curves and band curves. [48]

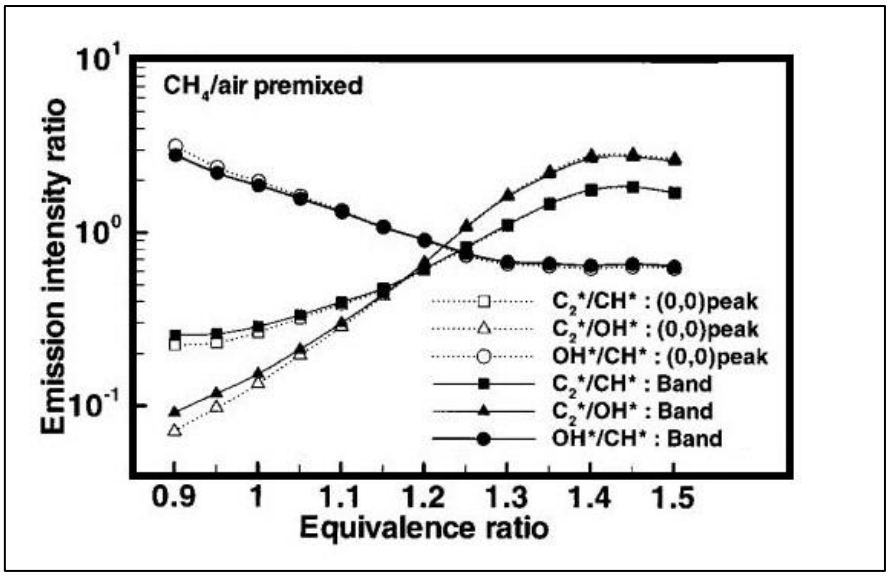

Figure 61: Correlation of the chemiluminescent emission intensity ratios (log [C_2/CH*], log[C_2*/OH*], and log[OH*/CH*]) to the equivalence ratio. Peak means the maximum intensity of each branch of the spectra. Band means the spectrally integrated emission [48].*

It can be seen that the correlation between the intensity ratio and the equivalence ratio is almost linear until $\Phi = 1.35$. This high degree of correlation indicates that the local flame stoichiometry in premixed flame fronts can be determined by spatially resolved chemiluminescence measurements [48]. In case of methane/air flames this linear correlation is applicable until the equivalence ratio becomes 1.35. Also, it is to be noted that this correlation using C_2*/CH* remains unaffected by self-absorption because the self-absorption of these radicals is negligible in small flames [54]. In this study, a similar observation of the peak intensities of the (0,0) C_2 band and (0,0) CH band, for different equivalence ratios was made and the peak intensity ratio data is tabulated below in Table 4.

Equivalence Ratio	**C_2 (0,0) Peak Intensity**	**CH (0,0) Peak Intensity**	**C_2(0,0)/CH(0,0) Peak Intensity Ratio**
0.85	0.019	0.040	0.49
0.90	0.042	0.076	0.55
0.95	0.062	0.130	0.47
1.00	0.095	0.183	0.51
1.05	0.154	0.192	0.80
1.10	0.225	0.185	1.21
1.15	0.245	0.160	1.53
1.20	0.223	0.135	1.65
1.25	0.198	0.105	1.88
1.30	0.194	0.090	2.15
1.35	0.189	0.051	3.70

Table 3: C_2(0,0)/CH(0,0) peak intensity ratio data

The peak emission intensity ratio of (0,0) transition of the C_2 radical and the (0,0) transition of the CH radical is plotted against the equivalence ratio as shown in Fig.62(right) below. The left-hand side of Fig.62 shows the same relationship taken from literature [48].

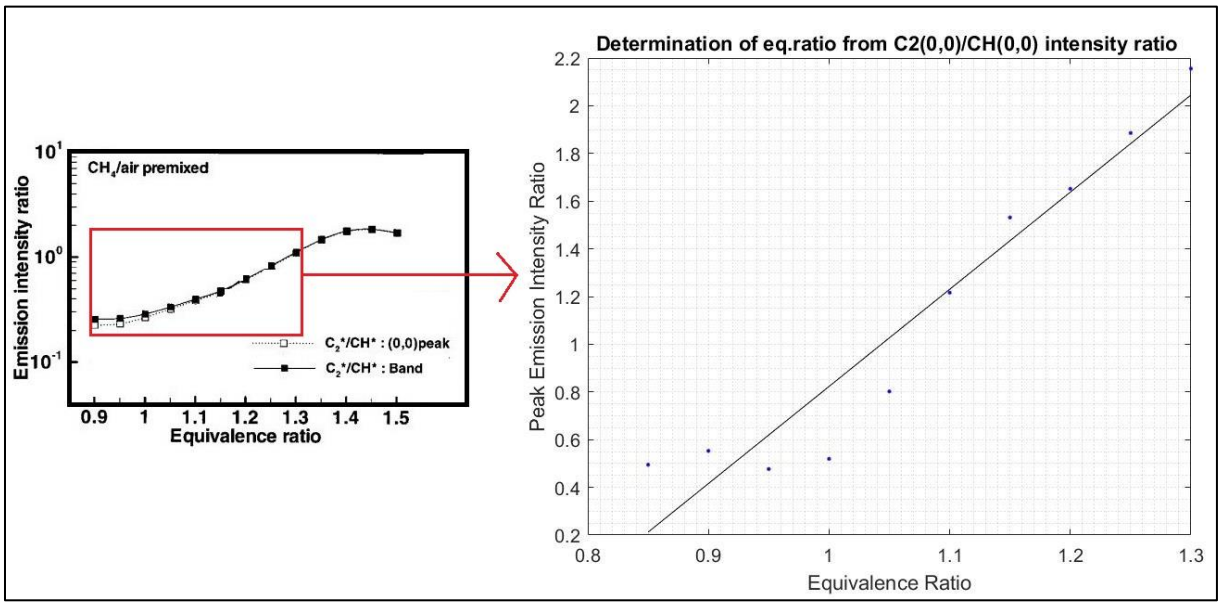

Figure 62: C_2(0,0)/CH(0,0) peak intensity ratio vs equivalence ratio (left- from literature[48], right-extracted from experimentally recorded spectrum)

The following inferences are made from the results obtained in Section 7.3 :

- The relative emission peak intensities of different radicals formed as intermediates in combustion is a function of the equivalence ratio. The relative emission peak intensities of different radicals depends on the relative radical populations of the corresponding energy levels.

- In lean combustion, for $\varphi<1$, the CH emission intensity is higher than the C_2 emission intensity.

- In rich combustion, for $\varphi<1.1$, the C_2 emission intensity is higher than the CH emission intensity.

- Still, between $\varphi=1$ and $\varphi=1.1$, the CH emission intensity is greater to that of the C_2 emission intensity.

- C_2(0,0)/C_2(1,1) Peak Intensity Ratio and the C_2(0,0)/CH(0,0) Peak Intensity Ratio has a high degree of correlation with the equivalence ratio, this correlation indicates that the local flame stoichiometry in premixed flame fronts can be determined by spectrally resolved chemiluminescence measurements.

Chapter 8. Conclusions and Recommendations

In this chapter the thesis study is concluded, highlighting the main contributions of the research work performed. Further possibilities of research in this arena are then discussed.

8.1 Conclusions

This thesis work has successfully investigated the feasibility of using chemiluminescent spectrum emitted by combustion flames as a tool for studying spatial distribution of radicals, analysing local flame stoichiometry and measurement of local flame temperature.

An experimental set-up was proposed to capture the emission spectra of a premixed, laminar, methane-air Bunsen flame at various spatial locations across the geometry of the flame. The emission spectra was analysed thoroughly to achieve the research objectives. Then a theoretical spectrum was synthesized, and the experimental spectra was fitted to it using open source software and spectroscopic thermometry was performed as well. The following important conclusions were drawn from this study:

- In combustion, local flame emission spectrum can be effectively exploited to study the local flame chemistry. The spatially resolved intensity profiles of the chemiluminescent C_2* radical and CH* radical across the reaction zone of a premixed laminar methane-air flame were experimentally recorded. Just at the beginning of the preheat zone slight emissions from the CH* radical is seen, and this grows until the mid-reaction zone. The emission from the C_2* radical in this zone is almost zero. Post this zone, the emission intensity from the C_2* radical is dominant and peaks higher than the CH* radical. This C_2* and CH* distribution is found to be in accordance with the way intermediate combustion reactions proceed across the reaction zone of a premixed laminar methane-air flame front.

- There is a strong correlation between peak intensity ratios of intermediate radicals and the local equivalence ratio. In this study the C_2*(0,0)/C_2*(1,1) peak intensity ratio and the C_2*(0,0)/CH*(0,0) peak intensity ratio were analysed in the flame front, it proved to have a high degree of correlation with the local equivalence ratio, this correlation indicates that the local flame stoichiometry in premixed flame fronts can be determined by spatially resolved chemiluminescence measurements.

- The use of C_2* radical emission spectra from the combustion flame front, for spectroscopic thermometry was presented. The presented methodology was able to extract the C_2* vibrational and rotational temperature for different equivalence ratios. It has been shown that there is a very close agreement between the rotational

temperature and the adiabatic flame temperature for the entire range of equivalence ratios in fuel rich combustion, wherein the Swan band emission signal intensity is strong. The average deviation of the extracted rotational temperature from the theoretical adiabatic temperature is only about 4.3%. Rotations and translations take very few collisions to exchange energy to establish a state of local thermal equilibrium, and so they are almost equal to each other. Due to the larger amounts of energy exchanged vibrations take longer to equilibrate thermally.

- The reaction zone emission thickness of the C_2 radical from literature is found to be only about 190 µm at $\varphi = 1.1$ and 280 µm at $\varphi = 1.5$. Hence, in order to perform such fine translational measurements with a "point"-measurement probe on the 2-D flame stabilized over the Bunsen burner, a translation stage with micrometer resolution is required. However, a millimeter translational stage has been used in this study as only this type of stage was available.

8.2 Future Recommendations

- The C_2*/OH* curve is more sensitive to local equivalence ratio and OH*/CH* curve is more reliable for determining local equivalence ratio in lean conditions($\varphi<0.9$) as the C_2* emission intensity is to weak in lean conditions. However, in this study, the comparatively less sensitive C_2*/CH* curve was used to establish a relationship between the emission intensity ratio of these radicals and the local equivalence ratio, due to the limitation that OH* emission spectra does not lie in the visible light region. And so recording of OH* emission spectrum in the ultraviolet region to investigate the correlation between emission intensity ratio radicals and the local equivalence ratio will prove more efficient. This could be of interest for future study for determination of local equivalence ratio with greater accuracy.

- For any system, complete thermodynamic equilibrium is an ideal situation that becomes more difficult to approach as the temperature of the system increases. In hot molecular gases, the molecules possess translational, rotational and vibrational degrees of freedom. Rotations and translations take very few collisions, only about 5 to 20 collisions to exchange energy to establish a state of local thermal equilibrium, and so they are often treated as having the same temperature. Due to the larger amounts of energy exchanged vibrations take longer to equilibrate thermally. A molecule makes about 400 collisions by the time it crosses the reaction zone. We know that it takes only 5 - 20 collisions for establishment of equilibrium between rotational and translational energies. Thus, theoretically, there cannot exist a state of disequilibrium between rotational and translational temperatures beyond the reaction zone. The extent of existence of such an equilibrium could be verified and studied experimentally by using spectroscopic thermometry.

References

[1] Gregory, O.J., You, T. “Ceramic Temperature Sensors for Harsh Environments” IEEE Sensors Journal Vol. 5(2005): pp 833-838.

[2] Passaro, Angelo, Carinhana Jr, Dermeval, Gonçalves, Enizete Aparecida, Silva, Marcio Moreira da, Guimarães, Ana Paula Lasmar, Abe, Nancy Mieko, & Santos, Alberto Monteiro dos. "The use of molecular spectra simulation for diagnostics of reactive flows." Journal of Aerospace Technology and Management Vol. 3(2011).

[3] Gord, J. R., Fiechtner, G. J. “Emerging Combustion Diagnostics” 39th AIAA Aerospace Sciences Meeting & Exhibit, Reno, USA.(2001): pp. A01-16608.

[4] Ballester, J., García-Armingol, T. “Diagnostic Techniques for the Monitoring and Control of Practical Flames” Progress in Energy and Combustion Science Vol. 36(2010): pp. 375-411.

[5] Guggenheim, Daniel. “AE3051 Experimental Fluid Dynamics - Temperature and Pressure Measurements in a Turbine Engine.” Georgia Institute of Technology.

[6] Kayabaşı, Murat, Brouckaert, J.-F. and Mersinligil, M. “Gas path temperature measurements in high temperature gas turbine environments.” Von Karman Institute Diploma Report (2009).

[7] Scervini, Michele and Rae, Catherine. “An Improved Nickel Based MIMS Thermocouple for High Temperature Gas Turbine Applications.” Journal of Engineering for Gas Turbines and Power Vol. 135(2013).

[8] Cumptsy, Nicholas. "Jet Propulsion": Cambridge University Press, Cambridge(2003).

[9] HEATTOP Project. Work Package 1 - Definitions and Sensor Specifications(2007).

[10] E.Gorton, Robert. “Temperature measurement for aircraft-turbine-engine development.” Experimental Mechanics Vol. 9 (1969).

[11] Childs, P. R. N., Greenwood, J. R. and Long, C. A. “Review of temperature measurement.” Review of Scientific Instruments Vol. 71(2000).

[12] Anonymous. "Laminar Premixed Flames." University of Toronto Lecture Notes <http://arrow.utias.utoronto.ca/~ogulder/ClassNotes6.pdf>.

[13] Jun Kojima, Yuji Ikeda, Tsuyoshi Nakajima. "Basic aspects of OH(A), CH(A) and C2(d) chemiluminescence in the reaction zone of laminar methane-air premixed flames." Combustion and Flame Vol. 140(2004): pp. 34-45.

[14] Swan, William. “On the prismatic spectra of the flames of compounds of carbon and hydrogen.” Transactions of the Royal Society of Edinburgh Vol. 21 (1857): pp. 411–430.

[15] H Nassar. “C_2 Swan spectrum used as a molecular pyrometer in transferred arc and the influence noise to signal ratio on the temperature values.” Journal of Physics Vol.511 (2014).

[16] Uhlenbeck, G.E. and Goudsmit, S. “Replacement of the hypothesis of non-mechanical force through a suggestion in regard to the inner-behaviour of all single electrons.” Naturwissenshaften Vol. 13 (1925): pp. 953-954.

[17] Born, M. and J.R.Oppenheimer. “On the quantum theory of the molecules.” Ann.PhysikVol. 84 (1927): pp. 457-484.

[18] Mavrodineanu, Radu and Boiteux, Henri. “Flame Spectroscopy.” John Wiley and Sons, Inc.,, (1965).

[19] Dickey, F.P and Hoffman, J.M. “Application of phase discrimination method of detection to the study of the spectrum of the OH radical in an oxy-actyleneflame.” Symposium (International) on Combustion Vol. 7 (1958): pp. 938-941

[20] Anonymous."Structure and spectra of diatomic molecules." Zürich, ETH. Lecture Notes <https://www.ethz.ch/content/dam/ethz/special-interest/chab/physical-chemistry/ultrafast-spectroscopy-dam/documents/lectures/spectroscopyFS13/scriptFS13/PCV_Ch3.pdf.>

[21] Morse, Philip M. “Diatomic molecules according to the wave mechanics. II. Vibrational levels .” Physical Review Vol. 34 (1929)

[22] Dunham, J.L. “The energy levels of a rotating vibrator.” Physics Review Vol. 41 (1932): pp. 721-731.

[23] Pekeris, C. L. “The Rotation-Vibration Coupling in Diatomic Molecules.” American Physical Society, Physics Review Vol. 45 (1934): pp. 98-103.

[24] Kratzer, A. “Infrared rotation spectra of hydrogenated halogens.” Z.Physik Vol. 3 (1920): pp. 289-307.

[25] Tipler, Paul A. and Llewellyn. “Ralph A. Modern Physics- 5th Edition” W. H. Freeman and Company.

[26] Demtröder, Wolfgang. "Atoms, Molecules and Photons - An Introduction to Atomic, Molecular and Quantum Physics. 2nd Edition." Springer (2010).

[27] Cooley, Joya. Rovibrational Spectroscopy. <https://chem.libretexts.org/Core/Physical_and_Theoretical_Chemistry/Spectroscopy/Rotational_Spectroscopy/Rovibrational_Spectroscopy>.

[28] Annie, Hanssona and James, K.G.Watson. “A comment on Hönl-London factors.” Journal of Molecular Spectroscopy Vol. 233 (2005) .

[29] Condon, Edward. “A theory of intensity distribution in band systems.” Physics Review Vol. 28 (1926).

[30] Bernath, Peter F. “Spectra of atoms and molecules.”(2016).

[31] Somoza, Mark M. "Franck–Condon principle." <https://en.wikipedia.org/wiki/Franck%E2%80%93Condon_principlE> (2006).

[32] Nikitin, E. E. and Zare, R. N. “ Correlation diagrams for Hund's coupling cases in diatomic molecules with high rotational angular momentum.”Molecular Physics Vol. 82 (1996).

[33] Einstein, Albert. “On the Quantum Theory of Radiation.” PhysikalischeZeitschrift Vol. 18 (1916): pp. 121-128.

[34] Rosmus, P. and H.J.Werner. “Einstein Transition-Probability coefficients in the electronic ground states of the diatomic hydrides.” Journal of Molecular Structure Vol. 60 (1980): pp. 405-408.

[35] Demtröder, W. “Laser spectroscopy : basic concepts and instrumentation.”(1996).

[36] H.P.Broida. “Temperature, Its Measurement and Control in Science and Industry.” Reinhold Publishing Corporation Vol. 2 (1955) .

[37] Goyette, A N, Jameson, W B and Lawler, L W Anderson and J E. “An experimental comparison of rotational temperature and gas kinetic temperature in a H2 discharge.” Journal of Physics D: Applied Physics Vol. 29 (1996).

[38] Smith, W. H. “Transition Probabilities for the Swan and Mulliken C_2 Bands.” Astrophysical Journal Vol. 156.

[39] Broida, Herbert P. and Shuler, Kurt E. “ Spectroscopic Study of Electronic Flame Temperatures and Energy Distributions.” The Journal of Chemical Physics Vol. 27 (1957).

[40] Bohr, N. “On the constitution of atoms and molecules.” Phil.MagVol. 26 (1913): pp. 1-25.

[41] A, Fareed M, et al.“Carbon molecules for intense high-order harmonics from laser-ablated graphite plume.” Journal of Physics B: Atomic, Molecular and Optical Physics Vol. 49 (2016).

[42] Gaydon, A. G. and Wolfhard, H. G. “Spectroscopic Studies of Low-Pressure Flames. III. Effective Rotational Temperatures and Excitation Mechanism for C2 Bands.” Proceedings of the Royal Society of London Vol. 201 (1950).

[43] Thorlabs, Inc. " Thorlabs' manual translation stages." <https://www.thorlabs.com/navigation.cfm?guide_id=2> .

[44] Mengqiu Zhangab, Gang Liab, Shao Hui Wang, Zhigang Fud, Yang Guand, Ling Lin. "The influence of different integration time on stoichiometric analysis in near infrared grating spectrometers." Infrared Physics & Technology Vol. 86 (2017): pp. 130-134.

[45] S Pellerindag, K Musiolddag, O Motretdag, B Pokrzywka and J Chapelledag. "Application of the (0,0) Swan band spectrum for temperature measurements." Journal of Physics D: Applied Physics Vol. 29 (2011).

[46] Christian G.Parigger, Alexander C.Woods, David M.Surmick, Ghaneshwar Gautam, Michael J.Witte, James O.Hornkohl. "Computation of diatomic molecular spectra for selected transitions of aluminum monoxide, cyanide, diatomic carbon, and titanium monoxide" Spectrochimica Acta Part B: Atomic Spectroscopy Vol. 107 (2015): pp. 132-138.

[47] Demtröder, Wolfgang. "Atoms, Molecules and Photons - An Introduction to Atomic, Molecular and Quantum Physics. 2nd Edition." Springer (2010).

[48] Jun Kojima, Yuji Ikeda, Tsuyoshi Nakajima. "Spatially resolved measurement of OH*, CH*, and C_2*chemiluminescence in the reaction zone of laminar methane/air premixed flames." Proceedings of the Combustion Institute Vol. 28 (2000): pp. 1757-1764.

[49] Lambert D. L., Danks A. C. "High-resolution spectra of C2 Swan bands from comet West 1976 VI" Astrophysical Journal, Part 1 Vol. 268(1983): pp. 428-446.

[50] B.Német, K.Musiol, I.Sánta, J.Zachorowski. "Time-resolved vibrational and rotational emission analysis of laser-produced plasma of carbon and polymers." Journal of Molecular Structure Vol. 511(1999): pp. 259-270.

[51] Carinhana Junior, D. “Determination of Flame Temperature by Emission Spectroscopy” (In Portuguese), Ph.D. Thesis, State University of Campinas, Campinas, SP, Brazil (2006).

[52] C.K.Law, T.Makino, F.Lua. "On the off-stoichiometric peaking of adiabatic flame temperature." Combustion and Flame Vol. 145(2006): pp. 808-819.

[53] T.S.Cheng. "Chemiluminescence measurements of local equivalence ratio in a partially premixed flame" Combustion Science and Technology Vol. 178(2006)

[54] Roby, R.J., Reaney, J.E., and Johnsson, E.L. "Detection of temperature and equivalence ratio in turbulent premixed flames using chemiluminescence." International Joint Power Generation Conference, Baltimore, MD, U.S.A. (1998).